Curtin
University of Technology

NOVIA

THE CFD SIMULATION OF FLUID CATALYTIC CRACKING

Curtin
University of Technology

Department of Chemical Engineering

The CFD Simulation of Fluid Catalytic Cracking

Novia

This thesis is presented for the Degree of
Doctor of Philosophy
of
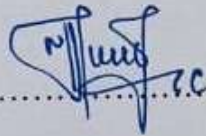**Curtin University of Technology**

May 2007

Declaration

To the best of my knowledge and belief this thesis contains no material previously published by any other person except where due acknowledgment has been made.

This thesis contains no material which has been accepted for the award of any other degree or diploma in any university.

Signature: .... 7.C.................................

Date: 07/05/2007

i

Acknowledgments

Dedications

What is with you must vanish: what is with Allah will endure.
And We will certainly bestow, on those who patiently persevere,
their reward according to the best of their actions.

The Holy Quran – An Nahl 96

To my beloved husband and children
Admansyah, Alif and Hanif

Publications

Journal

1. **Novia, M. S. Ray, and V. K. Pareek.** *Three-dimensional Hydrodynamics and Reaction Kinetics Analysis in FCC Riser Reactors*. The new Berkeley Electronic Press journal Chemical Product and Process Modeling (Submitted)

Conference Proceedings

2. <u>**N. Novia**</u>**, M. S. Ray, V. K. Pareek.** *Application of CFD for Transient Multiphase Flow and Reaction modelling in a Riser*. Fifth International Conference on Computational Fluid Dynamics in the Process Industries, December 13-15, 2006, Melbourne, Australia.

3. <u>**N. Novia**</u>**, M. S. Ray, V. K. Pareek.** *Unsteady State Simulation of Eulerian-Eulerian Multiphase Flow in FCC Riser Reactors*. Fifth International Conference on Computational Fluid Dynamics in the Process Industries, December 13-15, 2006, Melbourne, Australia.

4. <u>**N. Novia**</u>**, M. S. Ray, V. K. Pareek.** *CFD Analysis of Multiphase Flow and Reaction in FCC Riser reactors*. Curtin Engineering Faculty Research Colloquium (CERF), November 14, 2006, Perth, Western Australia.

5. <u>**N. Novia**</u>**, V. K. Pareek, M. S. Ray.** *Hydrodynamics and Kinetics Modelling of FCC Riser Reactors using CFD*. Australasian Chemical Engineering Conference (CHEMECA), September 17-20, 2006, Auckland, New Zealand.

6. <u>**N. Novia**</u>**, V. K. Pareek, M. S. Ray.** *CFD Simulation of Multiphase Flow in FCC Riser Reactors*. Australasian Chemical Engineering Conference (CHEMECA), September 25-28, 2005, Brisbane, Australia.

Table of contents

List of Figures

List of Tables

Abstract

Fluid catalytic cracking (FCC) is the refinery process used for the conversion of high molecular-weight hydrocarbons to produce higher valuable products such as gasoline. This research was especially concerned and motivated by the complex hydrodynamic and kinetic problems relating to the operation of FCC riser reactors, which affect both the design and optimization strategies. The catalytic cracking of hydrocarbons is a complex process due to the many reactions and chemical species involved. Therefore, the complexities of the reactions have been investigated by lumping together several chemical compounds. In this thesis, the Eulerian-Eulerian multiphase flow and the 3-lump kinetic model were assumed, in order to simulate three-dimensional hydrodynamics and cracking reactions occurring in the FCC riser reactors. The commercial CFD software, FLUENT version 6.2, was used for the modelling of these flow systems.

Computational fluid dynamics (CFD) is a powerful computer-based design technique that is used to optimize the industrial processes that incorporate complex reacting multiphase flows. CFD involves the numerical solution of the conservation equations for mass, momentum and energy in the flow geometry of interest, along with subsidiary sets of equations. The CFD model predicted the flow pattern of the solid and gas and many important aspects of a riser, such as the velocity profiles of the phases, solids hold-up, temperature and enthalpy distribution, yield distribution and feed injector geometry. It has also been used to describe how the FCC parameters such as catalyst-to-oil ratio (CTO) affect the final product distribution. It was found that the reliability of the estimated parameters and the predicted results were significantly improved when compared to those obtained by other studies, especially for gasoline yield.

Keywords: CFD; Fluid Catalytic Cracking (FCC); Hydrodynamics; Reaction Kinetics; Riser-Reactor.

<div align="center">

Chapter 1

OVERVIEW OF FCC AND RESEARCH OBJECTIVES

</div>

1.1   Background Information and Data

Fluid Catalytic Cracking (FCC) is the refinery industrial process for the conversion of high molecular-weight hydrocarbons to produce higher valuable products such as gasoline. The FCC and ancillary unit produce about 45% of gasoline worldwide. During its history of about 60 years, the FCC technology has been subjected to demands for improved product quality, as well as changing economics and stricter environmental regulations. The performance of a fluid catalytic cracking unit plays a significant role in the overall economics of the petroleum refinery due to its number of products, especially when optimization strategies are implemented. Determining optimal operating parameters for different modes of operation by experimentally changing the process conditions on a commercial FCC is neither feasible nor advisable. The development of improved design of FCC units was due to improved knowledge of several factors affecting the process (Murphy, 1992).

An FCC operation consists of two units: a riser-reactor and a regenerator. In the riser-reactor where catalytic cracking reactions occur, the hot regenerated catalyst is conveyed in contact with the feedstock. The riser usually operates in the turbulent regime, with fluctuations in velocity, pressure and concentration fields at the corresponding length and time scales . The flow behaviour in the FCC riser was studied experimentally and computationally. In the regenerator, burning the

coke catalyst in the presence of air regenerates the spent catalyst. This research was especially concerned on the FCC riser reactors. Since the gas-oil processing industry related to the riser unit directly. Predictive models for the FCC riser reactors using hydrodynamics and kinetics under a variety of operating conditions have been developed.

Knowledge of the hydrodynamics in multiphase reactors is not always available but it is crucially important for specifying optimal operation, design and scale-up. More research is required to provide a better understanding of the complex multiphase flow. In recent years a considerable research effort has been expended in order to obtain relevant CFD models (Krishna and van Baten, 2001, Hansen et al., 2003). The use of CFD has increased significantly as a powerful engineering tool in order to predict the flow behaviour in many types of industrial equipment. The velocity distribution of gas and solids, temperature, particle size and their distribution, inlet and exit configuration, and particle properties are important factors that determine flow behaviour. The applications of CFD can not only reduce the time and cost of scaling up, but can also forecast the performance of the industrial equipment before construction. Although the tools for applying single-phase flow in CFD are widely available, application of multiphase CFD still remains complex from both a physical and a numerical view point .

The catalytic cracking of hydrocarbons is a very complex process due to the many reactions that occur, and the catalyst activity changes rapidly during these reactions. A predictive kinetic description of fluid catalytic cracking processes is useful for the design, optimization and control of commercial plants (Jacob et al., 1976).

1.2   Objectives of This Research

This research was motivated by the complex hydrodynamic and kinetic problems relating to the operation of FCC riser reactors, which affect both the design and optimization strategies. Hydrodynamics play a crucial role in defining the performance of the riser. The specific objectives of the proposed research are as follows:

1. Modelling of riser hydrodynamics using CFD. The model will account not only for multiphase mixing but also the effect of riser internals such as mixing elbows.

2. Hydrodynamics of the riser system will also be simulated using the kinetic theory of granular flow (KTGF).

3. Kinetic modelling of the FCC riser reactors using CFD.

4. An integrated CFD model including hydrodynamics and reaction kinetics for the riser reactors will be developed. This will enable prediction of the transient behaviour of an FCC unit.

The overall aim of this research is to develop a rigorous hydrodynamics and kinetics model of the FCC riser reactors system.

1.3   Thesis Outline

This thesis focuses on FCC riser reactor system. The thesis can be subdivided into three main topics. (i) Hydrodynamic simulations of FCC riser reactors and the implications for design and optimisation with steady-state and unsteady-state conditions (Chapters 4 and Chapter 5).   (ii) The kinetic modelling of an FCC riser reactor for steady-state conditions (Chapter 6). (iii) Modelling of hydrodynamics and reaction kinetics of FCC riser–reactor with unsteady-state simulation (Chapter 7). Supplemental to this research is the overview and research objectives (Chapter 1), the literature review (Chapter 2), the modelling of FCC riser reactors (Chapter 3), conclusions and recommendations (Chapter 8), nomenclature (Chapter 9) and the reference listing (Chapter 10).

Chapter 2

LITERATURE REVIEW

2.1   Overview of Available Literature

Fluid catalytic cracking (FCC) is an important refinery unit operation. It converts high molecular weight petroleum fractions to useful low molecular weight products. The fluid catalytic cracking unit is usually operated to maximize gasoline production and to minimize coke formation in order to obtain the most economical process. The optimization of an FCC process yields the products which satisfy the current product quality demand. There are several mathematical models for the FCC in the literature which offer a simply cracking process description and use integration between the regenerator and riser. However, FCC technology is still facing the large challenge and far from being mature. FCC processes are known to be very difficult to model because of the large size of the process, complex hydrodynamics, and complex kinetics of both the cracking and coke-burning reactions .

At present, there are many large industrial organisations that have used CFD to solve a range of problems. Computational fluid dynamics is a powerful computer-based design technique used to optimize the industrial processes that incorporate complex multiphase flows. Computational fluid dynamics involves the numerical solution of the conservation equations for mass, momentum and energy in the flow geometry of interest, along with subsidiary sets of equations. Recently, there have been many efforts committed to the applications of CFD such as quicker

product-process development, optimization of an existing process for advanced energy efficiency, and the efficient design of new products and processes. According to Das, De Wilde et al. , the design of risers using conventional approaches faces difficulties in the calculations, such as: (i) the solid hold up in the reactor; (ii) the non-ideal flow and its effect on reactions; and (iii) the mixing of gas/solid at different length and time scales. These difficulties can be overcome using CFD. In order to predict optimum conditions of multiphase flow and cracking reactions in the riser-reactor, this research has used the simulation tool FLUENT 6.2 CFD package to model performance of the riser-reactor.

2.2 FCC Process Descriptions

A schematic of an FCC unit is shown in Figure 1. The FCC unit basically comprises two reactors, a riser-reactor and a regenerator. The riser-type reactor is commonly used in the fluid catalytic cracking process. The advantages of the riser-reactor are high contact efficiency of gas-solid, the flexibility of operating conditions and high gas/solid flux. The riser-reactor is divided into two zones: one is the feed-injecting zone at the bottom of the riser, and the other is the middle and upper sections. The preheated feedstock is injected with steam into the riser bottom through feed nozzles. The geometry of the feed-injection system increases the complexity of the riser, because flow in-homogeneities and back-mixing flow at the bottom of the riser lead to "hot spots" that can cause coke deposition, thermal cracking, and reduce the selectivity of primary products . Efficient feed-injection systems play a role in the plug-flow model by reducing unnecessary side reactions. The hot catalyst flows from the regenerator to the bottom of the riser. Contact between atomized feed and hot catalyst immediately induces vaporization. The upward velocity of the produced vapor pushes the catalyst up along the riser height. The produced vapours, due to reaction and vaporization,

increase the velocity of the flowing system. The instantaneous vaporization that takes places inside the reactor leads to three-phase flow (catalyst, liquid hydrocarbon and vapour hydrocarbon) at the riser bottom, and after completion of feed vaporization it becomes two-phase flow (catalyst and vapour hydrocarbon).

A series of cyclones separate the catalyst from hydrocarbon products. The catalyst is flushed with a counter-current flow of steam in the stripper to minimize hydrocarbon entrainment to the regenerator . After steam stripping, the deposited coke that is produced from the catalytic cracking reactions is entrained to the regenerator. In the regenerator, the coke is burned off the catalyst in the presence of air. The hot regenerated catalyst exits the regenerator and is recirculated into the bottom of the riser.
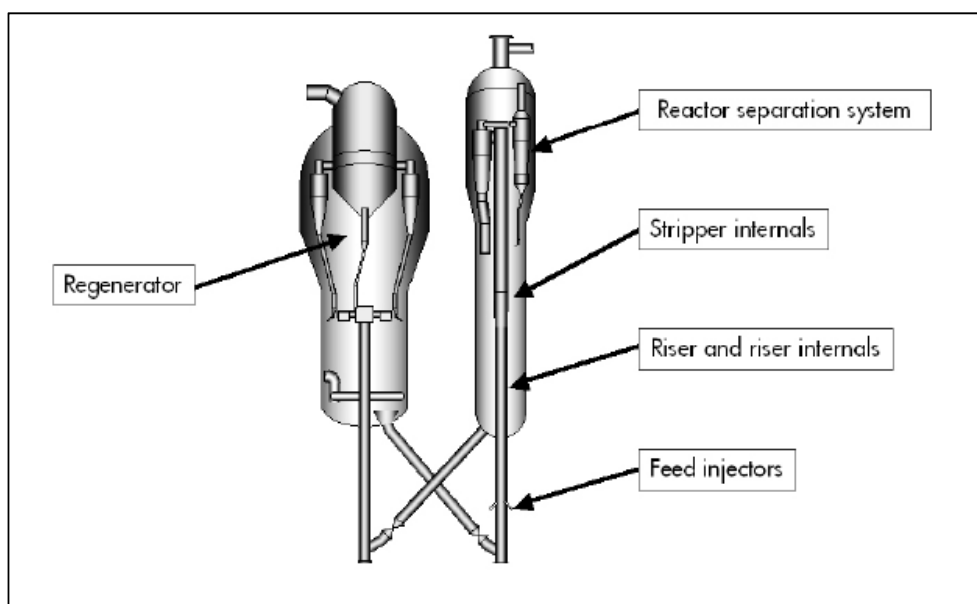
Figure 2.1. Schematic diagram of an FCC unit .

Performance of the riser and regenerator are intrinsically linked. Combustion of coke on catalyst particles is produced in the riser by cracking reactions; the regenerator supplies the heat which is needed for the vaporization of gas-oil feed and the endothermic heat of cracking reactions in the riser. The heat of combustion increases the temperature of the catalyst recycling from the regenerator.

2.3   Application of CFD

Computational fluid dynamics (CFD) is a powerful design technique that provides an analysis and understanding of the complex phenomena in the riser-reactor of an FCC unit. Recently, some CFD software such as FLUENT 6.2 has focused on simulating multiphase flow modelling to a higher level of reliability. Over the past few decades, CFD has been used to improve process designs and their optimization. The use of CFD allows engineers to solve problems involving complex geometries and boundary conditions. A CFD analysis gives the flow field of velocity, pressure, temperature and concentration on a computational grid of the solution domain. The advantages of using CFD are: (i) it costs less than laboratory experiments, because design parameters can be changed without the expense of hardware changes; (ii) using CFD requires less time than experiments; (iii) CFD gives important information about a flow field in a region where measurements are either difficult or impractical to obtain by experiment.

Although CFD models are well developed for single-phase flow, application of multiphase CFD remains more difficult. Therefore, many efforts have been committed to this area. Numerous models have been solved in a commercial CFD code and validated by plant data; therefore CFD model calculations can contribute to improved reactor design. Theologos and Markatos (1993) used a commercial

CFD code to simulate two-phase (gas-solid) reacting flow in a FCC riser-reactor. However, they did not consider turbulent flow in their model. Benyahnia, Arastoopour et al. (2002) simulated two-dimensional, transient, isothermal flow using CFD software (CFX). They obtained the flow profiles of velocity, volume fraction and pressure drop for each phase. Their research showed that both the inlet and exit conditions play a significant role in the overall mixing of the gas and particulate phases in the riser. Gao, Xu et al. solved a three-dimensional turbulent k-ε-k_p flow-reaction model using CFD code to predict the performance of FCC riser reactors. Das, Wilde et al. simulated a three-dimensional dilute-phase riser-reactor using a novel density-based solution algorithm. They used an Eulerian-Eulerian approach for multiphase flow, the kinetic theory of granular flow, and the k-ε model for gas phase turbulence. There was an unsteady behaviour of the flow and a core-annulus flow pattern in the riser as shown by their results. The concept of a 3-D analysis of a catalytic-cracking riser-reactor injection area using CFD techniques has been proven by the other researchers in order to evaluate atomization effects on feedstock vaporization rates, cracking reaction initiation, reactor selectivity and overall reactor performance. Van Wachem, Schoutten et al. developed a Eulerian-Eulerian multiphase CFD model for a freely bubbling gas-solid fluidised bed containing Geldart-B particles in order to study the dynamic characteristics at different superficial gas velocities, column diameters, and pressures. The dynamic characteristics are crucial for choosing the appropriate conditions to achieve stable operation and control. There is good agreement between their simulations and experimental data in the literature.

A detailed dynamic model of a modern riser-type FCC unit that consists of the reactor, regenerator, and catalyst transport lines with slide valves, was developed on the basis of the conservation principles . Elnashaie and co-workers extended their steady-state model to a simple dynamic model, and investigated the

sensitivity and stability of a bed-cracking-type FCC unit. Theologos, Nikou et al. presented a detailed dynamic model of a riser-reactor. This model consists of a set of three-dimensional partial differential equations that describe the distributions of catalyst and gas velocities, the pressure, component concentration, and temperature. However, they did not include the turbulent flow equation in their model. Their assumption was that the turbulent viscosity of the gas phase is 1000 times the laminar viscosity.

This research has used a Fluent 6.2 CFD code to optimize the process in modern riser FCC units, due to the application of CFD having been widely used to improve process design.

2.4 Alternative Modelling Approaches

A number of modeling approaches using different mathematical formulations have been published in the literature that predict the relationship between the solids concentration, operating conditions, and the geometry of the riser of an FCC unit. The main reason for studying the hydrodynamics of multiphase flow in the FCC riser is for the accurate prediction of their performance. Much research has attempted to develop the fundamental models used to describe the turbulent multiphase flow model. However, a detailed riser-reactor model considering the actual flow patterns is useful to change the operating conditions for improved performance. Many modern riser-reactors operate in the turbulent fluidization regime.

2.4.1 Riser Hydrodynamics

It is difficult to model the FCC riser reactor because of the combination of complex hydrodynamics, heat transfer, mass transfer and catalytic cracking kinetics. The parameters which influence these aspects also change along the riser height , namely:

    a. The feedstock is injected into the riser together with hot catalyst particles from the regenerator.

    b. Gas velocity increases due to feed vaporization and molar expansion resulting from cracking of the VGO to lower molecular weight products.

    c. Gas velocity influences the axial (and radial) profile of catalyst volume fraction.

    d. Catalyst temperature falls due to heat requirements for raising the sensible heat of the feed, its vaporization, and endothermic heat of cracking reactions.

    e. Catalyst activity falls due to deposition of coke on the catalyst surface.

Many FCC riser models are available in the literature, with various assumptions, as follows :

    i. Instantaneous vaporization of feed, and thermal equilibrium between catalyst and hydrocarbons.

    ii. Plug flow for gas and catalyst.

    iii. The slip factor, i.e. ratio between gas velocity and catalyst velocity, equal to 1.

    iv. Reactor is either isothermal or adiabatic.

    v. Lumped kinetics.

    vi. Catalyst activity varying either with time-on-stream or coke concentration on catalyst with non-selective deactivation.

According to Van Wachem and Almstedt , the reasons for the lack of fundamental knowledge on multiphase flows are:

1) Multiphase flow is a very complex physical phenomenon where many flow types can occur, and within each flow type several possible flow regimes can exist.

2) The complex physical laws and mathematical treatment of phenomena occurring in the presence of the two phases (interface dynamics, coalescence, break-up, drag) are still largely undeveloped. For example, there is still no agreement on the governing equations.

3) The numeric for solving the governing equations laws of multiphase flows are extremely complex. Very often multiphase flows show inherent oscillatory behaviour.

The riser hydrodynamics have been modelled using several modelling approaches. The most popular approach is the 1-D plug flow model with slip between the phases (Froment and Bischoff, 1990). This idealized model is not able to describe the complex hydrodynamics of the riser without the introduction of fitted parameter values, which depend on the natures of the particles and the pipe size . Arastoopour and Gidaspow used four different two-phase flow models to describe a one-dimensional steady-state pneumatic conveying system in order to obtain desirable solids flow behaviour. Later, Tsuo and Gidaspow (1990) simulated the two-dimensional numerical simulation of a cylindrical circulating fluidized bed with particle viscosity as an input parameter. Miller and Gidaspow (1992) also observed the hydrodynamics of gas/solid flow in the riser-reactor. They obtained the radial profile data at three different heights in the riser reactor. Theologos and Markatos (1993) simulated a two-phase model (the solid catalyst and the vapour hydrocarbon) in a riser-reactor. A two-dimensional transient model incorporating the kinetic theory for the solid particles used in the Fluent code is able to predict reasonably well the complex gas/solid flow behaviour in the riser section of a circulating fluidized bed . A 3D-simulation of gas-solid flow using the Eulerian-Eulerian approach with the kinetic theory of granular flow is

able to give insight into the complex hydrodynamics of circulating fluidized beds . Because complex flow patterns are basically 3D and have a major effect on the flow and reaction variables, the complete 3D simulation is desired.

Several researchers have studied multiphase flow in a riser, both theoretically and experimentally. Some experiments have been conducted to observe the flow pattern along the riser. Numerous research groups found a non-homogeneous distribution of particles along the radial and axial directions of the riser. Their results showed a core-annular flow regime with particles forming structures at the walls in the form of clusters and sheets for different operating conditions such as superficial gas velocity, particle diameter, pipe diameter and mass flux. The non-homogenous particles distribution influences the particle residence time distribution and the reactor performance. Martin, Derouin et al. (1992b) proposed the gas phase to be plug flow with radial dispersion. They calculated the catalyst suspension density based on an experimentally measured slip factor. The radial profile of the suspension density was assumed to be flat. Fligner, Schipper et al. used the experimentally measured radial density distribution from a cold-flow model of an FCC riser. Their model successfully demonstrated that the gasoline yield increased from 1.5 to 3% when a feeding strategy was used that led to a flatter radial density distribution. Berry et al. (2004) predicted conversion and yield patterns with a two-dimensional model in the riser section of an FCC unit. They found that increasing the droplet size from 50 to 500 μm decreased the gas-oil conversion by 4 wt%, while gasoline and light gas yields were reduced by 1.9 wt%.

As we know from the literature, the simulation of gas-solid flow using the Eulerian-Eulerian approach with the kinetic theory of granular flow is capable of solving the complex hydrodynamics of circulating fluidized beds. The complex flow patterns are basically 3D and have a major effect on the flow and reaction

variables. Furthermore, several researches has been developed in hydrodynamics simulation, however still much more works to be done in the future. Therefore, a complete model for FCC riser reactors is needed. This study has used the complete 3D simulation of Eulerian-Eulerian multiphase flow in a riser-reactor combined with the kinetic theory of granular flow in order to model the complex hydrodynamic of the riser-reactor.

2.4.2 Core-Annulus and Cluster Model

In the core-annulus type models, the solids velocity is either zero or negative in the annulus, which indicates solids moving downwards at the wall. Tsuo and Gidaspow (1990) proposed the prediction of core-annular flow of particles using a two-dimensional transient model with the finite difference technique, and with a solid viscosity determined from riser experiments. Other authors also used a particular viscosity value as an input variable into their models. Later, Neri and Gidaspow modelled the two-phase flow riser hydrodynamics and found a reasonable agreement between their modelling results and experimental data. Their results described the core-annular flow regimes and the radial and axial flow non-homogeneity. The three-dimensional model of an FCC riser-reactor using a novel density-based solution algorithm was simulated to show a core-annular flow pattern in the riser (Das et al., 2003). The higher solid fraction and lower solid velocity resulted in a higher conversion in the annulus region than in the core. For low flux risers, cold flow data show no catalyst downflow at the wall under FCC operating conditions .

Several researchers have studied cluster formation and its effects on the velocity profile calculations in risers. Tsuo and Gidaspow (1990) studied the simulation of a two-phase flow model in a riser, and investigated particle clusters in their

simulation for the case of relatively large particles (sand particles with diameter 520 μm). However, no clustering was observed in their simulation for the case of relatively small particles (diameter 76 μm) such as those found in fluid catalytic cracking operations. In contrast, Agrawal, Loezos et al. (2001) observed particle clustering in their simulation for small particles (diameter 75 μm). In some cases, the segregation of particles is concentrated near the pipe wall, however, large regions of high particle concentrations extend well into the centre of the pipe (Pita and Sundaresan, 1993). Fligner et al. presented a cluster model approach in order to observe high slip factors. They considered the riser as comprising two phases: a dispersed cluster phase (the catalyst particle), and a continuous (gas) phase. Sharma, Tuzla et al. investigated the parametric effects of particle size and superficial gas velocity on solid concentration in clusters. Their results showed that solid volume fractions in clusters were insensitive to particle size, but decreased significantly with increasing gas velocity. Heynderick, Das et al. (2004) have taken into account the effects of clustering/mesoscale fluctuations by using an effective interphase momentum-transfer coefficient. They calculated the effective interphase momentum-transfer coefficient from the single-particle interphase momentum transfer coefficient by taking into account the cluster volume fraction in the two-phase flow.

For low flux risers, cold flow data show no catalyst downflow at the wall under FCC operating conditions . According to Tsuo and Gidaspow (1990), no clustering was observed in their simulation for the case of relatively small particles (diameter 76 μm) such as those found in a fluid catalytic cracking operation. A disadvantage of the core-anulus models is that the application is limited to the fully developed flow zone of the riser, where the solid and the gas have been accelerated to their steady-state velocity, and the average solids holdup remains constant. According to Gidaspow et al. , the core-annular structure leads

to two main problems: (1) insufficient gas-solid contact, and (2) back-mixing due to non-uniform radial distribution. The models based on the core-annulus flow assumption were not able to describe the upflow of solids at the wall that has been reported to take place at high mass fluxes . Therefore, we have not considered the core-annulus and cluster model in our research.

2.4.3 The Eulerian-Eulerian Multiphase Model

Two approaches are used for the modelling of multiphase flow: the Eulerian-Eulerian and the Eulerian-Langrangian approaches. In the Eulerian-Eulerian approach, both the continuous and dispersed phases are considered in a Eulerian representation, which creates mass and momentum equations for each phase. The presence of each phase is described by a volume fraction. In the alternative Eulerian-Langrangian approach, the mixture is treated as a pseudo-continuous phase with variable density, but it is not suitable for application where the volume fraction of the dispersed phase is high. The Langrangian approach restricts the number of particles, and is not suitable for gas/solid flow systems such as the fluidized bed. The Eulerian-Langrangian approach is more computationally intensive than the Eulerian-Eulerian approach, because it allows the tracking of particles (bubbles) in the continuous phase. Recently, the Eulerian approach has been most often used and is preferable when considering gas/solids flow systems such as fluidized beds. A difficulty to be overcome with the Eulerian-Eulerian approach is the calculation of the physical properties appearing in the equations (i.e. the solid-phase pressure and viscosity). These solid properties can be calculated either on an empirical or theoretical basis . Recently, gas-particle two-fluid models which treated the particle phase as a continuous fluid based on the Eulerian method, were widely employed in modeling gas-particle flow (Ding and Gidaspow, 1990). Theologos et al used a Eulerian-Eulerian CFD model that

described both the gas/particle flow and the catalytic cracking, without modelling the turbulent motion of the phases.

There are two Eulerian modelling approaches for multiphase flows: the two-fluid model with constant solid phase viscosity, and the two-fluid model using the kinetic theory of granular flow (KTGF) for the solid phase . The advantages of a two-fluid model are that it needs less computational effort, it is more appropriate for engineering applications where no details of the individual particle motion are available, and it is the only practical way of approaching the modelling of denser flows . Recently, the KTGF has become the most widely used approach. The KTGF is principally an extension of the classical kinetic theory applied to dense particle dissipation where non-ideal particle-particle collisions are taken into account by means of the coefficient of restitution . In the KTGF, the collisions between particles are considered as interactions of the fluctuating and the mean motion of the particles. The solid-phase pressure and viscosity are related directly to the solid-phase turbulence, and using the granular temperature equation .

The kinetic-theory flow model is based on inter-penetrating continua for fundamental multiphase flow. In the kinetic-theory-based flow model, different phases can be present at the same time in the same computational volume. The conservation of mass, momentum and energy are solved for each phase. The constitutive equations have to be specified in order to describe the physical properties of each phase. Solid viscosity and pressure are derived from the solid velocity fluctuation and particle collision. Sinclair and Jackson (1989) were the first to present the granular flow model for the fully developed gas-solid flow in a small vertical pipe. They demonstrated lateral segregation of solids observed in the radial direction. To simplify the simulation, they took into account the drag force and the stress in the particle phase, in consequence neglecting the gas-phase turbulence. Ding and Gidaspow (1990) extended the granular flow model using

the Boltzmann equation for distribution of particle velocity. They used the Maxwellian velocity distribution as a single particle distribution. Their model is restricted to dense gas/solid flow applications. Samuelsberg and Hjertager (1996) also modelled the riser using a more complete kinetic theory model by solving the granular temperature equation. They compared their model results with experimental data from a pilot-scale circulating fluidized-bed reactor with different solid loadings and a range of gas superficial velocities. The granular temperature is essentially determined by the random oscillating kinetic energy of the particles. This theory gives rise to an equation of state that relates the granular temperature to the granular pressure and bulk density (Sun and Gidaspow, 1999).

The influence of direct particle-particle collisions has been modelled using the kinetic theory for granular flow based on the Chapman-Enskog theory of dense gas . The sensitivity of Eulerian models considering inelastic particle-particle collisions for simulations in the riser have been investigated by several authors (Pita and Sundaresan, 1991). Goldschnidt, Kuipers et al. studied the influence of the restitution coefficient on the segregation behaviour of dense gas-fluidized beds based on a multi-fluid Eulerian model.

We have applied the Eulerian-Eulerian multiphase flow model in this study, because this approach has been most often used (and literature data is available) and is preferable when considering gas/solids flow systems such fluidized beds. This approach is also appropriate for application where the volume fraction of the dispersed phase is high.

2.4.4 Feedstock Vaporization and Feed Injection

Cracking reactions, especially at the inlet of the riser-reactor, are affected by interphase heat transfer at the riser inlet area, feedstock vaporization inside the reactor, hydrocarbon-catalyst interaction, temperature-related reaction kinetics, and the complex geometry of the feed injector . Effects of feedstock vaporization and feed-injection configuration in a riser-reactor have been studied experimentally and also modelled using CFD techniques by a number of research groups (Theologos and Markatos, 1993). At the entrance region of the feed-injection zone, partial feed vaporization leads to a three-phase flow of catalyst, liquid hydrocarbon, and hydrocarbon vapour. Complete feed vaporization and then a two-phase flow of catalyst and hydrocarbon vapour begins at 3 to 4 m of the riser height. Rapid flash vaporization of the liquid feed reduces coke formation, does not allow heavy fractions to be exposed to the true catalyst temperature, eliminates thermal cracking, and contributes to a fast catalytic quenching process (Mauleon and Courcelle, 1985). Mirgain et al. (2000) have found that feed vaporization in a riser-reactor affects the yield of valuable products in risers. They studied homogeneous vaporization in the gas phase, and also heterogeneous vaporization, when the feedstock droplets sprayed into a fluid cracker. Mauleon and Courcelle (1985) found that the interphase heat transfer and feed-spray atomization have some impacts on feed vaporization and also affect the temperature and concentration distributions.

The inlet zone of the riser-reactor is where the catalyst is accelerating. This is the most complex part of the reactor where intense turbulence and non-homogeneous flow creates high temperature and concentration gradients. The ideal feed system will distribute the catalyst across the riser before contact with the feed, maximize the heat transfer between the oil and catalyst, atomize the oil into small droplets which evaporate faster, distribute the feed in a flat sheet across the riser, and create a narrow droplet size distribution (with a small Sauter mean diameter) which will increase the vaporization rate and allow uniform mixing of oil and

catalyst . Uniformity of solid particles distribution over the entire riser height is greatly affected by inlet and outlet configurations. Pita and Sundaresan (1993) studied the effects of different inlet configurations on the flow pattern. Hot spots at the inlet zone induce the secondary cracking reactions, which produce undesirable products and coke deposition. The feed injection may control the flow of catalyst and hydrocarbons and establish plug flow conditions in order to minimize undesirable temperature gradients (Theologos and Markatos, 1993). Theologos, Lygeros et al. developed the conceptual 3D analysis in the injection area of a catalytic cracking riser-reactor using CFD. They found that geometry of feed nozzles and the feed introduction method at the bottom of the riser have a significant influence on the distribution of catalyst.

In the present study, we have used an assumption that instantaneous vaporization of the feed occurs as it enters the riser-reactor. This research has used four feed injection nozzles due to the feed injector geometry, and the number of feed injection nozzles affects the multiphase mixing.

2.5   Reaction Kinetics

The catalytic cracking of hydrocarbons is a very complex process due to the many reactions that occur, and the catalyst activity changes rapidly during these reactions. A predictive kinetic description of fluid catalytic cracking processes is useful for the design, optimization and control of commercial plants (Jacob et al., 1976). Using a very active catalyst, the cracking reaction can be completed in short-contact-time riser-reactors. Gas residence time distributions have considerable importance in predicting conversion and selectivity for various operations, especially for catalytic cracking reactions. However, solid residence time distribution determines the degree of solids backmixing in a riser which in

turn affects the gas-solid contact, suspension-to-wall heat transfer, and the degree of catalyst deactivation and particle conversion for a gas-solid reaction involving the particle transformation (Xiaotao, 2004). The conversion obtaining in the FCC process is determined by the coke build-up on the catalyst. The amount of coke determines the heat generated in the regenerator and the amount of heat using for the cracking reaction.

The riser-type reactor has been used in the FCC process because the catalyst circulation rate has to be high because of rapid deactivation, an intermediate product is the desired product, reactivation of catalyst is needed, and the reactions are highly exothermic or endothermic (Kunii and Levenspiel, 1991). The continuous circulation of catalyst is important for the stable operation of an FCC unit. The functions of catalyst circulation are that it brings the deactivated catalyst into the regenerator to restore its activity, and it transfers the heat produced in the regenerator to the reactor.

The catalytic cracking reactions can be classified into two categories: primary cracking of gas-oil molecule and re-cracking of cracked products. According to Gates et al. (1979), the cracking reactions occurring in FCC is following:

1. Paraffins are cracked to olefins and smaller olefins:

   $C_{16}H_{34} \rightarrow C_9H_{18} + C_7H_{16}$

2. Olefins are cracked to smaller olefins:

   $C_{12}H_{24} \rightarrow C_7H_{14} + C_5H_{10}$

3. Aromatics side-chain scission:

   $C_6H_5\text{-}C_{12}H_{25} \rightarrow C_6H_5\text{-}C_8H_{15} + C_4H_{10}$

4. Naphthenes (cycloparaffins) are cracked to olefins and smaller ring compounds:

   $C_{20}H_{40} \rightarrow C_{12}H_{24} + C_8H_{16}$
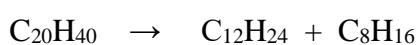
Catalytic cracking reactions over zeolite catalyst are mainly endothermic reactions.

2.5.1 Kinetic Modelling

The first step for improving the FCC product yields has been to determine the mechanism of the catalytic cracking reactions from appropriate kinetic models. The complex reactions have been studied by lumping numbers of chemical compounds. The kinetic models are formulated by grouping reactants and products into hydrocarbon lumps. The complexity of models used to define the feed-product lumps varies from the simplest model (using the 3-lump kinetic model) to models involving thousands of chemical species. The 3-lump kinetic model considers the heavy gas-oil, gasoline and the remaining component as the lumps. Weekman and Nace (1970) found that a 3-lump model is sufficient for reactor design purposes, because more lumps create complex mathematical models. A 5-lump kinetic model, and the prediction of coke yield separately from other lumps, has been presented by several authors . In 3-lump and 5-lump models, the primary gas-oil cracking is considered as a second-order reaction, and the gasoline cracking as a first-order reaction . According to Hagelberg, Eilos et al. , the apparent second-order behaviour of the gas-oil cracking is explained by the changing reactivity of gas-oil molecules, i.e. at low conversions the most reactive molecules crack first and as the conversion increases the reactivity of the feed molecules decreases, this leads to the apparent second-order reaction.

A more detailed 10-lump kinetic model to take into account other feed properties in addition to the boiling range was developed by Jacob, Gross et al. (1976). In the 10-lump kinetic model, the heavy and middle distillate fractions are subdivided into four different lumps; paraffins P_h, naphthenes N_h, aromatic substituents A_h,

and carbon atoms inside the aromatic rings F_h. Theologos, Nikou also applied a 10-lump kinetic model in their simulation. The prediction of coke yield separately from other lumps becomes very important in order to perform heat integration studies, and to design and simulate the air blowers and the FCC regenerator and reactor . In contrast to the lump models, is the detailed microscopic level definition of the reactions, known as single-event kinetic modelling, based on the mechanism of the various reactions involving carbenium ions (Das et al., 2003). Mathematical modelling of catalytic cracking becomes much more complex when considering factors due to macro-kinetics .

Pareek, Adesina et al. presented sensitivity analysis of the rate constants of Weekman's riser kinetics using the CATCRAK program. Van Landeghem, Nevicato et al. considered gas-oil cracking as a second-order reaction and gasoline as first-order. Weisz and Goodwin (1966) found that reaction kinetics are controlled by the rate of pore diffusion of oxygen to the coke surface. They also found that the reaction kinetics could be best described by a first-order rate equation for the combustion of coke in an FCC unit.

A 3-lump reaction scheme was chosen in our study for simplicity and computational economy. In this scheme, the gas-oil feed is converted to gasoline and dry gas plus coke, and a part of the gasoline is also converted to dry gases plus coke. We used this scheme because (Theologos and Markatos, 1993):

1. a 3-lump model is still capable of illustrating the interactions between the process variables and the reaction rate and catalyst decay velocity;

2. a 3-lump model predicts gasoline selectivity that represents the most significant contribution to the profitability of catalytic cracking reactor;

3. a simplified reaction scheme can perfectly illustrate the capabilities of computational fluid dynamic techniques for modelling complex process operations, within acceptable computational costs.

2.5.2 Catalyst Deactivation

A very active zeolite-based catalyst is widely used in FCC unit operations. The development of these catalysts allowed the cracking reaction to be completed in short-contact-time riser-reactors. The catalyst performance is influenced by diffusion of reactants and products in the catalyst substrate. Therefore, the overall performance is influenced by the interaction between the intrinsic kinetics and the transport processes such as heat, mass and momentum transfer in the catalyst support . Loss of catalyst activity is due to the formation of carbonaceous deposits on the pore space of the catalyst, which is known as coking. Furthermore, the catalyst is deactivated by poisoning the active sites and by pore plugging. Deactivation of catalyst is important in fluid catalytic cracking reactors. Coke-on-catalyst is an important FCC variable, and a small variation in its value can significantly affect the FCC operation in general, and the regenerator operation in particular . Coke formed during the reaction is deposited on the catalyst, blocking the internal and the external surface, and results in a substantial reduction in the catalyst activity and selectivity. The coke is burned in the regenerator in order to restore the catalyst activity . Faltsi-Saravelou found that a step change in the coke yield of cracking reactions resulted in an increase in the regenerator temperature, but no increase in carbon on the regenerated catalyst. Coke combustion provides the thermal energy necessary to vaporize the feedstock and to compensate for the endothermic reaction . Den Hollander, Makkee et al. studied experimentally the coke deposition and its effect on the catalyst activity in the micro-riser-reactor. Their result showed that the timescale of coke formation (within 0.15 s) is much shorter than the timescale for conversion (0 – 5 s). They concluded that the initial coke deposition is the main cause of deactivation.

The effect of various types of catalyst decay on selectivity have been reviewed by several authors (Froment and Bischoff, 1990, Masamune and Smith, 1966). Poor atomization due to the formation of feed droplets that are too heavy to be moved upwards by the vapour stream can cause rapid catalyst deactivation . The degree of feedstock atomization controls the residence time of the liquid phase inside the reactor, and affects the initiation of cracking reactions and influences reaction selectivity.

2.5.3 Heat of Reaction

An accurate overall heat balance around the reactor-regenerator system in an FCC unit includes: (1) the enthalpy of combustion of coke-on-catalyst; (2) the endothermic heat of cracking reactions; (3) the heat of vaporization of gas-oil at the entrance of the riser; and (4) other enthalpies such as the heat of feed air, product stream, exit flue gas from regenerator . The heat of FCC reaction is a complex function of various factors, such as feed composition and temperature, and is a major unknown in FCC operation. Additionally, the heat of reaction at any particular height is also dependent on the overall conversion level and distribution at that height . Elnashaie and Elshishini assumed a constant average heat of reaction for all the cracking reactions.

2.5.4 Riser Heat Balance

Theologos, Lygeros et al. reported that the heat lost by the hot regenerated catalyst in the riser is distributed between the mechanisms of heating and vaporization of the liquid feed (between 60-80%), endothermic heat of cracking (10-35%), and heat losses (5%). Therefore, an FCC riser model should also include the riser energy balance. Their results also showed that good feed injection is essential for controlling the heat balance when processing heavy fuels.

The FCC reactor temperature is controlled by automatically adjusting the catalyst circulation rate, so that the heat transferred to the reactor is at the required rate to keep the reactor temperature constant . Pareek, Adesina et al. found that the temperature in the riser-reactor decreases progressively from the bottom to the top of the riser. The temperature drop as a result of the cracking reactions affects the

gasoline yield and the overall conversion in the riser and the regenerator . Pareek, Adesina et al. developed a non-isothermal riser model for the FCC riser-reactor in order to estimate the temperature drop due to the cracking reactions as a function of riser length. According to Theologos, Lygeros et al. interphase heat transfer is critical when establishing the heat balance in the three-phase-flow system at the bottom of the riser, and its determination plays an important role since it affects phase temperatures that in turn control the reaction kinetics.

2.6 Conclusions and Significant Findings

The optimization of an FCC process means that the products satisfy current quality control demands. CFD is a powerful engineering tool that can be used to optimize industrial FCC processes, and provides an analysis and understanding of the complex phenomena in a riser-reactor. Several researchers have used CFD to solve problems with complex geometries and boundary conditions. A CFD analysis provides the flow field of velocity, pressure, temperature and concentration on a computational grid of the solution domain. The advantages of using CFD are lower costs and less time required than performing experiments. CFD also gives important information about the flow field in a region where measurements are either difficult (or not feasible) to obtain from experiments. This research has used the Fluent 6.2 CFD code to optimize the process, due to the application of CFD having been widely used to improve process designs of modern FCC riser reactors.

The riser-type reactor is commonly used in the FCC process because of the high contact efficiency of the gas and solids, the flexibility of operating conditions, and high gas/solid flux. There are many considerations when choosing a riser-type reactor, i.e. the catalyst circulation rate has to be high because of rapid

deactivation, an intermediate product is the desired product, reactivation of catalyst is needed, and the reactions are highly exothermic or endothermic (Kunii and Levenspiel, 1991). However, it is difficult to model the FCC riser reactor because of complex hydrodynamics, heat transfer, mass transfer and the catalytic cracking kinetics. Multiphase flow mixing in the riser influences the yield and selectivity of a fluid catalytic cracking process. Two approaches are used in modelling of multiphase flow: the Eulerian-Eulerian and the Eulerian-Langrangian approaches. The Eulerian-Langrangian approach is more computationally intensive than the Eulerian-Eulerian approach. The Eulerian-Eulerian multiphase flow model has been applied in this study, because this approach has been most often used and is preferable when considering gas/solids flow systems such fluidized beds. This approach is also appropriate for application where the volume fraction of the dispersed phase is high. A 3D-simulation of multiphase flow using the Eulerian-Eulerian approach with the kinetic theory of granular flow is capable of solving the complex hydrodynamics of FCC riser reactors.

Many factors influence the modelling of multiphase flow. Numerous research groups have investigated a core-annular flow regime with particles forming structures at the walls in the form of clusters and sheets for different operating conditions such as superficial gas velocity, particle diameter, pipe diameter and mass flux. The feed nozzle geometries and the feed introduction method at the bottom of the riser have a significant influence on the catalyst distribution. The inlet zone of the riser-reactor, where the catalyst is accelerating, is the most complex part of the reactor. Here intense turbulence and flow non-homogeneity result in high temperature and concentration gradients. In the present study, we have made the assumption that instantaneous vaporization of the feed occurs as it enters the riser-reactor. This research has used four feed injection nozzles, because

the feed injector geometry and the number of feed injection nozzles affect the multiphase mixing.

FCC riser-reactor is expected to maximize the gasoline production. The riser hydrodynamics has been predicted in the 3-D model. Catalyst sizes have been simulated under varying gas flow rates and feed temperatures, because some simulation results in the literature showed the performance of the riser was influenced by these factors.

A predictive kinetic description of fluid catalytic cracking processes is useful for the design, optimization and control of commercial plants. Our research has evaluated the applicability of the Fluent 6.2 CFD package to predict the steady-state and transient 3D-simulation of multiphase flow and kinetic modelling in an FCC riser-reactor, using the Eulerian-Eulerian approach and the kinetic theory of granular flow. A 3-lump reaction scheme was chosen for this study for reasons of simplicity and computational economy.

<div align="center">

Chapter 3

CFD MODELLING AND SIMULATION

</div>

3.1   Previous Modelling Approaches

Modelling and CFD simulation of FCC riser reactors has obtained good results during the last 15 years. However the precise analysis of the flow field has not yet been achieved and it still restricted to two-dimension flow. In order to improve the process performance of an actual system, detailed knowledge about modelling and CFD simulation is required. The CFD approach is becoming ever more useful with improvements in computer technology. Using CFD to design and simulate reactors has some advantages because of its capability to take account of the complex flow process.

Computational fluid dynamics (CFD) is a body of knowledge that provides numerical solution of the conservation equations for mass, momentum and heat of flow geometry, together with subsidiary sets of equations. Some examples of such subsidiary equations are equations for turbulence in the Reynolds-averaged formulation, equations describing chemical species in the flow, and equations describing the dynamics of solid particles, liquid droplets and gas bubbles in the flow . These equations are solved at several thousand discrete points in the defined flow domain.

The motion of solid particles suspended in a Newtonian gas or liquid can be described by the Navier-Stokes equations for the fluid, and the Newtonian equations of motion for suspended solid particles. Because of the complexity of

the Navier-Stokes equations, it is almost impossible to obtain an analytical solution for these equations. Therefore, suitable numerical methods need to be considered. The main objective of this chapter is to describe the procedure of the numerical solution applied for the work presented in the further chapters.

3.2   CFD Analysis

The application of CFD for some process equipment comprises a number of steps (Versteeg and Malalasekera, 1995, Ranade, 2002). First, the flow problem is described in terms of physical and chemical phenomena acceptable in this situation. The second step is the conceptualization of the appropriate flow geometry. Simplicity of the geometry is needed in order to meet the accuracy and adequacy of the representation. A three-dimensional CFD simulation is desirable, especially for complex flow, because it can provide a better understanding of flow and reaction variables .

When the geometry for the CFD analysis has been determined, the next task is the discretization of the computational domain to make possible the numerical solution of the related partial differential equation. The discretization of the geometry is defined as mesh (or grid) generation. The grids can be classified in two types: structured grids and unstructured grids (Ranade, 2002). In structured grids, all interior nodes have an equal number of adjacent elements. However, unstructured grids allow any number of elements to meet at single nodes.

Furthermore, the next step of CFD analysis is the numerical solution of the partial differential equations (PDEs). There are three main methods to solve PDEs numerically; these are finite difference, finite element, and finite volume. The final step in the CFD analysis is the visualization of a variety of solution variables in the computational domain.

3.3   CFD Simulation Packages

CFD codes are structured around the numerical algorithms that handle problems of fluid flow (Versteeg and Malalasekera, 1995). A number of commercial CFD codes have been developed such as FLUENT, CFX, STAR-CD, PHOENICS and FLOW3D. In order to provide easy access to their solution power, all commercial CFD packages include user interfaces to input problem parameters and to examine the results. All codes contain three key elements: (i) a pre-processor; (ii) a solver; and (iii) a post-processor. The pre-processor will construct and discretize the geometry of the computational domain and define boundary types of the constructed geometry. One of several pre-processors in the FLUENT solver is known as GAMBIT. In GAMBIT a user can create the geometry, mesh the geometry and define boundary types. The Solver solves the partial differential equations using one of three numerical methods: (i) finite difference; (ii) finite element; and (iii) finite volume (most widely applied). The post-processor in the CFD codes are provided to help the user to visualize the data. These include the domain geometry, vector plots, line and shaded contour plots, 2D and 3D surface plots, particle tracking, view manipulation (translation, rotation, scaling) and colour postscript output (Versteeg and Malalasekera, 1995). The CFD codes have also included animation facilities to visualize transient processes.

FLUENT is a state-of-the-art computer program for modelling multiphase flow, heat transfer and reaction kinetics in complex geometries. It provides the complete mesh flexibility and solving the flow problems with unstructured meshes that can be generated from complex geometries with relative simplicity .

FLUENT is written in the C computer language and makes full of the flexibility and power by the language. Consequently, true dynamic memory allocation, efficient data structures, and flexible solver control are all made possible. In addition, FLUENT uses a client / server architecture, which allows it to run as separate simultaneous processes on client desktop workstations and powerful compute servers, for efficient execution, interactive control, and complete flexibility of machine or operating system. In FLUENT, all functions required to compute solution and display the simulation results are accessible through the interactive, menu-driven interface . Therefore, this research has used the CFD software FLUENT 6.2 in order to solve the multiphase flow and kinetic modelling together with turbulence and heat transfer of the FCC riser reactors.

3.3.1 The Use of FLUENT

Once a grid has been read into FLUENT, all remaining operations are performed within the solver including setting boundary conditions, defining fluid properties, executing the solution, refining the grid, and viewing and post processing the results. FLUENT is ideally suited for incompressible and compressible fluid flow simulations in complex geometries. It also offers other solvers that address different flow regimes and incorporate alternative physical models.

FLUENT uses unstructured meshes in order to reduce the amount of time to generate meshes, simplify the geometry modelling and mesh generation process, model more-complex geometries and adapt the mesh to resolve the flow field features.

The procedure steps for solving the problem in FLUENT are following:

1. Create the model geometry and grid.
2. Start the appropriate solver for 3D modelling.
3. Import the grid.
4. Check the grid.
5. Select the solver formulation.
6. Choose the basic equations to be solved: laminar or turbulent, chemical species or reaction, heat transfer models, etc.
7. Specify material properties.
8. Specify the boundary conditions.
9. Adjust the solution control parameters.
10. Initialize the flow field
11. Calculation a solution
12. Examine the results
13. Save the results
14. If necessary, refine the grid or consider the revisions to the numerical or physical model.

FLUENT provide three different solver formulations:

- Segregated
- Coupled implicit
- Coupled explicit

All three solver formulations will provide accurate results for a broad rang of flows, but in some cases one formulation may perform better than the others. The segregated solver has been used for incompressible and middle compressible flow. On the other hand, the coupled approach was designed for high-speed

compressible flow. The segregated solver provides several physical models that are not available with the coupled solver such as: Eulerian multiphase model.

3.3.2 Defining Boundary Conditions by FLUENT

Boundary conditions specify the flow and thermal variables on the boundaries of the physical model. Therefore Boundary conditions are a critical component of FLUENT simulations and it is crucial that they are specified appropriately. The boundary types available in FLUENT are classified as following:

- Flow inlet and exit boundaries: pressure inlet, velocity inlet, mass flow inlet, inlet vent, intake fan, pressure outlet, pressure far-field, outflow, outlet vent, exhaust fan.
- Wall, repeating, and pole boundaries: wall, symmetry, periodic, axis
- Internal cell zones: fluid, solid
- Internal face boundaries: fan, radiator, porous jump, wall, interior

FLUENT provides ten types of boundary zone types for the specification of flow inlets and exits: velocity inlet, pressure inlet, mass flow inlet, pressure outlet, pressure far-field, outflow, inlet vent, intake fan, outlet fan, and exhaust fan

1. Velocity inlet boundary conditions are used to define the velocity and scalar properties of the flow at inlet boundaries.
2. Pressure inlet boundary conditions are used to define the total pressure and other scalar quantities at flow inlets.
3. Mass flow inlet boundary conditions are used in compressible flows to prescribe a mass flow rate at an inlet, It is not necessary to use mass flow rate inlets for incompressible flows because when density is constant, velocity inlet boundary condition will fix the mass flow.

4. Pressure outlet boundary conditions are used to define the static pressure at flow outlets.

5. Pressure far-field boundary conditions are used to model a free-stream compressible flow at infinity, with free-stream Mach number and static condition specified.

6. Outflow boundary conditions are used to model flow exits where the details of the flow velocity and pressure are not known prior to solution of the flow problem. They are appropriate where the exit flow is close to a fully developed condition, as the outflow boundary condition assumes a zero normal gradient for all flow variables except pressure. They are not appropriate for compressible flow calculations.

7. Inlet vent boundary conditions are used to model an inlet vent with a specified loss coefficient, flow direction, and ambient (inlet) total pressure and temperature.

8. Intake fan boundary conditions are used to model an outlet vent with a specified pressure jump, flow direction, and ambient (inlet) total pressure and temperature.

9. Outlet vent boundary conditions are used to mod4l an outlet vent with a specified loss coefficient, flow direction, and ambient (inlet) total pressure and temperature.

10. Exhaust fan boundary conditions are used to model an external exhaust fan with a specified pressure jump, flow direction, and ambient (discharge) static pressure.

3.4   Conservation Equations

The governing conservation equations of fluid flow represent mathematical statements of the conservation law of mass (continuity), momentum and energy. The most popular form of the momentum conservation equation is the Navier-Stokes equation. The detailed derivation of the equations for mass, momentum and energy can be found in the literatures (Versteeg and Malalasekera, 1995, Bird et al., 1960, Brodkey and Hershey, 1988).

3.4.1   Continuity Equation

The mass conservation (continuity) equation for species i can be written (Ranade, 2002) as:

$$\frac{\partial}{\partial t}\left(\rho\varepsilon_i\right)+\nabla.\left(\rho\mathbf{U}\varepsilon_i\right)=-\nabla.(J_i)+S_i \tag{3.1}$$

where t is time, ρ is density, ε_i is the mass fraction of species i and $\mathbf{U}$ is velocity. S_i is the source term of species i and represents the net rate of mass of species i due to chemical reaction or interphase transfer per unit volume. J_i is rate of diffusive flux of species i (mass per unit area per unit time) and is formulated by:

$$J_i = -\rho D_i \nabla x_i \tag{3.2}$$

D_i is diffusivity of species i in the fluid. Substitution of Equation (3.1) in Equation (3.2) gives:

$$\frac{\partial}{\partial t}(\rho \varepsilon_i) = -\nabla.(\rho \mathbf{U} \varepsilon_i) + \nabla.(\rho D_i \nabla \varepsilon_i) + S_i \tag{3.3}$$

Consequently, for all species in the system, it can be written:

$$\frac{\partial}{\partial t}(\rho) + \nabla.(\rho \mathbf{U}) = \sum_i S_i \tag{3.4}$$

For single-phase flows, right-hand side will be zero. However, for multiphase flows this term can account for interphase mass transfer.

3.4.2 Momentum Equation

The law of momentum conservation yields a basic set of equations governing the motion of fluids, and these are used to calculated velocity and pressure fields (Ranade, 2002). The momentum equations can be written:

$$\frac{\partial}{\partial t}(\rho \mathbf{U}) = -\nabla.(\rho \mathbf{U}\mathbf{U}) - \nabla.p - \nabla.\boldsymbol{\tau} + \rho \mathbf{g} + \mathbf{F} \tag{3.5}$$

where $\mathbf{F}$ is external body forces.

Stress tensor (τ) for Newtonian fluids is formulated (Ranade, 1999, Bird et al., 1960) as:

$$\boldsymbol{\tau}_{ij} = -\mu(\nabla \mathbf{U} + \nabla \mathbf{U}^T) + \frac{2}{3}\mu\delta_{ij}(\nabla.\mathbf{U}) \tag{3.6}$$

where δ_{ij} is the kronecker delta ($\delta_{ij} = 1$ if i = j and $\delta_{ij} = 0$ if i $\neq$ j) and μ is viscosity.

Substituting Equation (3.6) into (3.5) will produce three momentum balance components:

(i) x-momentum

$$\frac{\partial}{\partial t}(\rho U_x) + \nabla.(\rho \mathbf{U} U_x) = -\frac{\partial P}{\partial x} + \nabla.(\mu \nabla U_x) + S_{mx} \qquad (3.7)$$

(ii) y- momentum

$$\frac{\partial}{\partial t}(\rho U_y) + \nabla.(\rho \mathbf{U} U_y) = -\frac{\partial P}{\partial y} + \nabla.(\mu \nabla U_y) + S_{my} \qquad (3.8)$$

(iii) z-momentum

$$\frac{\partial}{\partial t}(\rho U_z) + \nabla.(\rho \mathbf{U} U_z) = -\frac{\partial P}{\partial z} + \nabla.(\mu \nabla U_z) + S_{mz} \qquad (3.9)$$

where $S_{mx} = \rho \mathbf{g}_x + \mathbf{F}_x$, $S_{my} = \rho \mathbf{g}_y + \mathbf{F}_y$, $S_{mz} = \rho \mathbf{g}_z + \mathbf{F}_z$

3.4.3 Energy Equation

The equation for internal energy is given by:

$$\frac{\partial}{\partial t}(\rho H) + \nabla.(\rho \mathbf{U} H) = -\nabla.(q) + \frac{Dp}{Dt} - (\tau : \nabla \mathbf{U}) - \nabla.\left(\sum_i H_i J_i\right) + S_i \qquad (3.10)$$

where H is the enthalpy:

$$H = \sum \varepsilon_i H_i \qquad (3.11)$$

$$H_i = \int_{Tref}^{T} C_{pi} dT \qquad (3.12)$$

3.4.4 Generic Transport Equation

The conservation equation for a general scalar ψ can be written (Ferziger and Peric, 1999) as:

$$\frac{\partial}{\partial t}(\rho\psi) + \nabla.(\rho\mathbf{U}\psi) = \nabla.(\rho\Lambda\nabla\psi) + S_{\psi} \qquad (3.13)$$

where Λ is diffusivity of scalar ψ and S_{ψ} is corresponding source term.

Table 3.1. Substitution variables for generic transport equation.

Scalar	ψ	Λ	S_{ψ}
Continuity equation	ε_i	D_i	S_i
x-momentum	U_x	μ/ρ	$\frac{\partial P}{\partial x} + S_{mx}$
y-momentum	U_y	μ/ρ	$\frac{\partial P}{\partial y} + S_{my}$
z-momentum	U_z	μ/ρ	$\frac{\partial P}{\partial z} + S_{mz}$
Energy equation	C_vT	$k/Cv\rho$	$-\nabla.(\mathbf{U}p) - \tau:\nabla\mathbf{U} - \left(\sum H_i\mathbf{J}_i\right) + S_i$

3.5   Numerical Methods

There are many numerical techniques that can be used to solve partial differential equations such as finite difference, finite element and finite volume. The numerical solution of these methods involves the discretization of the computational domain and approximation of unknown dependent variables to provide a set of algebraic equations (Ferziger and Peric, 1999). All methods yields the same solution if the grid (number of discrete locations used to represent the differential equations) is sufficiently fine (Ranade, 2002).

3.5.1   Finite Difference Method

Finite difference is the oldest numerical method for solving partial differential equations. The approximation for the first and second derivatives of dependent variables is obtained by using Taylor series expansions. The finite difference approximation at several grid points creates many linear algebraic equations. The finite difference method is restricted to simple geometries and structured grids, however most industrial reactors have complex geometrical constructions.

3.5.2   Finite Element Method

In the finite element method, the solution domain is divided into a number of discrete volumes or finite elements (generally unstructured grid). The feature of this method is that the equations are multiplied by a weight function before they are integrated over the entire domain. The advantage of using the finite element method is its capability to solve complex geometry problems. However, it is

difficult to develop solution methods for coupled and non-linear equations using the finite element.

3.5.3 Finite Volume Method

The finite volume method is used in most of the commercially available CFD codes. This method uses the integral form of the conservation equations in a control volume. The solution domain is divided into a number of finite volumes (computational cells). The differential equation is integrated over the volume of each computational cell in order to obtain the algebraic equations. Variable values are stored at the cell centres, and interpolation is applied to provide variable values at cell faces. Approximation of surface and volume integrals uses an appropriate quadrature formula. The finite volume method is suitable for any type of grid and also handles complex geometries. The numerical algorithm consists of the following steps (Versteeg and Malalasekera, 1995): (i) a formal integration of the governing equations of fluid flow over all the control volumes of the solution domain; (ii) discretisation technique involves some approximations in the integrated equation representing flow processes such as convection, diffusion and sources, it converts the integral equations into a system of algebraic equations; (iii) The set of algebraic equations is solved by an iterative method.

Consider a 3D-control volume in Figure 3.1, cell centre at P surrounded by six neighbouring control volumes with cell centres at *E* (east), *W* (west), *T* (top), *B* (bottom), *N* (north) and *S* (south). Six control faces are represented by *e*, *w*, *n*, *s, t and b*. Equation (3.13) is integrated over the control volumes in the computational domain. This equation can be written as:

$$\int\limits_{\Delta V_P} \frac{\partial}{\partial t}(\rho\psi)dV + \int\limits_{\Delta V_P} \nabla.(\rho\psi\mathbf{U})dV = \int\limits_{\Delta V_P} \nabla.(\Lambda\rho\nabla\psi)dV + \int\limits_{\Delta V_P} S_\psi dV \qquad (3.14)$$

For steady state condition and using Gauss's divergence theorem (for a vector **b**):

$$\int\limits_{\Delta V_P} \nabla.\mathbf{b}dV = \int\limits_A \hat{\mathbf{n}}.\mathbf{b}dA \qquad (3.15)$$

Equation (3.14) becomes:

$$\int\limits_A \hat{\mathbf{n}}.(\rho\psi\mathbf{U})dA = \int\limits_A \hat{\mathbf{n}}.(\Lambda\rho\nabla\psi)dA + \int\limits_{\Delta V_P} S_\psi dV \qquad (3.16)$$

Figure 3.1. Control volumes and the notation used for a Cartesian grid for three-dimensional flow.

Integration of the first term on the left and right side over all the faces of the control volumes, for 3D constant density system of Equation (3.16), gives:

$$\left[A_e U_{xe}\psi_e - A_w U_{xw}\psi_w\right] + \left[A_n U_{yn}\psi_n - A_s U_{ys}\psi_s\right] + \left[A_t U_{zt}\psi_t - A_b U_{zb}\psi_b\right]$$

$$= \left\{A_e \Lambda_e \left(\frac{\partial \psi}{\partial x}\right)_e - A_w \Lambda_w \left(\frac{\partial \psi}{\partial x}\right)_w\right\} + \left\{A_n \Lambda_n \left(\frac{\partial \psi}{\partial x}\right)_n - A_s \Lambda_s \left(\frac{\partial \psi}{\partial x}\right)_s\right\} \quad (3.17)$$

$$+ \left\{A_t \Lambda_t \left(\frac{\partial \psi}{\partial x}\right)_t - A_b \Lambda_b \left(\frac{\partial \psi}{\partial x}\right)_b\right\} + \frac{S_\psi \Delta V_P}{\rho}$$

where A_j is surface area of jth face of control volume. Approximation of the finite difference type is substituted into equation (3.17) so it replaces the diffusive fluxes, where:

$$\left\{A_e \Lambda_e \left(\frac{\partial \psi}{\partial x}\right)_e - A_w \Lambda_w \left(\frac{\partial \psi}{\partial x}\right)_w\right\} = \left\{A_e \Lambda_e \left(\frac{\psi_E - \psi_P}{\delta x_{PE}}\right) - A_w \Lambda_w \left(\frac{\psi_P - \psi_W}{\delta x_{WP}}\right)\right\}$$

$$(3.18)$$

$$\left\{A_n \Lambda_n \left(\frac{\partial \psi}{\partial x}\right)_n - A_s \Lambda_s \left(\frac{\partial \psi}{\partial x}\right)_s\right\} = \left\{A_n \Lambda_n \left(\frac{\psi_N - \psi_P}{\delta x_{PN}}\right) - A_s \Lambda_s \left(\frac{\psi_P - \psi_S}{\delta x_{SP}}\right)\right\}$$

$$(3.19)$$

$$\left\{A_t \Lambda_t \left(\frac{\partial \psi}{\partial x}\right)_t - A_b \Lambda_b \left(\frac{\partial \psi}{\partial x}\right)_b\right\} = \left\{A_t \Lambda_t \left(\frac{\psi_T - \psi_P}{\delta x_{PT}}\right) - A_b \Lambda_b \left(\frac{\psi_P - \psi_B}{\delta x_{BP}}\right)\right\}$$

$$(3.20)$$

Substituting Equations (3.18), (3.19) and (3.20) into Equation (3.17) gives:

$$\left[F_e \psi_e - F_w \psi_w\right] + \left[F_n \psi_n - F_s \psi_s\right] + \left[F_t \psi_t - F_b \psi_b\right] = \left\{D_e\left(\psi_E - \psi_P\right) - D_w\left(\psi_P - \psi_W\right)\right\}$$

$$+ \left\{D_n\left(\psi_N - \psi_P\right) - D_s\left(\psi_P - \psi_S\right)\right\} + \left\{D_t\left(\psi_T - \psi_P\right) - D_b\left(\psi_P - \psi_B\right)\right\} + {S_\psi \Delta V_P}\Big/{\rho}$$

$$(3.21)$$

where:

$$F_e = A_e U_{xe} \tag{3.22}$$

$$F_w = A_w U_{xw} \tag{3.23}$$

$$F_n = A_n U_{yn} \tag{3.24}$$

$$F_s = A_s U_{ys} \tag{3.25}$$

$$F_t = A_t U_{zt} \tag{3.26}$$

$$F_b = A_b U_{zb} \tag{3.27}$$

$$D_e = \frac{A_e \Lambda_e}{\delta x_{PE}} \tag{3.28}$$

$$D_w = \frac{A_w \Lambda_w}{\delta x_{WP}} \tag{3.29}$$

$$D_n = \frac{A_n \Lambda_n}{\delta x_{PN}} \tag{3.30}$$

$$D_s = \frac{A_s \Lambda_s}{\delta x_{SP}} \tag{3.31}$$

$$D_t = \frac{A_t \Lambda_t}{\delta x_{PT}} \tag{3.32}$$

$$D_b = \frac{A_b \Lambda_b}{\delta x_{BP}} \tag{3.33}$$

The face value of variables (ψ_e, ψ_w, ψ_n, ψ_s, ψ_t, and ψ_b) in Equation (3.21) should be written in terms of nodal value of variables (ψ_E, ψ_W, ψ_N, ψ_S, ψ_T, and ψ_B). There are many schemes to solve this task, such as a central differencing scheme (CDS), upwind scheme, quadratic upstream interpolation for convective kinetics (QUICK), and hybrid differencing scheme. The algorithms of this scheme have been discussed in several books (Versteeg and Malalasekera, 1995, Ferziger and

Peric, 1999). The disadvantage of using a central differencing scheme is its inability to identify flow direction. In the upwind scheme that we have used, its upstream cell centre replaces the face value of a variable. When the flow is in a positive direction (U_{xe}, U_{xw}, U_{yn}, U_{ys}, U_{zt} and U_{zb} are positive), then:

$$\Psi_e = \Psi_P;\ \Psi_w = \Psi_W;\ \Psi_n = \Psi_P;\ \Psi_s = \Psi_S;\ \Psi_t = \Psi_P;\ \Psi_b = \Psi_B \qquad (3.34)$$

If the flow is negative direction, the upwind scheme sets:

$$\Psi_e = \Psi_E;\ \Psi_w = \Psi_P;\ \Psi_n = \Psi_N;\ \Psi_s = \Psi_P;\ \Psi_t = \Psi_T;\ \Psi_b = \Psi_P \qquad (3.35)$$

Substitution of Equations (3.34) and (3.35) into Equation (3.21) produces:

$$a_P \psi_P = a_W \psi_W + a_E \psi_E + a_N \psi_N + a_S \psi_S + a_T \psi_T + a_B \psi_B + S_\psi \Delta V_P / \rho \qquad (3.36)$$

where,

$$a_W = D_W + \max(F_w, 0) \qquad (3.37)$$

$$a_E = D_E + \max(0, -F_e) \qquad (3.38)$$

$$a_S = D_S + \max(F_s, 0) \qquad (3.39)$$

$$a_N = D_N + \max(0, -F_n) \qquad (3.40)$$

$$a_B = D_B + \max(F_b, 0) \qquad (3.41)$$

$$a_T = D_T + \max(0, -F_w) \qquad (3.42)$$

$A_e = A_w = \Delta x_P$; $A_n = A_s = \Delta y_P$; $A_t = A_b = \Delta z_P$ and $\Delta V_P = = \Delta x_P \Delta y_P \Delta z_P$.

Equation (3.36) is implemented for the nodes of the computational domain in order to obtain a set of algebraic equations that can be solved by an iterative method with appropriate boundary conditions.

3.6   Solution Algorithms for Pressure-Velocity Coupling

Two algorithms are used widely for the solution of PDE's, the pressure-based method and the density-based method. The density-based method is restricted to single phase flow simulators. Many multiphase simulations of multiphase in risers have used the pressure-based solution methods . Therefore in this work, we use the pressure-based solution methods for multiphase flow. In the pressure-based methods, pressure and velocity are solved iteratively for each time step in a sequential manner. The basic steps, especially for unsteady-state conditions are taken as:

a. Both the pressure and velocity fields are assumed

b. The correction of velocity field is obtained using the assumed values in the momentum equation

c. The continuity equation is used to obtain the correction for the pressure field

d. The corrections for other scalar quantities such as concentration, temperature, etc., are obtained by solving the species balance and energy conservation equations

e. The above steps (b)-(d) are repeated for each time step until the corrections are within acceptable limits.

The corrections are iteratively brought down to zero for convergence. An example of pressure-based methods is the SIMPLE method of Patankar and Spalding (Versteeg and Malalasekera, 1995). A difficulty with pressure-based methods is the discretisation of the pressure field, so these methods often use heavy under relaxation for pressure correction.

The velocity component appears in each momentum equation and in the continuity equation. Meanwhile the pressure appears in the momentum equations but there is no equation for pressure. If the flow is incompressible, the density is constant so the pressure may not be obtained from P = P (ρ, T). Therefore, coupling between pressure and velocity should produce the solution of the flow field. If the correct pressure flow field is applied in the momentum equations the resulting velocity field should satisfy the continuity(Versteeg and Malalasekera, 1995). The non-linearity problems in the equation set and the pressure-velocity relationship can be determined by an iterative solution strategy such the SIMPLE algorithm of Patankar and Spalding (1972). Pressure, velocity, scalar quantities and a vector are stored in the grid. If the velocity and pressure are stored at the same set of grid nodes (colocated), we have obtained a 'check-board' pressure field (Versteeg and Malalasekera, 1995). A staggered grid, which uses a different location of nodes for storing velocity and pressure, can overcome a 'check-board' pressure field problem. In a staggered grid, the velocities are centred at the cell faces and indicated by arrows. The scalar variables (pressure, temperature, density) are stored at nodes marked (•). The staggered gird arrangement for a two-dimensional flow is shown in Figure 3.2. In a three-dimensional flow the *u*-velocities are stored at scalar faces *e* and *w*, the *v*-velocities are stored at scalar faces *n* and *s*, and the *w*-velocities are stored at scalar faces *t* and *b*. In Figure 3.2 the dashed lines constructing the scalar cell faces (pressure field) are numbered by lower case letters *I* and *J*. The unbroken grid lines have been numbered using capital *i* and *j*. Therefore a point P is identified by (I*, j*).
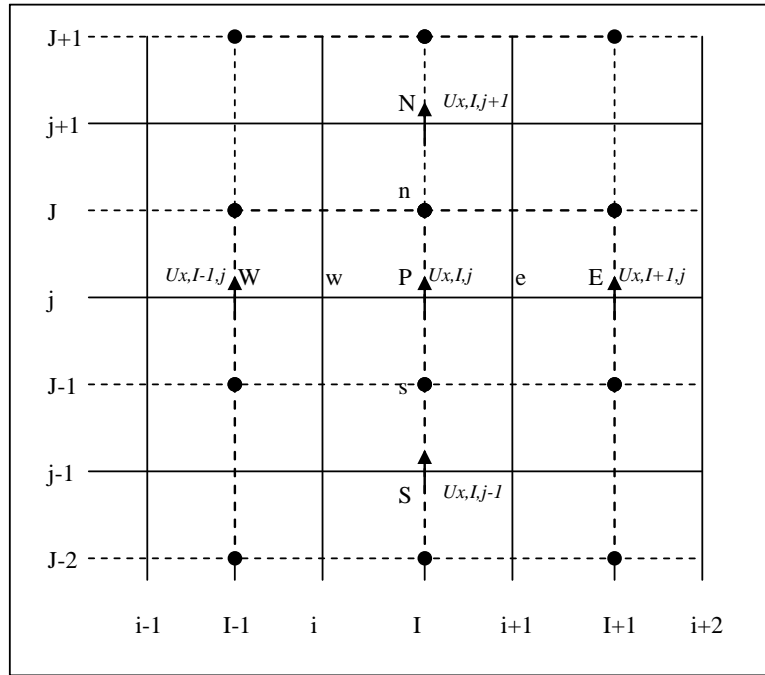
Figure 3.2. A *v*-control volume and its neighbouring velocity component for a two-dimensional flow.

For simplification, we consider the one-dimensional pipe flow in order to illustrate the staggered grid, in Figure 3.3. The x-momentum is to be neglected. Using generic transport equation (equations (3.16) and (3.36)) and substitution from Table 3.1 ($\psi=U_y$, $\Lambda=\mu/\rho$ and $S_\psi = \dfrac{\partial P}{\partial y} + S_{my}$), the discretized y-momentum equation can be obtained:

$$a_P U_{yP} = a_W U_{yW} + a_E U_{yE} + a_N U_{yN} + a_S U_{yS} - \int_{\Delta V_P} \frac{\partial p}{\partial y} dV + S_{my} \Delta V_P / \rho \qquad (3.43)$$

Equation (3.43) can be written as:

$$a_{I,j}U_{y,I,j} = a_{I-1,j}U_{y,I-1,j} + a_{I+1,j}U_{y,I+1,j} + a_{I,j+1}U_{y,I,j+1} + a_{I,j-1}U_{y,I,j-1} +$$
$$+ \left(P_{I,J-1} - P_{I,J}\right)A_{I,j} + S_{my}\Delta V_P / \rho \tag{3.44}$$
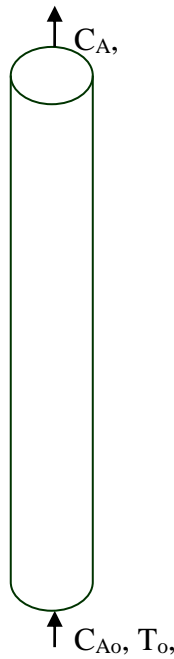
Figure 3.3. Schematic of a pipe flow reactor.

$$F_e = \frac{F_{i+1,J} + F_{i+1,J-1}}{2} = \frac{A_{i+1,J}U_{x,i+1,J} + A_{i+1,J-1}U_{x,i+1,J-1}}{2} \tag{3.45}$$

$$F_w = \frac{F_{i,J} + F_{i,J-1}}{2} = \frac{A_{i,J}U_{x,i,J} + A_{i,J-1}U_{x,i,J-1}}{2} \tag{3.46}$$

$$F_n = \frac{F_{I,j} + F_{I,j+1}}{2} = \frac{A_{I,j}U_{y,I,j} + A_{I,j+1}U_{y,I,j+1}}{2} \tag{3.47}$$

$$F_s = \frac{F_{I,j-1} + F_{I,j}}{2} = \frac{A_{I,j-1}U_{y,I,j-1} + A_{I,j}U_{y,I,j}}{2} \tag{3.48}$$

$$D_e = \frac{A_{I-1,J-1}\Lambda_{I-1,J-1} + A_{I,J-1}\Lambda_{I,J-1} + A_{I-1,J}\Lambda_{I-1,J} + A_{I,J}\Lambda_{I,J}}{4(x_i - x_{i-1})} \tag{3.49}$$

$$D_w = \frac{A_{I,J-1}\Lambda_{I,J-1} + A_{I+1,J-1}\Lambda_{I+1,J-1} + A_{I,J}\Lambda_{I,J} + A_{I+1,J}\Lambda_{I+1,J}}{4(x_i - x_{i-1})} \tag{3.50}$$

$$D_s = \frac{A_{I,J-1}\Lambda_{I,J-1}}{y_j - y_{j-1}} \tag{3.51}$$

$$D_n = \frac{A_{I,J}\Lambda_{I,J}}{y_{j+1} - y_j} \tag{3.52}$$

The discrete equation of temperature is also obtained by integration of the generic transport Equations (3.16) and (3.24), where $\psi = C_v T$ and $\Lambda = k/C_v\rho$. The source term for the energy equation is:

$$S_\psi = S_H = -\nabla.(\mathbf{U}p) - \tau : \nabla\mathbf{U} - \nabla.\left(\sum H_k\mathbf{J_k}\right) + S_h \tag{3.53}$$

$$a_P T_p = a_W T_W + a_E T_E + a_N T_N + a_S T_S + a_T T_T + a_B T_B + S_h\Delta V_P / C_v\rho \tag{3.54}$$

The discretization of the momentum equations (Equation 3.44) produces additional unknown variables (pressure node). Therefore, a scheme is required to calculate the pressure field. The SIMPLE (Semi-Implicit Method for Pressure-Linked Equations) algorithm is a method for calculating pressure and velocities.

The sequence of operations in a CFD procedure which employs the SIMPLE algorithm is given by Figure 3.4 (Versteeg and Malalasekera, 1995). The SIMPLE algorithm has been successfully implemented in numerous CFD procedures especially for steady-state conditions. There are many types of SIMPLE algorithms, such as SIMPLER (SIMPLE Revised), SIMPLEC (SIMPLE consistent) and PISO (Pressure Implicit with Splitting of Operators) (Ranade, 2002). The PISO algorithm is a non-iterative transient calculation procedure. Therefore, it requires less computation than the implicit SIMPLE algorithm. In the transient algorithm, all time-dependent terms are retained in the momentum and continuity equations. The PISO method has produced accurate results with small time steps. The algorithm of PISO is shown by Figure 3.5.

START

Initial guess p^*, u^*, v^*, ϕ^*

STEP 1: Solve discretised momentum equations

$$a_{i,J}u^*{}_{i,J} = \sum a_{nb}u^*{}_{nb} + (p^*{}_{I-1,J} - p^*{}_{I,J})A_{i,J} + b_{i,J}$$

$$a_{I,J}v^*{}_{I,J} = \sum a_{nb}v^*{}_{nb} + (p^*{}_{I,J-1} - p^*{}_{I,J})A_{I,J} + b_{I,J}$$

u^*, v^*

STEP 2: Solve pressure correction equation

$$a_{I,J}p'{}_{I,J} = a_{I-1,J}p'{}_{I-1,J} + a_{I+1,J}p'{}_{I+1,J} + a_{I,J-1}p'{}_{I,j-1} + a_{I,J+1}p'{}_{I,J+1} + b'{}_{I,J}$$

p'

STEP 3: Correct pressure and velocities

$$p_{I,J} = p^*{}_{I,J} + p'{}_{I,J}$$

$$u_{i,J} = u^*{}_{i,J} + d_{i,J}(p'{}_{I-1,J} - p'{}_{I,J})$$

$$v_{I,j} = v^*{}_{I,j} + d_{I,j}(p'{}_{I,J-1} - p'{}_{I,J})$$

Set
$p^*=p$, $u^*=u$
$v^*=v$, $\phi^*=\phi$

p, u, v, ϕ^*

STEP 4: Solve all other discretised transport equations

$$a_{I,J}\phi_{I,J} = a_{I-1,J}\phi_{I-1,J} + a_{I+1,J}\phi_{I+1,J} + a_{I,J-1}\phi_{I,J-1} + a_{I,J+1}\phi_{I,J+1} + b\phi_{I,J}$$

ϕ

No

Convergence?

Yes

STOP

Figure 3.4. The SIMPLE algorithm.

$$\text{START}$$

Initial guess p^*, u^*, v^*, ϕ^*

Perform STEPS 1-3 of SIMPLE algorithm
- Solve discretised momentum equations
- Solve pressure correction equation
- Correct pressure and velocities

p^*, u^*, v^*, ϕ^*

STEP 4: Solve second pressure correction equation
$$a_{I,J}P^{'}_{I,J} = a_{I-1,J}P^{''}_{I-1,J} + a_{I+1,J}P^{''}_{I+1,J} + a_{I,J-1}P^{''}_{I,J-1} + a_{I,J+1}P^{''}_{I,J+1} + b^{''}_{I,J}$$

STEP 5: Correct pressure and velocities
$$P^{***}_{I,J} = P^{*}_{I,J} + P^{'}_{I,J}$$

$$u^{***}_{i,J} = u^{*}_{i,J} + d_{i,J}\left(p^{'}_{I-1,J} - p^{'}_{I,J}\right) + \frac{\sum a_{nb}\left(u^{**}_{nb} - u^{*}_{nb}\right)}{a_{i,J}} + d_{i,J}\left(p^{''}_{I-1,J} - p^{''}_{I,J}\right)$$

$$v^{***}_{I,j} = v^{*}_{I,j} + d_{..}\left(p^{'}_{...} - p^{'}_{..}\right) + \frac{\sum a_{nb}\left(v^{**}_{nb} - v^{*}_{nb}\right)}{} + d_{..}\left(p^{''}_{I,J-1} - p^{''}_{I,J}\right)$$

Set
$$p = p^{***}$$
$$u = u^{***}$$
$$v = v^{***}$$

Set
$p^*=p, u^*=u$
$v^*=v, \phi^*=\phi$

p^*, u^*, v^*, ϕ^*

STEP 6: Solve all other discretised transport equations
$$a_{I,J}\phi_{I,J} = a_{I-1,J}\phi_{I-1,J} + a_{I+1J}\phi_{I+1,J} + a_{I,J-1}\phi_{I,J-1} + a_{I,J+1}\phi_{I,J+1} + b\phi_{I,J}$$

ϕ

No ← Convergence?
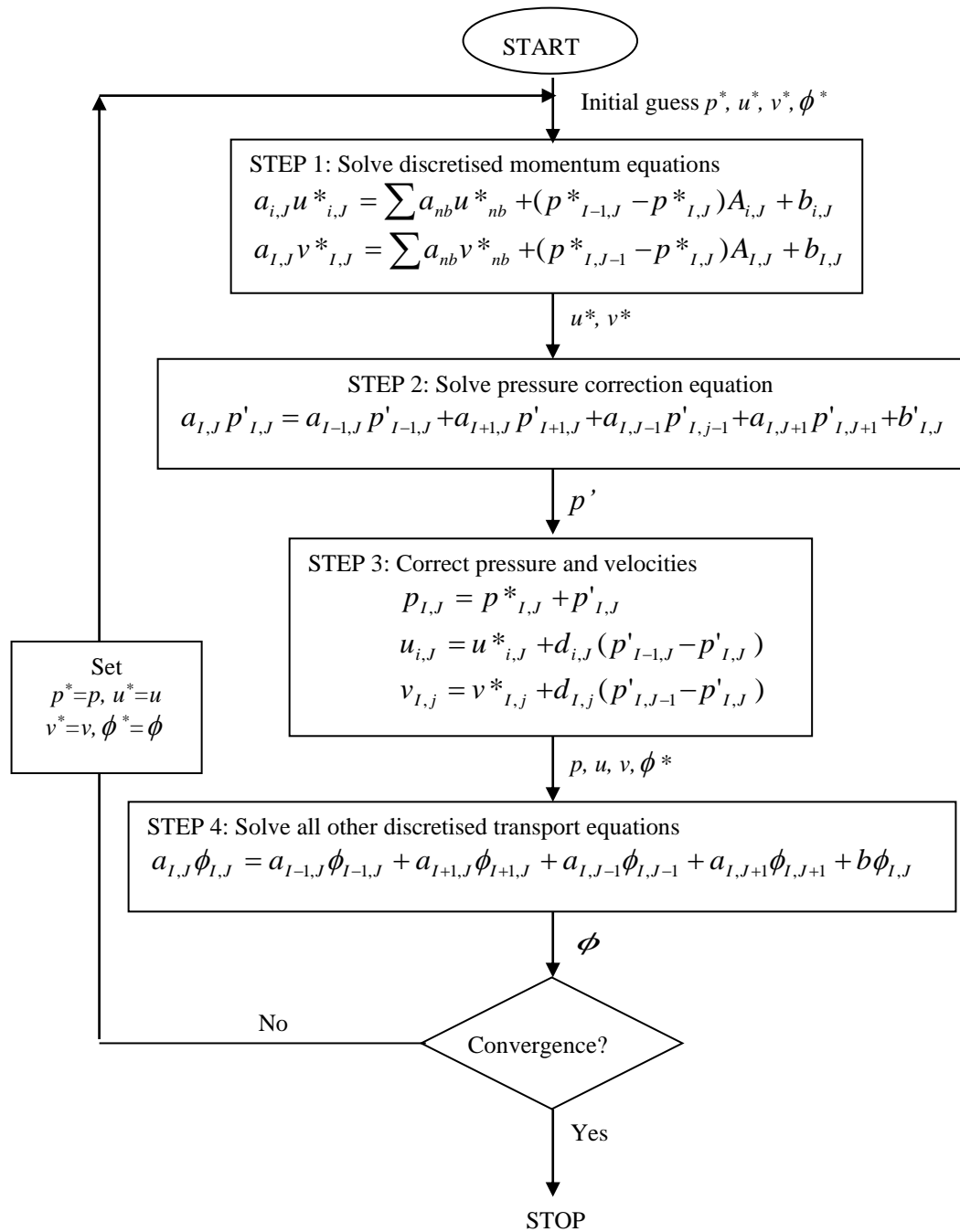
Yes

STOP

Figure 3.5. The PISO algorithm.

3.7   Turbulence Model

A fluid flow is described as turbulent if it is irregular, random, chaotic, rotational, intermittent, highly disorder, diffusive and dissipative (Ranade, 2002, Versteeg and Malalasekera, 1995). The turbulent motion is inherently unsteady and three-dimensional. The rate of scalar mixing in turbulent flow is greater than in laminar flows. The rates of heat and mass transfer are also significantly higher in turbulent flows. Turbulence is the most complicated type of fluid motion. Although it is difficult to model the turbulence phenomena accurately, turbulence is often used to improve the performance of chemical reactors in order to make the desired operation realizable and more efficient. Therefore, it is crucial to develop appropriate methods to predict and control turbulent flow processes.

The modelling approaches in turbulent flow can be classified into three categories: direct numerical simulation (DNS), large eddy simulations (LES), and Reynolds-averaged Navier-Stokes equations (RANS). DNS simulates directly all the dynamical scales of turbulent flows. In DNS, all the motions in the flow are resolved. It is based on the hypothesis that direct simulations are carried out by decreasing the Reynolds number to the point where important scales can be simulated accurately by computer. DNS models are widely used as learning models. The application of DNS needs large computer resources. Therefore, if the accuracy of the input data to the model is limited, then it is better to use other alternative approaches. LES is based on the hypothesis that the relevant scales in turbulent flows can be separated into large-scale and small-scale components. In LES, large-scale motions are resolved rigorously and small-scale motions are modelled using the sub grid scale (SGS) models. LES models are less costly than DNS. However, the LES model is still computationally intensive especially for steady-state conditions. In RANS, it is not necessary to resolve all the small-scale

phenomena because the variation of time-averaged quantities occurs at much larger scales. This approach requires more significant computing resources than the LES or DNS approaches. However, the RANS model is not resolving the small-scale phenomena that cause the closure problem. Recently, much research into simulations of turbulent flows has used the RANS-based turbulence models.

Generally, the FCC riser reactor is under turbulent flow conditions. Therefore it is important to use an appropriate turbulence model to describe the effect of turbulent fluctuations of velocities and scalar variables for the basic conservation equations. A $k\text{-}\in$ model was used to describe the turbulent motions in both phases. The two-equation $k\text{-}\in$ model of turbulence is most widely used in RANS-based models due to its computational efficiency, robustness and reasonable accuracy. It has been extensively studied and is recommended as a baseline model for typical internal flows encountered by reactor designers. In the $k\text{-}\varepsilon$ model, turbulent viscosity is related to k and $\in$ by:

$$\mu_{t,i}{}^{(t)} = \rho_i \varepsilon_i C\mu \frac{k_i{}^2}{\in_i} \tag{3.55}$$

where C_μ is empirical coefficient. The turbulence kinetic energy, k, and its rate of dissipation, $\in$, can be calculated from the following transport equations (Launder and Spalding, 1972):

$$\frac{\partial}{\partial t}\left(\rho_i \varepsilon_i k_i\right) + \nabla.(\rho_i \varepsilon_i k_i U_i) = \nabla.\left(\varepsilon_i \frac{\mu_t}{\sigma_k}\nabla k_i\right) + \left(\varepsilon_i G_k - \varepsilon_i \rho_i \in_i\right) \tag{3.56}$$

$$\frac{\partial}{\partial t}\left(\varepsilon_i \rho_i \in_i\right) + \nabla.\left(\rho_i \varepsilon_i \in_i U_i\right) = \nabla.\left(\varepsilon_i \frac{\mu_t}{\sigma_k}\nabla \in_i\right) + \frac{\in_i}{k}\left(C_{1\in}\varepsilon_i G_k - C_{2\in}\varepsilon_i \rho_i \in_i\right) \tag{3.57}$$

where G_k is the turbulence generation term, which is expressed by:

$$G_k = \tfrac{1}{2} \mu_T \left[\nabla \overline{U} + \left(\nabla \overline{U} \right)^T \right]^2 \tag{3.58}$$

The model constants C_1, C_2, $C\mu$, σ_k, σ_ε have values as following:

 $C_{1e} = 1.44$, $C_{2e} = 1.92$, $C\mu = 0.09$, $\sigma_k = 1.0$, $\sigma_\varepsilon = 1.3$

The assumptions have been used in the k-$\in$ model (Ranade, 2002) are:

- Turbulence is nearly homogeneous;

- The spectral distributions of turbulent quantities are similar;

- Diffusion is of the gradient type with constant effective Prandtl numbers;

- High Reynolds numbers.

The RNG (renormalization group) of the k and $\in$ model has been extended to use a differential form of the equation in order to calculate the effective viscosity from k and $\in$ (Fluent, 2005) by:

$$v_{eff} = v \left(1 + \sqrt{\frac{C_\mu}{v} \frac{k}{\sqrt{\in}}} \right)^2 \tag{3.59}$$

Turbulence flows are significantly influenced by the presence of wall. The mean velocity field is affected by the no-slip condition that has to be satisfied at the wall. However, the turbulence is also changed by the presence of the wall in non-trivial ways. Very close to wall, viscous damping reduces the tangential velocity fluctuations, while kinematic blocking reduces the normal fluctuations (Fluent, 2005).

Numerous experiments have shown that the near-wall region can be largely subdivided into three layers. In the innermost layer, called the "viscous sub-layer", the flow is almost laminar, and the (molecular velocity plays a dominant role in momentum and heat or mass transfer. In the outer layer, called the fully-turbulent layer, turbulence plays a major role. There is an interim regime between the viscous sub-layer and the fully-turbulent layer where the effects of molecular viscosity and turbulence are equally important. (Fluent, 2005). Figure 3.6 describes these subdivisions of the near-wall region, plotted in semi-log coordinate.

There are two approaches to model the near-wall region. Firstly, if the viscosity-affected inner region (viscous sub-layer and buffer layer) is not resolved, semi-empirical formulas called "wall function" are used to bridge the viscosity-affected region between the wall and the fully-turbulent zone. In the other approach, the turbulence models are modified to enable the viscosity-affected region to be resolved with a mesh all the way to the wall, including the viscous sub-layer (Fluent, 2005). These two approaches are shown schematically in Figure 3.7.
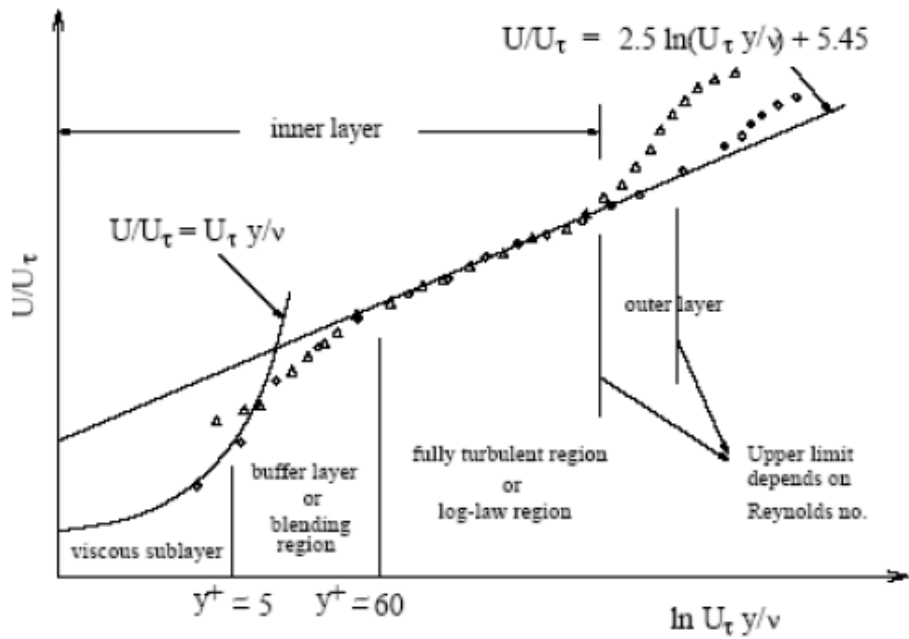
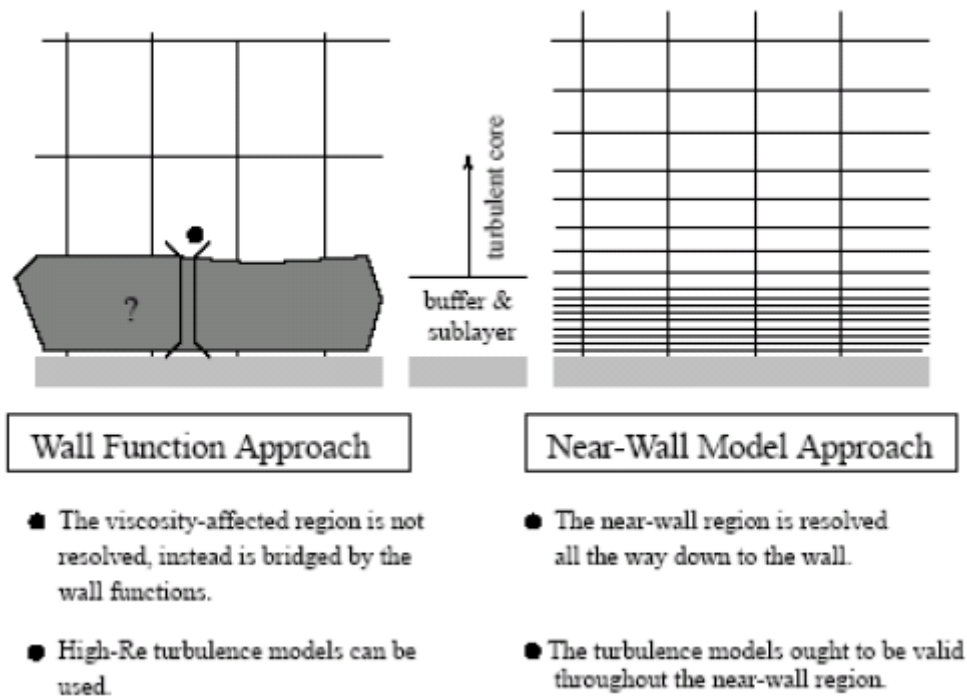**Figure 3.6. Subdivisions of the Near-Wall Region (Fluent, 2005) .**

Figure 3.7. Near-wall treatments in FLUENT (Fluent, 2005).

3.8   Multiphase Flow Model

Multiphase flow processes are key elements of several important reactor technologies such as fluid catalytic cracking reactors. Multiphase flow processes can be classified by different flow regimes depending upon the operating conditions and the geometry of the process equipment. Modelling multiphase flow processes is complex. There are two approaches for the numerical calculation of multiphase flows: the Eulerian-Langrangian approach and the Eulerian-Eulerian approach. In the Eulerian-Langrangian approach, the fluid phase is treated as a continuum by solving the time-averaged Navier-Stokes equations; tracking a large number of particles, bubbles, or droplets through the calculated flow field solves the dispersed phase. This model is appropriate for modelling spray dryers, coal and liquid-fuel combustion, cyclones, electrostatic precipitators, but is inappropriate for the modelling of fluidized beds or any application where the volume fraction of the second phase is not negligible (Fluent, 2005). In the Eulerian-Eulerian approach, the different phases are treated mathematically as interpenetrating continua. The concept of phasic volume fraction is introduced, because the volume of a phase cannot be occupied by the other phases. These volume fractions are assumed to be continuous functions of space and time and their sum is equal to one. The Eulerian-Eulerian approach is more suitable for modelling dispersed multiphase systems with a significant volume fraction of dispersed phase (>10%).

In the Fluent CFD package, there are three different Eulerian-Eulerian multiphase models: the volume of fluid (VOF) model, the mixture model, and the Eulerian model. In the VOF model, the motion of all phases is modelled by formulating local, instantaneous conservation equations for mass, momentum and energy. In

this approach, a single set of momentum equations are shared by the fluids and the volume fraction of each the fluids in each computational cell is tracked throughout the domain. However this approach is limited to modelling the motion of only a few dispersed phase particles. It is not suitable for simulations of dispersed multiphase flows in large equipment. It is also requires significant computational resources. The mixture model solves the mixture momentum equation, and prescribes relative velocities in order to describe the dispersed phases. This model is suitable for applications of sedimentation and cyclone separators. The Eulerian model is the most complex of multiphase models in Fluent. It solves a set of 'n' momentum and continuity equations for each phase. How this coupling is achieved through the pressure and interphase exchange coefficients. This coupling is handled depends on the type of phases involved, i.e. granular (fluid-solid) flows and non- granular (fluid-fluid) flow. For granular flows, the properties are obtained from application of the kinetic theory. Applications of the Eulerian multiphase model include risers, fluidized beds and bubble columns.

A granular Eulerian-Eulerian approach was used to simulate the hydrodynamics of the multi phases. In Fluent 6.2 CFD code, the conservation equations were discretized by finite volume method. The Eulerian-Eulerian approach is used to solve the equations.

Conservation Equations

The continuity equation of phase i (i = gas, solid):

$$\frac{\partial}{\partial t}\left(\rho_i \varepsilon_i\right) + \nabla.\left(\rho_i \varepsilon_i \mathbf{U}_i\right) = 0 \tag{1}$$

With definition: $\varepsilon_g + \varepsilon_s = 1$

Based on Newton's law, the change momentum is the sum of the net force on a domain. The important forces in multiphase flow model are:

- Static pressure gradient
- Solid pressure gradient
- Viscous force
- Body force
- Interphase force (drag)

Therefore, the conservation of momentum of phase i (i = gas, solid, k≠i) can be written as:

$$\frac{\partial}{\partial t}\left(\rho_i \varepsilon_i \mathbf{U}_i\right) + \nabla.\left(\rho_i \varepsilon_i \mathbf{U}_i \mathbf{U}_i\right) = -\varepsilon_i \nabla P + \nabla.\boldsymbol{\tau}_i + \rho_i \varepsilon_i \mathbf{g} - \beta(\mathbf{U}_i - \mathbf{U}_k)$$

(2)

The conservation of energy for phase i yield:

$$\frac{\partial}{\partial t}\left(\varepsilon_i \rho_i H_i\right) + \nabla.\left(\varepsilon_i \rho_i \mathbf{U}_i H_i\right) = -\varepsilon_i \frac{\partial P_i}{\partial t} + \boldsymbol{\tau}_i : \nabla \mathbf{U}_i - \nabla.\mathbf{q}_i + S_i$$

(3)

Interphase Exchange Coefficients

For Eulerian-Eulerian multiphase flow model, momentum exchange between the phases is based on the value of the fluid-solid exchange coefficients (β).

$$\beta = \frac{3}{4} C_D \frac{\rho_g}{d_s} \frac{1}{v_{r,s}^2} \left| \mathbf{U}_s - \mathbf{U}_g \right|$$

(3.60)

The drag coefficient for Syamlal-O'Brian model, C_D is given by:

$$C_D = \left(0.63 + \frac{4.8}{\sqrt{\mathrm{Re}_s / v_{r,s}}} \right)^2$$

(3.61)

where:

$$\text{Re}_s = \frac{\rho_g d_s |\mathbf{U}_s - \mathbf{U}_g|}{\mu_g} \tag{3.62}$$

$v_{r,s}$ is the terminal velocity correlation for the solid phase:

$$v_{r,s} = 0.5\left(A - 0.06\,\text{Re}_s + \sqrt{(0.06\,\text{Re}_s)^2 + 0.12\,\text{Re}_s(2B - A) + A^2} \right) \tag{3.63}$$

$$A = \varepsilon_g^{4.14} \tag{3.64}$$

$$B = 0.8\varepsilon_g^{1.28} \text{ for } \varepsilon_g \le 0.85 \text{ and } B = \varepsilon_g^{2.65} \text{ for } \varepsilon_g > 0.85 \tag{3.65}$$

Pressure of Solids

The solids phase pressure (P_s), which consists of both kinetic and collisional pressure, is obtained from an equation of state similar to the van der Waals equation of state for gases (Chapman and Cowling, 1970):

$$P_s = \left(1 + 2(1 + e_s)\varepsilon_s g_o\right)\varepsilon_s \rho_s \Theta_s \tag{3.66}$$

$$= \rho_s \varepsilon_s \Theta + 2 g_o \rho_s \varepsilon_s^2 \Theta(1 + e) \tag{3.67}$$

The first part of the solids pressure represents the kinetic contribution, and the second part represents the collisional contribution. The kinetic part of the stress tensor physically represents the momentum transferred through the system by particles moving across imaginary shear layers in the flow; the collisional part of the stress tensor denotes the momentum transferred by direct collisions . Θ_s is the granular temperature related to the kinetic turbulent energy of particle motion. e_s is the coefficient of restitution for particle collisions, which is $0 \le e_s < 1$ for inelastic collision. g_o is the radial distribution function (Sinclair and Jackson, 1989), which is equal to one if the particles are loosely packed and become infinite if they are so closely packed:

$$g_o = \left[1 - \left(\frac{\varepsilon_s}{\varepsilon_{s,max}} \right)^{\frac{1}{3}} \right]^{-1}$$ (3.68)

The maximum solid packing, $\varepsilon_{s,max}$, which is used in the simulation, is 0.6. Because this averaged value is assumed to be valid for various kinds of particles.

Solids Shear Stress

The solid phase bulk viscosity accounts for the resistance of the granular temperature to compression and expansion is given by:

$$\mu_b = \frac{4}{3} \varepsilon_s \rho_s d_s g_o (1 + e_s) \left(\frac{\Theta_s}{\pi} \right)^{\frac{1}{2}}$$ (3.69)

The solids phase shear viscosity for dense and dilute flow can be written as:

$$\mu_s = \frac{2\mu_{s,dil}}{(1+e)g_o} \left[1 + \frac{4}{5}(1+e_s)g_o\varepsilon_s \right]^2 + \frac{4}{5}\varepsilon_s \rho_s d_s g_o (1+e_s) \left(\frac{\Theta_s}{\pi} \right)^{\frac{1}{2}}$$ (3.70)

Solid phase dilute viscosity:

$$\mu_{s,dil} = \frac{5}{16} \rho_s \varepsilon_s l_s \sqrt{2\pi\Theta_s}$$ (3.71)

With $l_s = \frac{\sqrt{2}}{12} \frac{d_s}{\varepsilon_s}$ (3.72)

Granular Temperature

Concepts gas kinetic theory (Chapman and Cowling, 1970) can be used to describe the effective stress in the solid phase resulting from kinetic and collisional contributions when the motion of particle is dominated by collisional interactions . Lun et al. (1984) have presented the constitutive relations of the solid phase stress based on kinetic theory concepts for inelastic particle-particle collision.

Analogues to the thermodynamic temperature for gases, the granular temperature can be introduced as a measure of the particle velocity fluctuation.

$$\Theta_s = \left(\Theta_s = \frac{1}{3} \langle U_s \rangle \right) \tag{3.73}$$

Because the solid phase stress depends on the magnitude of these particle-velocity fluctuations, a balance of the granular energy (3/2 Θ) associated with these particle fluctuation is needed to supplement the continuity and momentum balance for both phases.

$$\frac{3}{2} \frac{\partial}{\partial t} \left(\rho_s \varepsilon_s \Theta_s \right) + \nabla . \left(\rho_s \varepsilon_s \mathbf{U}_s \Theta_s \right) = T_s : \nabla \mathbf{U}_s + \nabla . \left(k_s \nabla \Theta_s \right) - \gamma_s \tag{3.74}$$

The net change of fluctuation energy (left hand side) is equal to the sum of fluctuating energy (right hand side). The first term on the right side represents the creation of fluctuating energy due to shear in the particle phase. The second term represents the diffusion of fluctuating energy in the solid. γ_s represents the dissipation of fluctuating energy due to inelastic particle and collisions.

The diffusion coefficient for granular energy, k_s is expressed as:

$$k_s = \frac{2k_{s,dil}}{(1+e_s)g_o} \left(1 + \frac{6}{5}(1+e_s)g_o \varepsilon_s \right)^2 + 2\varepsilon_s^2 \rho_s d_s g_o (1+e_s) \left(\frac{\Theta_s}{\pi} \right)^{1/2} \tag{3.75}$$

Where

$$k_{s,dil} = \frac{75}{64} \rho_s \varepsilon_s l_s \sqrt{2\pi\Theta_s}$$

(3.76)

The collisional energy dissipation, γ_s, is represented by:

$$\gamma_s = 3\left(1 - e_s^2\right)\varepsilon_s^2 \rho_s g_o \Theta_s \left[\frac{4}{d_s}\left(\frac{\Theta_s}{\pi}\right)^{1/2} - \nabla\mathbf{U}_s\right]$$

(3.77)

3.9   Conclusions and Key Decisions

Our research has used the finite volume method to solve PDEs numerically. This method uses the integral form of the conservation equations in a control volume. The finite volume method is suitable for any type of grid and also handles complex geometries.

In this work, we have used the pressure-based solution methods for multiphase flow. In the pressure-based methods, pressure and velocity are solved iteratively for each time step in a sequential manner. The corrections are iteratively brought down to zero for convergence. An example of pressure-based methods is the SIMPLE method. In this study, we have used the SIMPLE algorithm because it has been successfully implemented in numerous CFD procedures especially for steady-state conditions.

Many researchers into the simulation of turbulent flows have used RANS-based turbulence models. The RANS model is not resolving the small-scale phenomena that cause the closure problem. The two-equation $k\text{-}\epsilon$ model of turbulence is the

most widely used in RANS-based models because of its computational efficiency, robustness and reasonable accuracy. It has been recommended as the basic model for the typical internal flows encountered by reactor designers.

Multiphase flow processes are key elements of several important reactor technologies such as fluid catalytic cracking reactors. A granular Eulerian-Eulerian approach was used to simulate the hydrodynamics of the multiphase flow in FCC rise reactors. In the Eulerian-Eulerian approach, the different phases are treated mathematically as interpenetrating continua. The concept of phasic volume fraction is introduced, because the volume of a phase cannot be occupied by the other phases. These volume fractions are assumed to be continuous functions of space and time and their sum is equal to one. The Eulerian-Eulerian approach is more suitable for modelling dispersed multiphase systems with a significant volume fraction of dispersed phase (>10%). Applications of the Eulerian multiphase model include risers, fluidized beds and bubble columns.

<div style="text-align:center">

Chapter 4

HYDRODYNAMICS MODEL OF

FCC RISER REACTORS

</div>

4.1   Overall Objectives

The complex hydrodynamics of FCC riser reactors is related to the characteristics of the two-phase flow. A model is a very useful tool for better design and optimal operation and to predict the flow pattern in the riser as a function of reactor geometry, operating conditions, and the characteristics of feed and catalyst. Most models reported in the literature are based on a two-phase description, one gas and one solid phase, where all the particles are assumed to have identical diameter, density and restitution coefficient. Multiphase flow is a very complex physical phenomenon where many flow types can occur, and within each flow type several possible flow regimes can exist .

Multiphase flow structure in FCC riser reactors is very complex. Attempts have been made by several researchers to model multiphase flow structure using many assumptions and different mathematical formulation. Harris and Davidson classified the kind of models that have been published in the literature to become three broad groups: (i) the model that predict the axial variation of the solids suspension density, but not the radial variation; (ii) the model that calculate the radial variation and the high average slip velocities which assume two or more regions, such as core-annulus and clustering annular flow models; and (iii) the model that apply the fundamental equations of fluid dynamics to predict the two phase gas-solid flow.

From three classifications of hydrodynamic models as mentioned above, the type (iii) models is the most rigorous. However, for the complex process, the models require the simplifying assumptions. The model type (i) gives the good agreement with experimental data and most of the model is not mathematically complex. However, the empirical models hinder their simplification for design and scale-up reason. The models based on the core-annulus flow assumption, the model type (ii), were not capable of describing the up-flow of solids at the wall that has been reported at take place at high solids mass fluxes . Incapability of the core-annulus model of predicting up-flow of solids at the wall is inherent in the definition of the core-annulus behaviour which assumes an annular region where the solids are moving down-wards. Therefore, it is important to develop a hydrodynamic model that will capable of describing up-flow of solids at the wall for high solids mass flux conditions.

This chapter is especially concerned on multiphase flow hydrodynamics of the riser and do not treat heat transfer and kinetic modelling. The steady state simulation of hydrodynamics model considers the catalyst as a particulate phase and the vapour hydrocarbon as a gas phase. Using a computational fluid dynamic (CFD) package Fluent 6.2 different catalyst sizes were simulated under varying gas-oil flow rates. The details of the governing and subsidiary equations for multiphase flow together with numerical solution procedure of CFD are given in the previous chapter (Chapter 3). The CFD model in this current work described the capability of CFD model to predict up-flow solids at the wall.

The model is used to predict velocity profiles of both phases; and solid volume fraction and to obtain the appropriate description of the flow pattern of solid and gas in the riser. In order to produce the satisfactory predicted results and a higher

level of reliability of the model, the calculated results of CFD model were validated by published experimental data.

4.2   The Boundary Conditions of FCC Riser Reactors

The performance of multiphase FCC riser reactors depends on its geometrical design. The geometries of the FCC riser section are shown in Figure 4.1. The solid catalyst (zeolite) was injected from the bottom of the riser. Gas-oil feed was fed to the reactor through four nozzles. The angle between the axes of the riser and the nozzles was 30°.

The riser diameter varied from 1m at the bottom to 1.4 m at the top. The total riser height used in the simulation was 13.8 m. In order to minimize computational requirements, the geometries of the FCC riser section were split into a quarter part of the unit with 5631 computational grids. A three-dimensional FCC riser was constructed using GAMBIT 2.3 (pre-processor for FLUENT 6.2). Structured (hexahedral) and unstructured (tetrahedral) grids were used throughout.

The solid catalyst entered the riser at the 1 m diameter section. The inlet flow rate of the catalyst was 235 kg/s. The volume fraction of solid was 40%. The average diameter of catalyst particle was varied at 30, 60 and 100 μm, and density of about 1500 kg/m^3. The gas-oil velocity inlet was varied at 4, 6, 8 and 10 m/s.

Boundary Conditions:

In order to produce acceptable simulation results and to obtain convergence, the selections of appropriate boundary conditions are very important. At the inlet, all velocities and volume fractions of both phases were specified. At the wall, the gas velocities were set at zero (non-slip condition). It was assumed that instantaneous vaporization of feed occurs as it enters the riser.
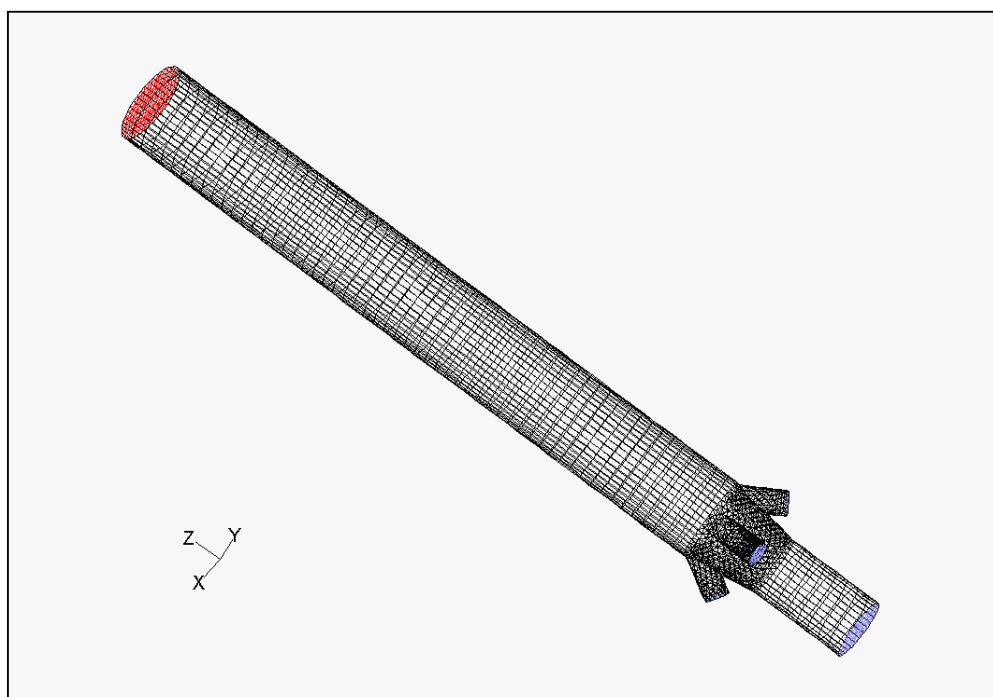

Figure 4.1. Geometry of FCC riser reactors (red: outflow; blue: velocity inlet; black: wall).

4.3   Computational Results

The simulations were carried out in order to observe the effects of a range of different operating conditions, and to be able to describe the multiphase flow pattern in the FCC riser reactors. The contours of the solid velocity are plotted to show the effects on the phase distribution of the flow pattern.

4.3.1 Solid volume fraction profiles

Solid volume fraction was acquired for each operating condition. Figures 4.2, 4.3 and 4.4 illustrate the distribution of the volume fraction of the solid phase obtained for gas-oil inlet velocities of 4, 6, 8, and 10 m/s, a solid mass flow rate of 235 kg.m^{-2}s^{-1}, and catalyst diameter of 30 to 100 μm. The volume fraction of the solid phase decreases across the entire riser diameter as the gas-oil inlet velocity increased. In addition, the solid volume fraction increases with increasing catalyst size. The figures show that for gas-oil inlet velocity of 4 m/s, the volume fraction of solid increases uniformly from the centre to the wall. The uniform solid volume fraction significantly benefited in the riser reactor. It indicates that good solid contact and less solid aggregation. It means good heat and mass transfer in the particles which is very important for rapid reactions. Furthermore, the model is able to describe quantitatively the accumulation of solid at the wall for all catalyst sizes chosen.
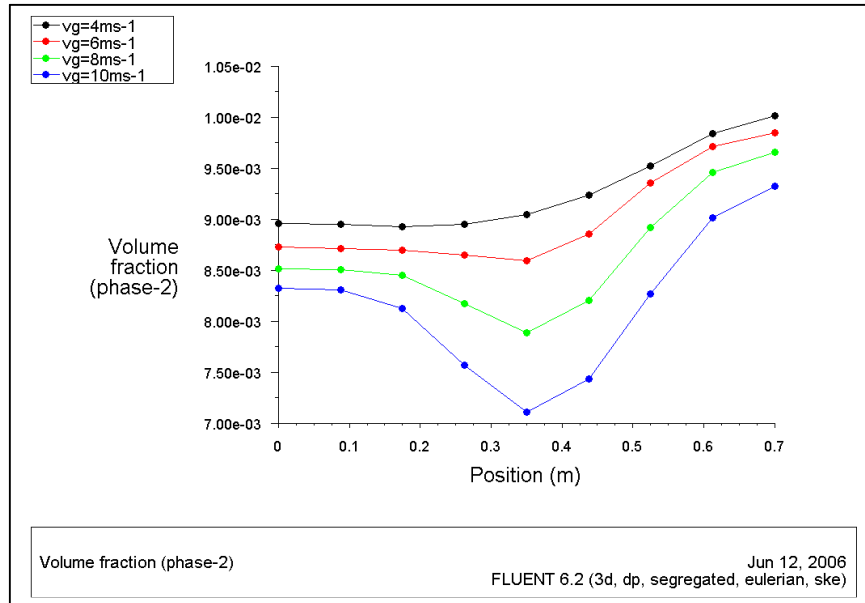
Figure 4.2. Effect of gas-oil inlet velocities on radial solid volume fraction profiles (dp = 30 μm, ρ_s =1,500 kg.m^{-3}, G_s = 235 kg.m^{-2}s^{-1}).

Figure 4.3. Effect of gas-oil inlet velocities on radial solid volume fraction profiles (dp = 60 μm, ρ_s =1,500 kg.m^{-3}, G_s = 235 kg.m^{-2}s^{-1}).

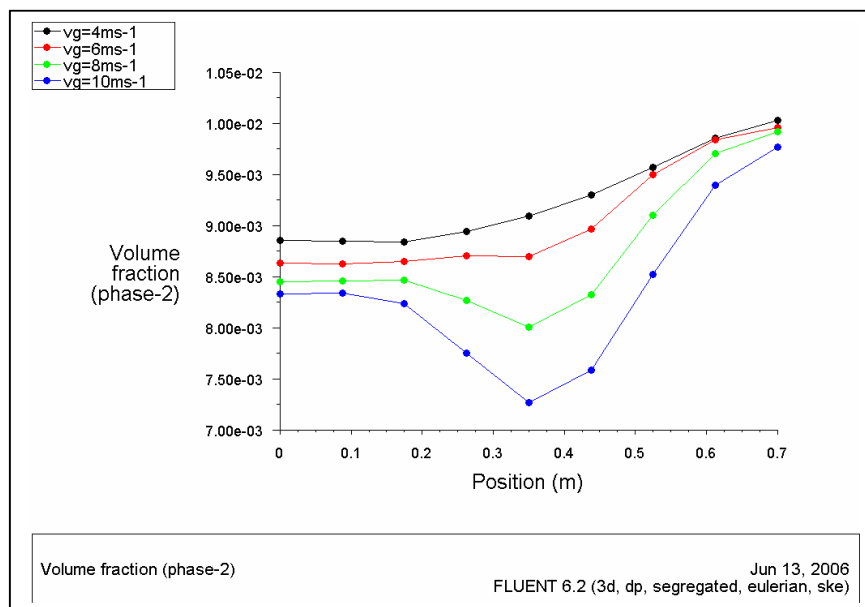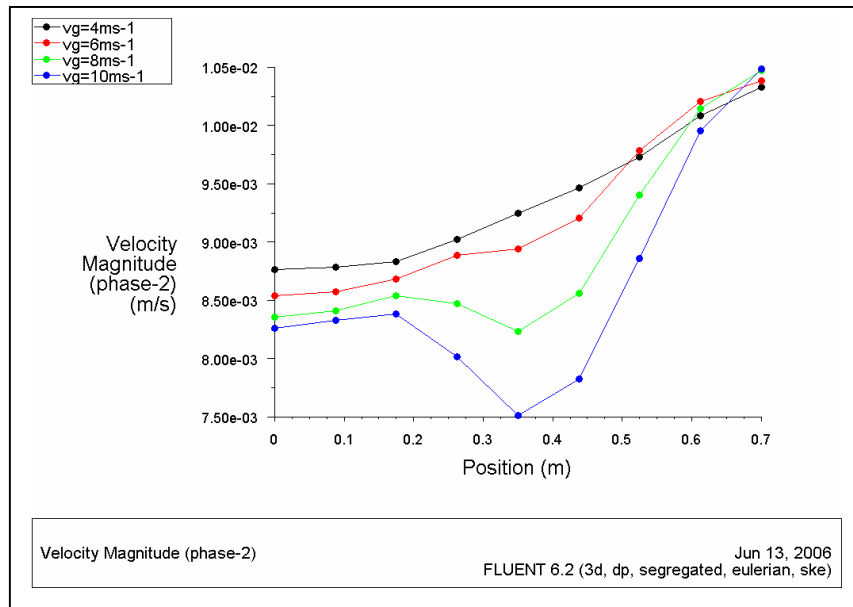**Figure 4.4. Effect of gas-oil inlet velocities on radial solid volume fraction profiles (dp = 100 μm, ρ_s =1,500 kg.m^{-3}, G_s = 235 kg.m^{-2}s^{-1}).**

4.3.2 Velocity profiles of the solid phase

Figures 4.5 and 4.6 show the velocity profiles of the gas and the solid phases for gas-oil inlet velocity of 10 m/s, a solid mass flow rate of 235 kg.m^{-2}s^{-1}, and catalyst diameter of 60 μm. The velocity profiles are plotted at the x-y direction with two different cross-sectional z-planes, that is at z = 10 m and z = 13.8 m, where z is the axial distance of the cross-section from the catalyst inlet. The minimum velocity is observed at the wall, and the solid and gas velocities increased toward the centre. The predicted radial profiles of gas and solid velocity are almost the same value.

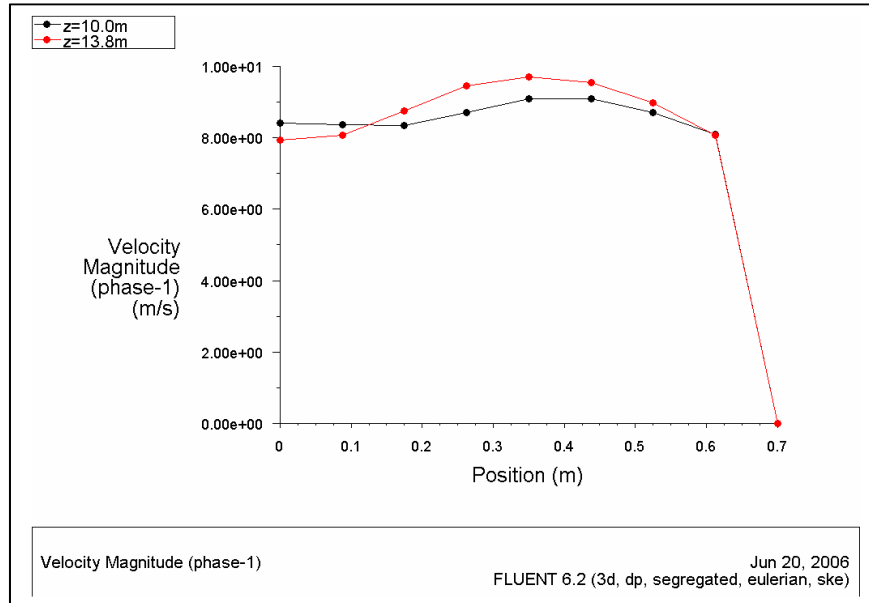**Figure 4.5. Gas velocity profiles (Ug = 10 m.s^{-1}; dp = 60 µm, ρ_s =1,500 kg.m^{-3}, G_s = 235 kg.m^{-2}s^{-1}).**
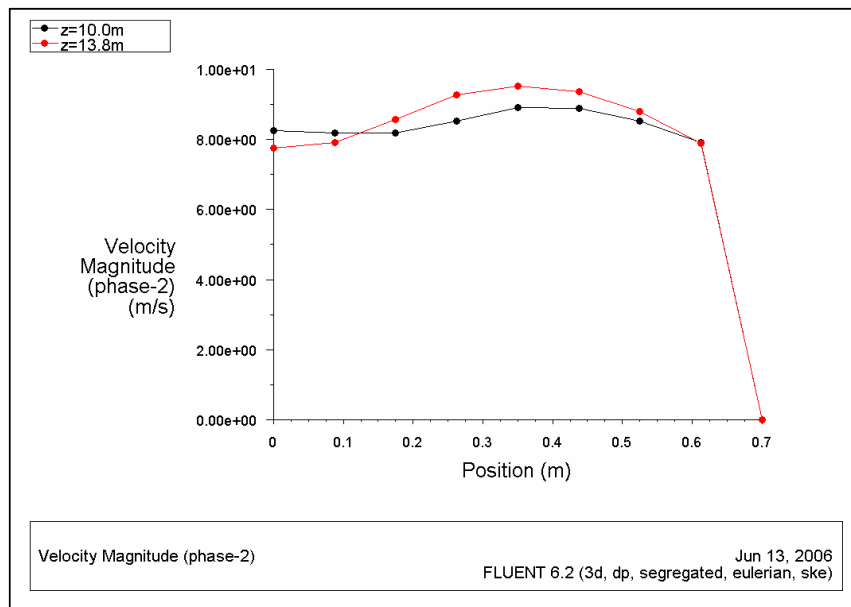
Figure 4.6. Solid velocity profiles (Ug = 10 m.s^{-1}; dp = 60 µm, ρ_s =1,500 kg.m^{-3}, G_s = 235 kg.m^{-2}s^{-1}).

Figures 4.7, 4.8, and 4.9 show the solid velocity profiles inside the riser for three different catalyst sizes (30, 60 and 100 μm). The solid velocity profiles are plotted for a solid mass flux of 235 kg.m^{-2}s^{-1} and gas-oil inlet velocities of 4, 6, 8, and 10 m/s. These figures show that in the region close to the wall, the solid velocity was a minimum and lower than that in the riser centre. Due to the solid velocity was lower and for lower gas velocities, the area swept by the gas becomes smaller, the thicker solid boundary layer zone increased. The solid velocity moves in the direction of flow and remains positive for all simulation results. It can be seen that a smaller gas-oil inlet velocity leads to a flatter profile for the solid velocity, except near the riser wall. As shown, at higher gas-oil inlet velocity, the solid velocity is higher. This is probably due to the larger amount of drag exerted on the solid by the gas, because the drag force is proportional to the relative velocity between the gas and the solid particles. However, at the riser centre, the predicted results show that the difference between the solid velocities is not significant.

This flow behaviour is similar to the average velocity of the FCC particles measured experimentally by Zhang and Arastoopour . They used Laser Doppler Anemometry (LDA) to measure the velocity and size distribution in the riser. They concluded that the solid velocity increased with superficial gas velocity due to the low solid void fraction, the collision interaction was very small so that each individual particle followed its own flow pattern with somewhat lower interaction with other particles. Arastoopour et al. have also observed similar profiles in their model. They concluded the higher drag force exerted on solid particles at the entrance zone. At higher gas-oil inlet velocity, the particles accelerate more and move at a higher speed at every cross-section of the vertical pipe.
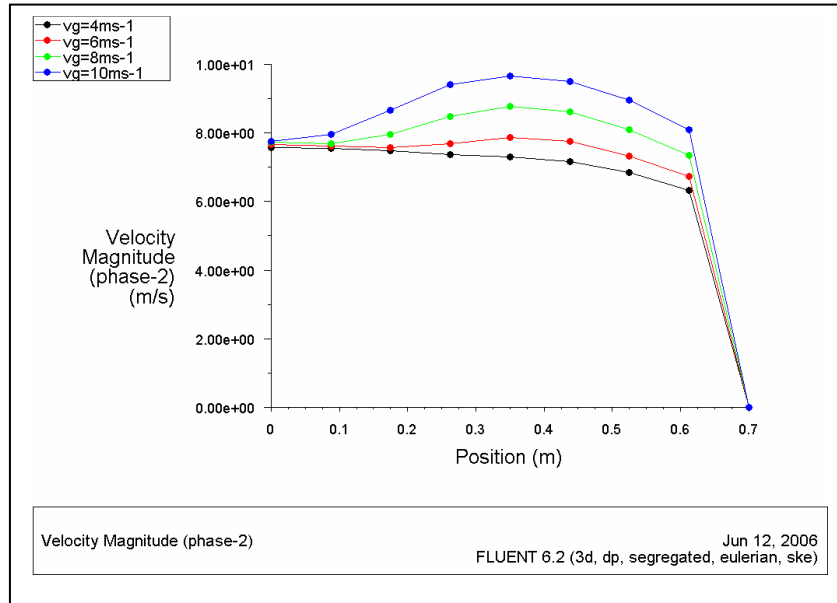
Figure 4.7. Solid velocity profiles at various gas-oil inlet velocities (dp = 30 μm, ρ$_s$ =1,500 kg.m^{-3}, G$_s$ = 235 kg.m^{-2}s^{-1}).
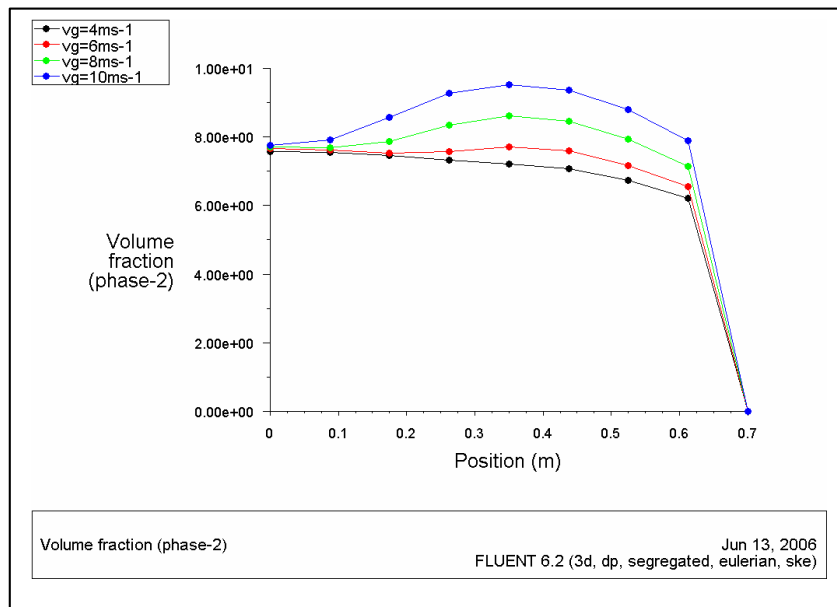
Figure 4.8. Solid velocity profiles at various gas-oil inlet velocities (dp = 60 μm, ρ$_s$ =1,500 kg.m^{-3}, G$_s$ = 235 kg.m^{-2}s^{-1}).
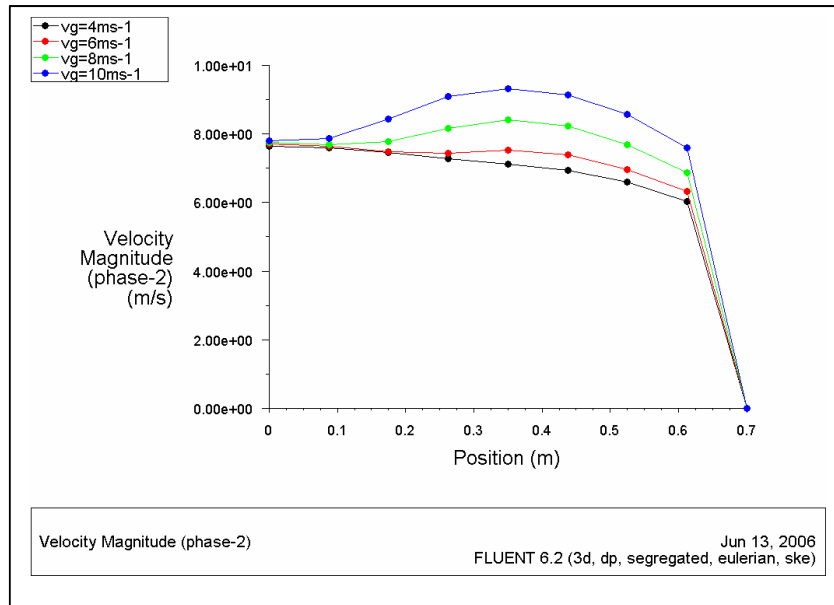
Figure 4.9. Solid velocity profiles at various gas-oil inlet velocities (dp = 100 μm, ρ_s =1,500 kg.m^{-3}, G_s = 235 kg.m^{-2}s^{-1}).

4.3.3 Contours and velocity vector of solid

The contours of the solid velocity are presented in Figure 4.10. High upward velocity was observed near the feed injection nozzles. This is due to low acceleration occurring at the area between the nozzles. The blue area represents the low velocity of solid and the red area for higher of solid velocity. It can be seen that the velocity profiles of catalyst show an off-centre maximum due to bypassing of the solid particles by gas. For this axial direction, the maximum catalyst velocity is observed between the centre and the wall. De Wilde et al. observed similar flow pattern in their experimental result.
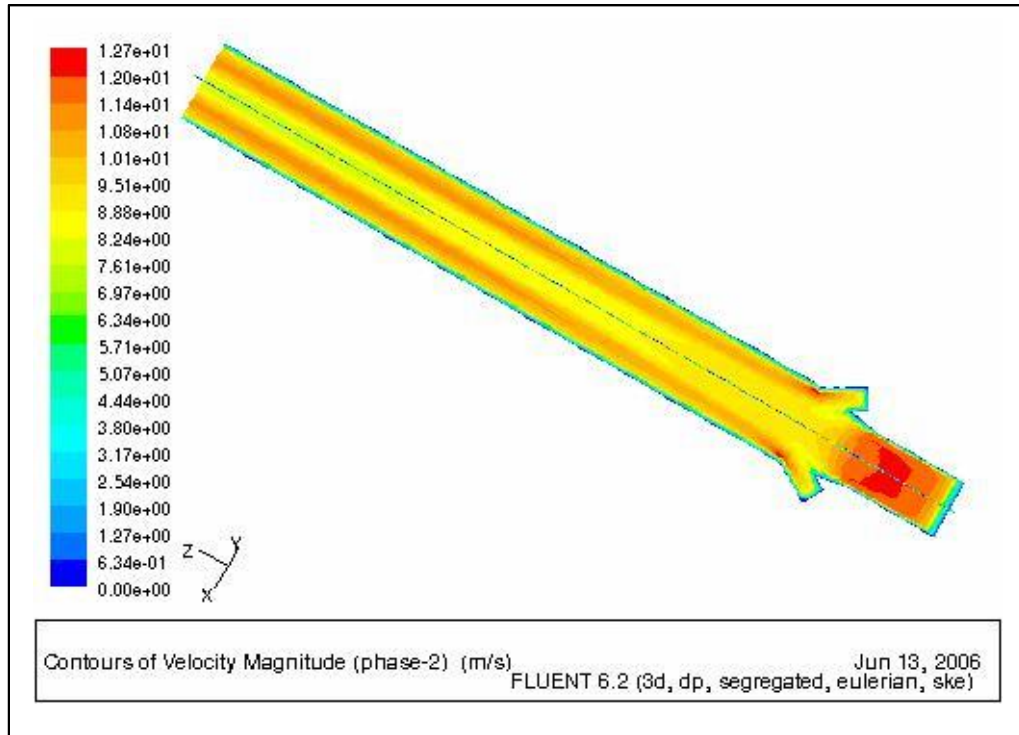
Figure 4.10. Contours of velocity magnitude of solid phase (Ug= 10 m.s^{-1}, dp = 60 μm, ρ_s =1,500 kg.m^{-3}, G_s = 235 kg.m^{-2}s^{-1}).

Figures 4.11, 4.12 and 4.13 illustrate the velocity vector of the catalyst which is moving upward. At higher gas velocity, the solid velocity is higher. This is due to the higher drag force exerted on solid particles at the riser entrance zone . At higher gas velocity, the particles accelerate more and travel at a higher speed at every cross-section of the riser. The velocity of catalyst is higher near the wall. At the riser bottom, the effect of feed geometry was apparent and leads to inhomogeneous flow. However, in the middle of the riser section, the flow is more defined along the riser height. In this work, the model was successful in relation to the significant up flow near the riser wall. The up flow at the wall can be seen if the simulations are performed with considering the gas phase turbulence model (Ranade, 1999).
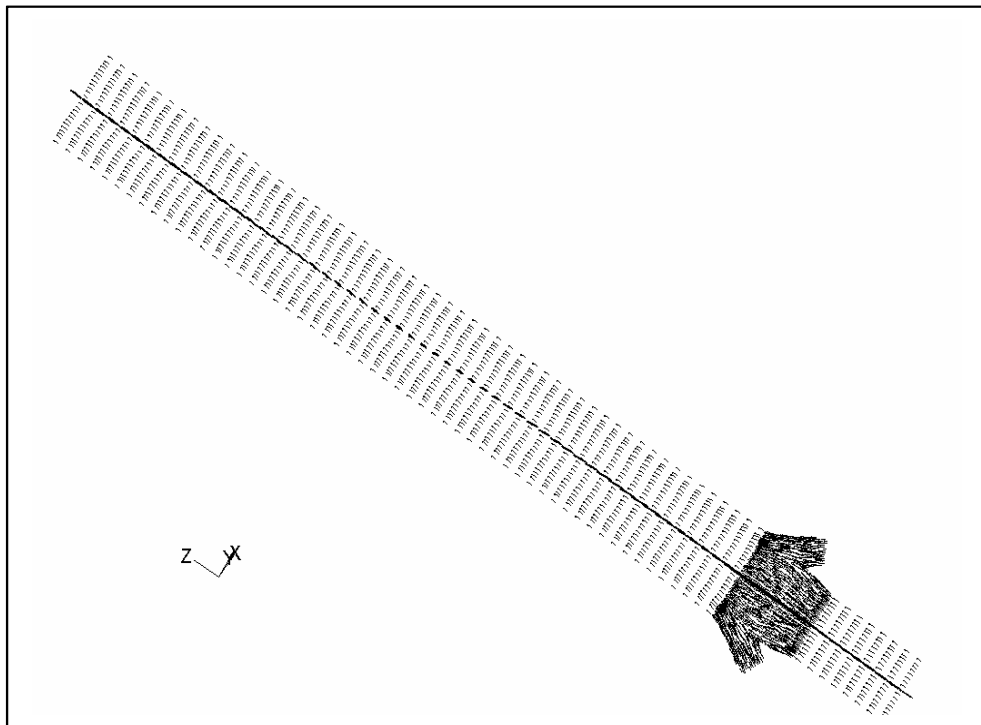
Figure 4.11. Vector velocity of solid phase (Ug= 10 m.s^{-1}, dp = 60 μm, ρ$_s$ =1,500 kg.m^{-3}, G$_s$ = 235 kg.m^{-2}s^{-1}).
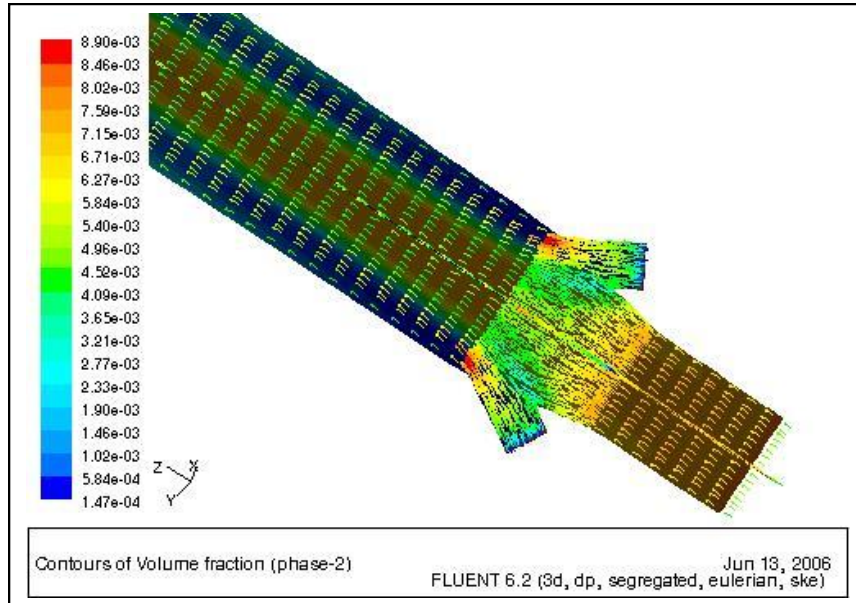
Figure 4.12. The velocity vector and volume fraction of solid at the bottom of the riser (Ug= 10 m.s^{-1}, dp = 60 μm, ρ_s =1,500 kg.m^{-3}, G$_s$ = 235 kg.m^{-2}s^{-1}).
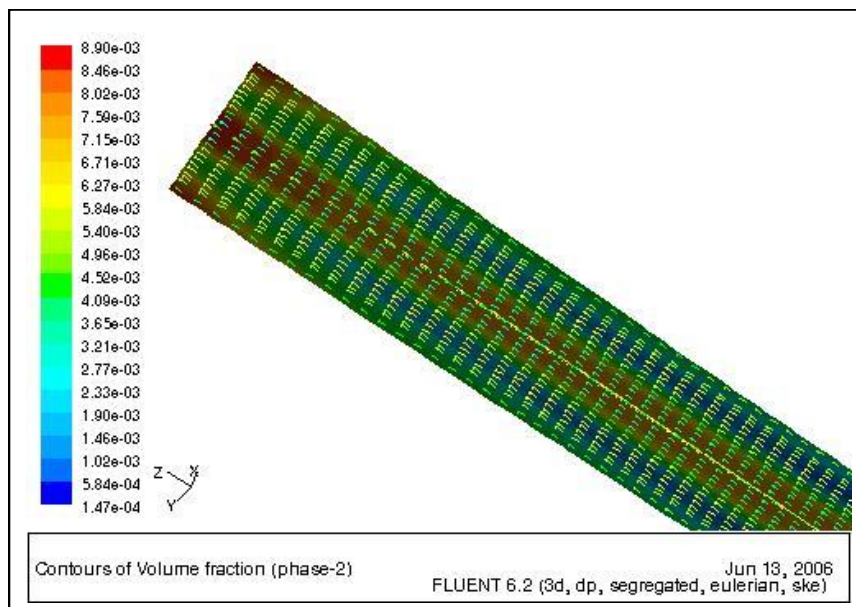
Figure 4.13. The velocity vector and volume fraction of solid at the top of the riser (Ug= 10 m.s^{-1}, dp = 60 μm, ρ_s =1,500 kg.m^{-3}, G$_s$ = 235 kg.m^{-2}s^{-1}).

4.4 Validation of Model with Experimantal Data

In the preliminary study, we have simulated multiphase flow corresponding to experimental conditions of Nieuwland . The accuracy of the numerical results was performed by comparing the solid velocity profiles of the predicted results to those experimental data. Table 4.1 shows operating condition and physical properties (sand as solid-phase and air as a gas-phase) employed in the verification. Figure 4.14 shows a comparison of radial solids velocity profile between the present model and experimental data measured by Nieuwland . They carried out their measurements at a solid flux of 350 kg m^{-2} s^{-}1 and a superficial gas velocity of 14.4 ms^{-1}.

The radial solids velocity profile predicted with CFD model using the correlation proposed in this work are in good agreement with the experimental data. Interestingly, the predicted solid velocity has the same value at position of 0.02 m from the centre. The radial solids velocity profile predicted with the CFD model using the relations proposed in this work is in good reasonable agreement, although close to centreline of the riser, the solid velocity profile is underpredicted slightly. The under prediction of the axial solids velocity in the riser centre is balanced by an overprediction in the wall region to satisfy the imposed solids mass flux.

Table 4.1. Operating condition and Physical Properties used in the verification.

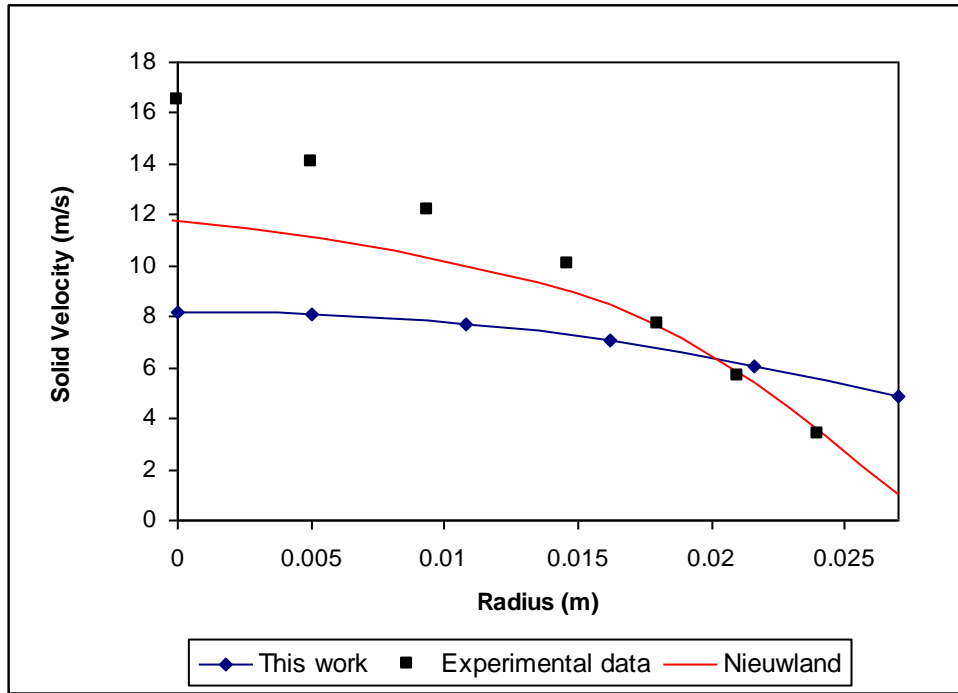| Parameter / Property	Value
Riser height (m)	8
Riser diameter (m)	0.054
Temperature (K)	293
Particle diameter (μm)	129
Particle density (kg m^{-3})	2540
Coefficient restrition (e)	1.0
Solid Flux (kg m^{-2} s^{-1})	350
Solid volume fraction	0.6
Gas velocity (m s^{-1})	14.4

Figure 4.14. **A comparison of predicted radial solids velocity with experimental results and model of Nieuwland at 2.5 m above the riser base. (R = 0.027 m, u_g = 14.4 m.s^{-1}, G_s = 350 kg.m^{-2}.s^{-1}, dp = 129 µm, ρ_s = 2,540 kg.m^{-3}).**

4.5   Conclusions and Key Decisions

This chapter discusses the two-phase flow model that considers the catalyst as a particulate phase and the vapour hydrocarbon as a gas phase. The computational model predicted the flow pattern of the solid and gas; velocity profiles of both phases; and solid volume fraction. The model was developed in order to provide reliable predictions of hydrodynamics multiphase flows in the FCC riser reactors. As expected, the model was successful in predicting the significant up flow of solid near the riser wall due to the inclusion of the gas phase turbulence model.

The developed model is able to describe quantitatively the accumulation of solid at the wall for all the catalyst sizes chosen. The volume fraction of the solid phase decreases across the entire riser diameter as the gas velocity is increased. In addition, the solid volume fraction increases as the catalyst size is increased. The uniform solid volume fraction significantly benefited in the riser reactor. It indicates that good solid contact and less solid aggregation. It means good heat and mass transfer in the particles which is very important for rapid reactions.

The solid velocity moves in the direction of flow and remains positive for all simulation results. A predictive result show that a smaller gas-oil inlet velocity leads to a flatter profile for the solid velocity, except near the riser wall. Furthermore, at higher gas-oil inlet velocity, the solid velocity is higher. This is probably due to the larger amount of drag exerted on the solid by the gas, because the drag force is proportional to the relative velocity between the gas and the solid particles. At higher gas velocity, the particles accelerate more and travel at a higher speed at every cross-section of the riser. However, at the riser centre, the

predicted results show that the difference between the solid velocities is not significant.

The velocity profiles of catalyst show an off-centre maximum due to bypassing of the solid particles by gas. For this axial direction, the maximum catalyst velocity is observed between the centre and the wall. High upward velocity was observed near the feed injection nozzles due to low acceleration occurring at that cross-sectional area. The velocity vector of the catalyst shows that the catalyst is moving upward and the velocity of catalyst is higher near the wall. At the riser bottom, the effect of feed geometry was apparent and leads to inhomogeneous flow. However, in the middle of the riser section, the flow is more defined along the riser height. The model was successful in relation to the significant up flow near the riser wall. The up flow at the wall can be seen if the simulations are performed with considering the gas phase turbulence model (Ranade, 1999). The calculated results of CFD model were validated by published experimental data in order to obtain the satisfactory predicted results and a higher level of reliability of the model. The radial solids velocity profile predicted with the CFD model is in good reasonable agreement with published experimental data.

Chapter 5

UNSTEADY STATE SIMULATION OF EULERIAN MULTIPHASE FLOW IN FCC RISER REACTORS: EFFECT OF GAS-OIL INLET VELOCITY AND CATALYST SIZE

5.1 Overall Objectives

An uncertain aspect of a fluid catalytic cracking (FCC) unit is the description of fluid-solid mixing at the riser entrance. Most of the existing models assume an instant mixing of solids and gaseous reactants. However, a finite mixing length at the bottom of the riser may have a pronounced effect on FCC operation, particularly, when only very short residence times are allowed in the current commercial FCC risers. Good solid-fluid mixing is essential to guarantee complete feed vaporization which is important for several reasons, including assuring thorough catalyst-to-oil contact and minimizing coke deposition. The uniform distribution of the solid particles results an advanced overall efficiency of a riser.

Knowledge of the hydrodynamics in multiphase reactors is crucially important for optimal operation, design and scale-up. In this chapter, transient multiphase hydrodynamics are predicted in the 3-D riser section of the FCC unit. The mixing of gas-oil feed and catalyst particles has been investigated using an Eulerian-Eulerian approach. The Eulerian-Eulerian approach is still the only advisable approach to perform parametric investigations scale-up and studies . In this approach, the governing equations are formulated with the concept of interpenetrating continua.

In the solid phase, stress is passed on by forces exerted at points of mutual contact between the particles. The solid phase shear stress is usually written in a Newtonian form by introducing a solid phase pressure and solid phase viscosity. These closure terms can be calculated by introducing the kinetic theory of granular flow. In the KTGF, the collisions between the particles are known as interactions of the fluctuating and the mean motion of the particles. The solid phase pressure and viscosity are related to the solid phase turbulence which is generally known as the granular temperature. A transport equation for the solid phase turbulence is obtained by the KTGF and solved simultaneously with the conservation equations of mass and momentum. Simulation of multiphase flows requires solution of a large number of governing equations. The main difficulties when simulating multiphase flow are handling the pressure-velocity coupling and non linearity, and the strong coupling between various equations which causes extremely slow convergence (Ranade, 2002).

A two-equation k-ϵ for gas-solid interactions is used for the calculation of the gas phase turbulent kinetic energy and dissipation. In this work, it was tried to include the mutual influence of gas-solids turbulence by gas-solids drag. Because of turbulence correlation of the gas-solid, enhancement of the gas-solids turbulence by gas-solid drag is possible.

This chapter discusses a transient multiphase flow model that considers the catalyst as a particulate phase and the vapour hydrocarbon as a gas phase. A number of simulations were performed to evaluate the effect of various parameters (such as gas-oil inlet velocity, catalyst size, and geometry of feed injector); and to obtain the description of the multiphase flow pattern in the FCC

riser. It was found that the geometry of the gas-oil feed nozzle affects the flow pattern in the riser.

The model predictions indicated that most of the complex mixing phenomena occur in the first 3 to 4 meters of the riser reactor. A gaseous feed is favourable for better mixing; however, for better temperature control and to avoid thermal cracking, an optimum phase distribution is required.

5.2   Initial and Boundary Conditions

The geometries of the riser section are similar to Figure 4.1 in Chapter 4. The solid catalyst entered the riser at 1 m diameter with flow rate of 235 kg m^2 s^{-1}. The volume fraction of catalyst was 40%. The average diameter of catalyst particle was varied from 10, 60 and 100 μm, and a density of approximately 1400 kg m^{-3}. The inlet gas-oil velocities were 5, 10 and 15 m s^{-1}.

Initially the riser was empty, and it was assumed that instantaneous vaporization of feed occurs as it enters the riser. For each simulation, all velocities and volume fractions of both phases were specified. At the wall, the gas velocities were set at zero (non-slip condition). A turbulence intensity of 5% is imposed for the gas phase. Calculations were started using the initial assumptions similar to the specified velocities and volume fractions. A constant time step of 0.001 seconds was used.

5.3 Multiphase Flow Pattern

CFD provides important information about the multiphase flow pattern in regions where measurements are either difficult or impossible to obtain by experiment. A CFD analysis predicts the flow field of velocity and concentration on a computational grid of the solution domain.

5.3.1 Contours of velocity magnitude of catalyst particle

Figure 5.1 shows the contour plots of the simulated velocity magnitude of the catalyst particles for three different times (1.4 s; 7.4 s; and 9.4 s) for the gas-oil inlet velocity of 10 m s^{-1}; the catalyst flow rate of 235 kg m^2 s^{-1}; and the catalyst size of 60 μm. It is found that the velocity profiles of catalyst show an off-centre maximum due to bypassing of the catalyst particles by gas. For this axial direction, the maximum catalyst velocity is observed between the centre and the wall. De Wilde et al. observed similar flow pattern in their experimental result. They revealed that the particles can not follow the gas motion from the central tube to the wall of the reactor due to inertia and the gas flow in the outer ring. As shown, the upward velocity of catalyst was quite high at the feed injection nozzles due to low acceleration occurring at the area between the nozzles.
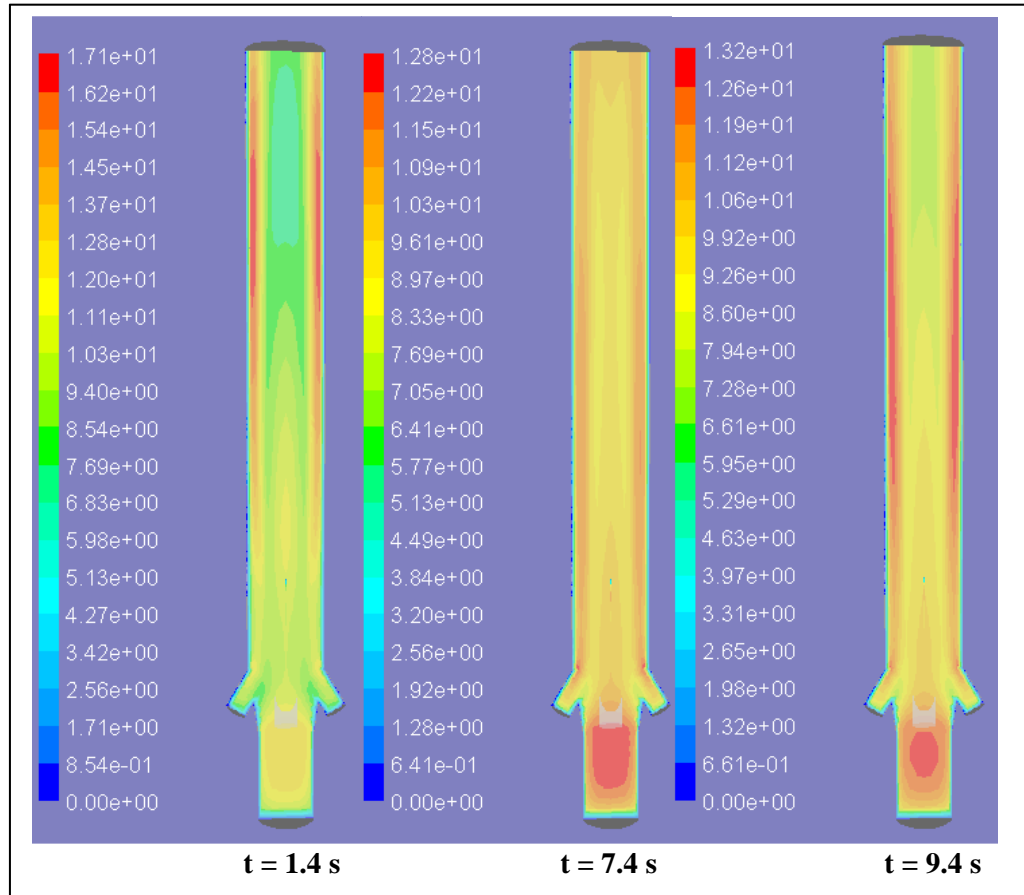
Figure 5.1. Time-dependent calculation of the velocity magnitude of catalyst (Ug= 10 m.s⁻¹, dp = 60 μm, ρₛ =1,400 kg.m⁻³, Gₛ = 235 kg. m².s⁻¹).

5.3.2 Velocity vector of catalyst particle

Figure 5.2 presents the time-dependent behaviour of the velocity vector of catalyst particles. Vector plots refer to three different times (1.4 s; 7.4 s; and 9.4 s) for the gas-oil inlet velocity of 10 m s⁻¹; the catalyst flow rate of 235 kg m² s⁻¹; and the catalyst size of 60 *μm*. It can be seen that the catalyst is moving upward closely plug flow. The model was not successful in demonstrating the significant

downflow of catalyst near the riser wall due to high velocity and turbulence in the gas phase. In addition, the downflow of catalyst may cause overcracking of gasoline to produce dry gas and coke. As shown in Figure 5.2, the flow pattern in the bottom region of the riser is still affected by the geometry of the gas-oil feed nozzle and leads to non-homogeneous flow. However, in the upper region, the flow is more uniform along the riser height.

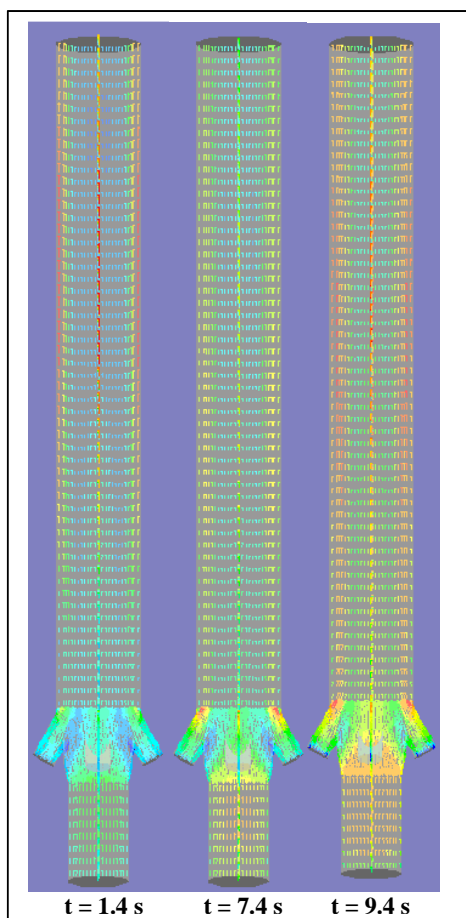**Figure 5.2. Time-dependent calculation of the velocity vector of catalyst (Ug= 10 m.s^{-1}, dp = 60 µm, ρ_s =1,400 kg.m^{-3}, G_s = 235 kg. m^2.s^{-1}).**

5.3.3 Contours of catalyst volume fractions

Figure 5.3 illustrates the simulated flow pattern of the catalyst volume fractions in the axial cross section of the riser, for the gas-oil inlet velocity of 10 m s^{-1}; the catalyst flow rate of 235 kg m^2 s^{-1}; and the catalyst size of 60 *μm*. These distributions are presented for three different times (7.4 s; 8.4 s; and 9.4 s) from the start of the simulation. The blue area representing the low solids concentration indicates dilute region. The red area is for the denser region with high solids concentration. Because the catalyst particles enter from the bottom and move toward the top, the increase of solid volume fraction grows from the bottom toward the top of the riser. It can be observed that the radial mixing of solid was hindered due to bypassing of the gas through feed nozzles. The typical of radial mixing of particles, as presented in figure 5.3, show similarities with the previous study by De Wilde et al.. They concluded that radial mixing is better in the bottom zone of the riser. Tinaburri (1996) also observed similar flow pattern.   The geometry of the riser used in their study is similar to this work.

In an assemblage of particles supported by a flowing fluid, random fluctuation of the local assemblage concentration appear . Because the drag force and other constituents of the interphase interaction force are non linear functions of the concentration, so the concentration fluctuations induce a fluctuating random force exerted by the fluid on the particles, thus violating the balance of gravity, and drag forces. Buyevich   found that in a vertical fluidized bed supported by an upward flowing fluid, the fluctuating forces accelerate the particles either upward or downward, depending on the sign of the concentration fluctuations, so that primarily vertical fluctuations occur. This is clearly demonstrated from this calculation results.
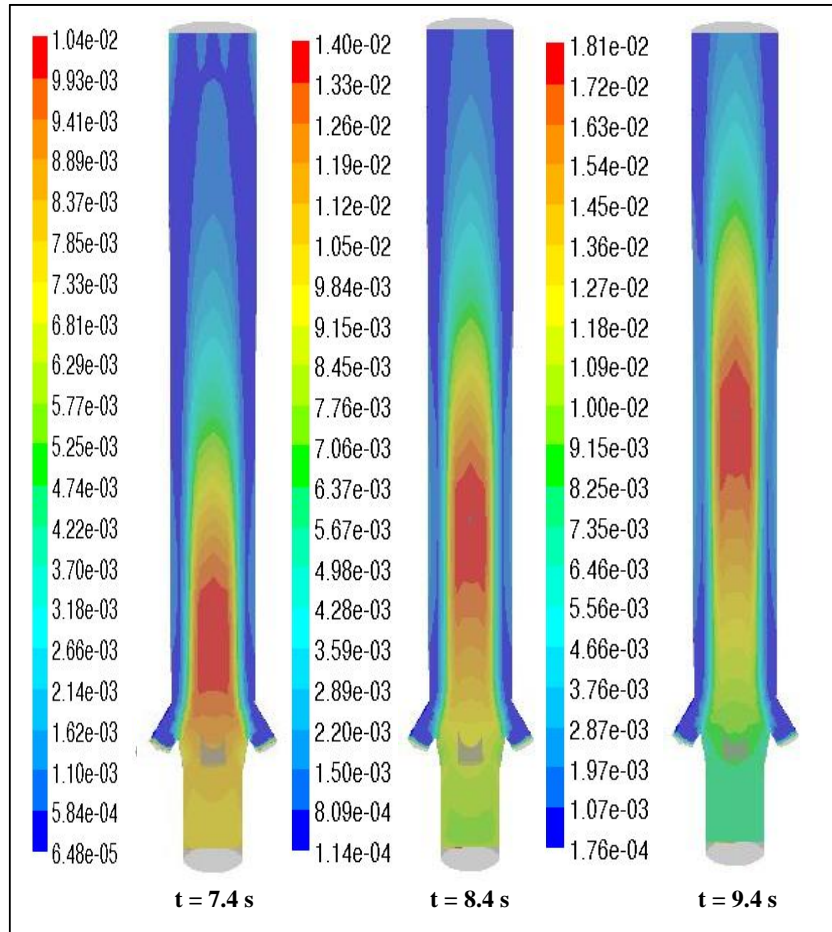
Figure 5.3. Instantaneous simulated flow pattern of catalyst volume fractions (Ug= 10 m.s⁻¹, dp = 60 μm, ρs =1,400 kg.m⁻³, Gs = 235 kg. m².s⁻¹).

5.3.4 Flow pattern of catalyst volume fractions and vectors

The simulated flow pattern of the catalyst volume fractions and vectors is shown in Figure 5.4 with the gas-oil inlet velocity of 10 m s^{-1}; the catalyst flow rate of 235 kg m^2 s^{-1}; and the catalyst size of 60 μm. These simulation results indicate that the geometry of the feed nozzle affects the flow pattern of the FCC riser reactor. As expected, the flow is more uniform after the injection point and there is no instantaneous reversal flow of catalyst at wall. Catalyst and gas move upward in a flow pattern approaching more closely the plug flow. The top part of the riser is dilute and the bottom part is dense. It is interesting to note that the radial mixing of solid was hindered due to bypassing of the gas through feed nozzles.

Figure 5.4. Instantaneous catalysts volume fraction flow pattern and velocity vector at t = 9.4 s (Ug= 10 m.s^{-1}, dp = 60 μm, ρ$_s$ =1,400 kg.m^{-3}, G$_s$ = 235 kg. m^2.s^{-1}).

5.4   Effect of Gas-Oil Inlet Velocity

Figure 5.5 shows the typical radial distribution of the time averaged volume fraction of the catalyst obtained for cases wit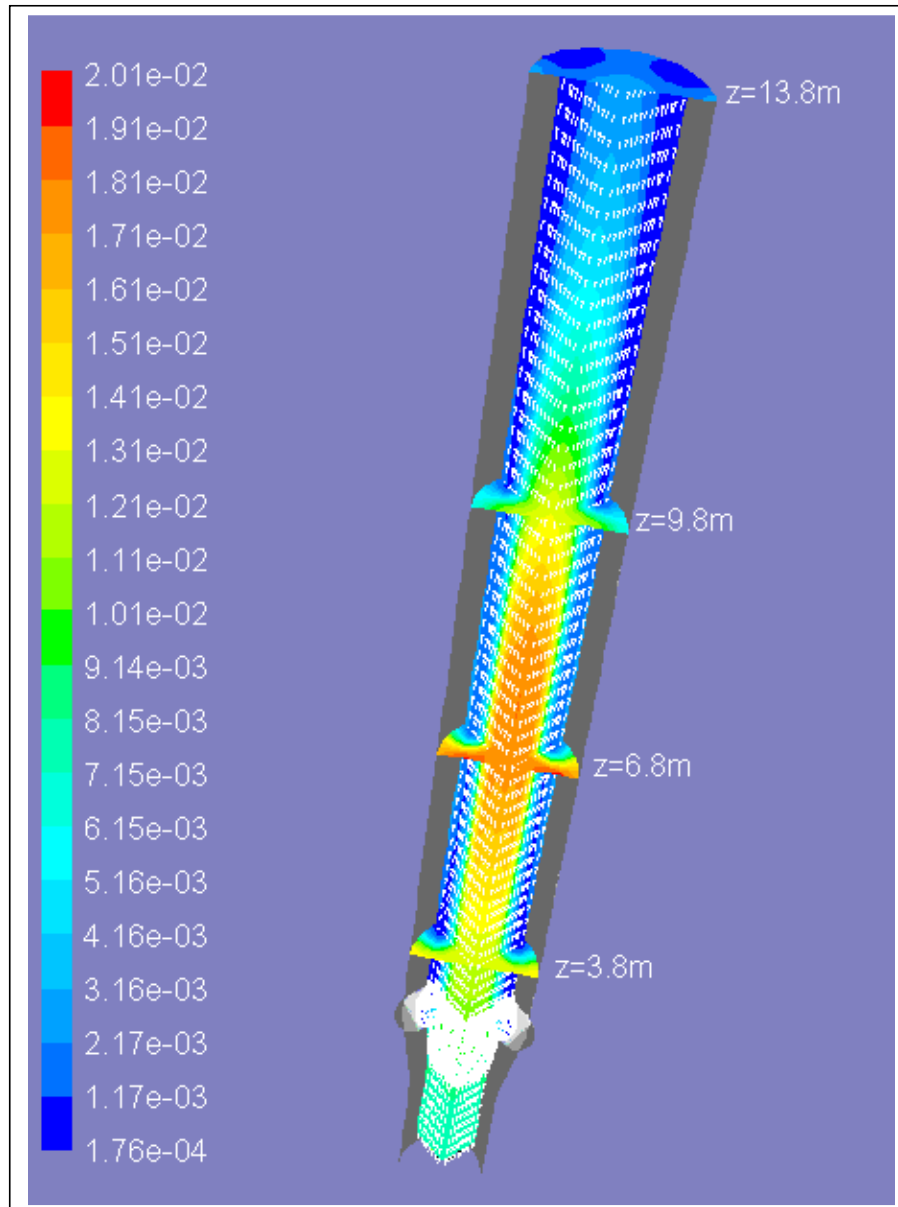h gas-oil inlet velocities of 5, 10, and 15 m s^{-1}; solid mass flow rate of 235 kg m^2 s^{-1}; and catalyst diameter of 60 μm. As shown in Figure 5.5, at the higher value of the gas-oil inlet velocity, the average catalyst volume fraction in the wall region of the riser is much lower, while the central region remains effectively unchanged. As evident from this figure, with decreasing gas-oil inlet velocity, a more pronounced lateral solids segregation results, which is in accordance with the observations of Nieuwland et al. . It is also observed that the catalyst volume fraction is lower at the central region and increases uniformly to the wall. The previous researchers, Wang et al. , investigated experimentally the radial profile of fine FCC particle (36 μm) using a dual-beam optical density sensor. They revealed that the uniform solid volume fraction significantly benefited the fine FCC particle. It indicates that good gas-solid contact and less solid aggregation. It means good heat and mass transfer in the particles which is very important for rapid reactions. The catalyst volume fraction in the centre region of the riser is about 0.001. For reference, results from the published literature are also plotted. As can been seen, the results match reasonably well.

Figures 5.5 and 5.6 compare results from the current model with both the experimental and computed results of Nieuwland et al. . Good qualitative agreement between the two models was observed. As shown in these figures, with decreasing gas velocity, a more pronounced lateral solids segregation results. The properties of gas and solids phase used in the current model, and the experimental data of Nieuwland et al. , are shown in Table 5.1.

Table 5.1. Physical properties for the gas and solid phase.

Nieuwland et al.	*Solid phase*	*Sand*
	Mean particle diameter, d_p	129 μm
	Particle density, ρ_s	2540 kg m^{-3}
	Coefficient of restitution, e	1.00
	Gas phase	Air
	Temperature, T	293 K
This Work	Solid phase	FCC particle
	Mean particle diameter, d_p	60 μm
	Particle density, ρ_s	1400 kg m^{-3}
	Coefficient of restitution, e	0.90
	Gas phase	Gas-oil
	Temperature, T	300 K

In this study, a particle-particle restitution coefficient (*e*) of 0.9 was used. Pita and Sundaresan (1993) investigated the high sensitivity of their computed solids density and mass flux to the restitution coefficient. They concluded that only a value of the restitution coefficient, (*e*) = 1, was appropriate to accurately compute the experimental data of Bader et al. . However, because the particle-particle collisions in the FCC riser reactors are not elastic, this value of restitution coefficient is not appropriate to be applied in the current work.

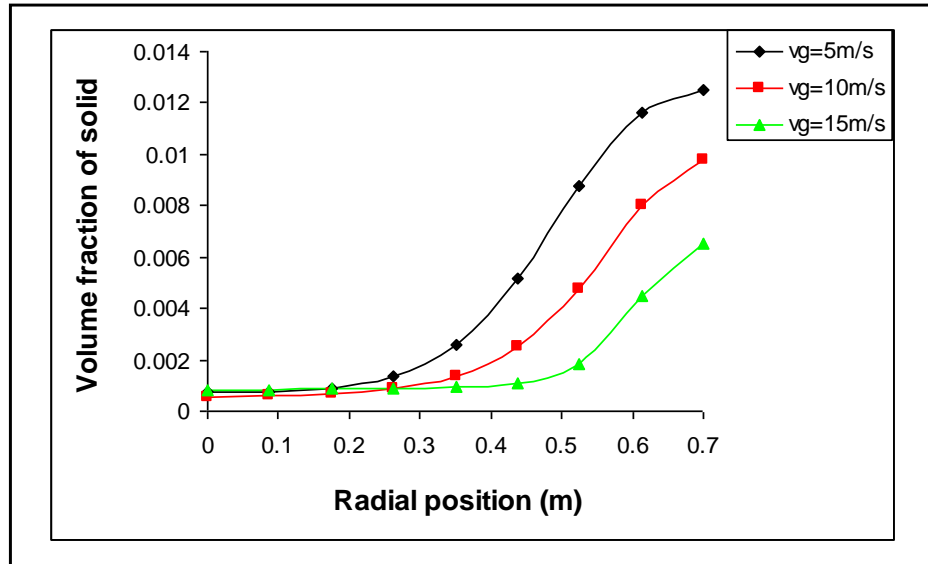**Figure 5.5. Time-averaged catalyst volume fractions at various gas-oil inlet velocities (dp = 60 μm, ρ_s =1,400 kg.m^{-3}, G_s = 235 kg.m^2. s^{-1}).**
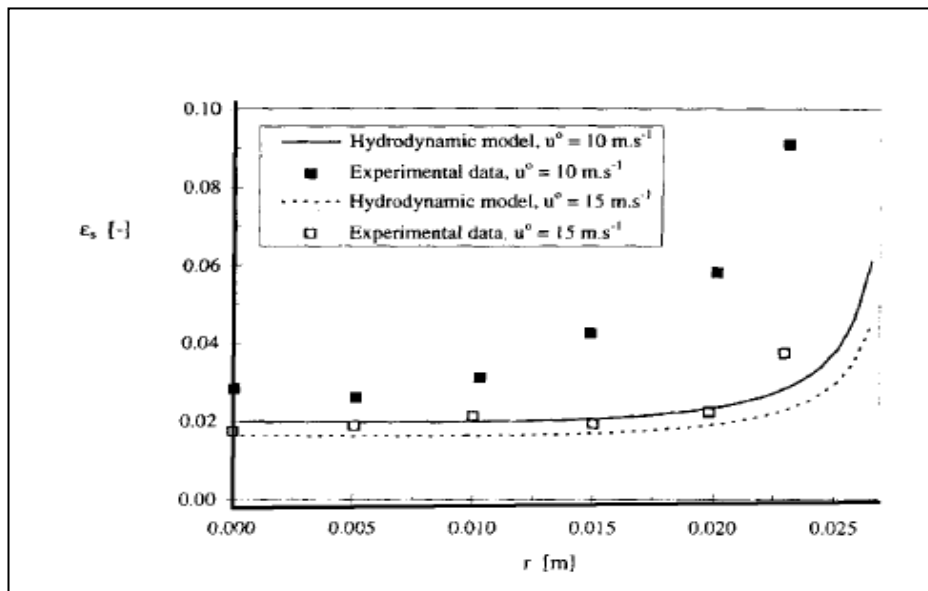
Figure 5.6. Calculated and experimentally determined solid volume fraction as a function of the radial position; reproduced from (dp = 129 μm, ρ_s =2,540 kg.m^{-3}, G_s = 100 kg.m^2. s^{-1}).

5.5   Effect of Catalyst Size

Figure 5.7 shows the profiles of the catalyst volume fraction for catalyst sizes of 10, 60 and 100 μm, gas-oil inlet velocity of 10 m.s^{-1}, and solid mass flow rate of 200 kg s^{-1}. From this figure it can be seen that, the catalyst size only slightly influences the solids volume fraction profiles in the riser. Near to the wall, the catalyst volume fraction increases with increasing values of the catalyst size. Hence, the model is able to describe quantitatively the accumulation of catalyst at the wall for all different catalyst sizes. Nieuwland also reported the same profiles especially for solids mass flux of 100 kg m^2 s^{-1} and particle diameter of 129 μm. They used the optical probe system to measure the particle concentration.

Figure 5.7. Time-averaged catalyst volume fractions at various catalyst sizes (dp = 60 μm, ρ_s =1,400 kg.m^{-3}, G_s = 235 kg.m^2. s^{-1}).

5.6   Conclusions and Key Decisions

Knowledge of the hydrodynamics in multiphase reactors is crucially important for optimal operation, design and scale-up. In this chapter, transient multiphase hydrodynamics are predicted in the 3-D riser section of the FCC unit. The mixing of gas-oil feed and catalys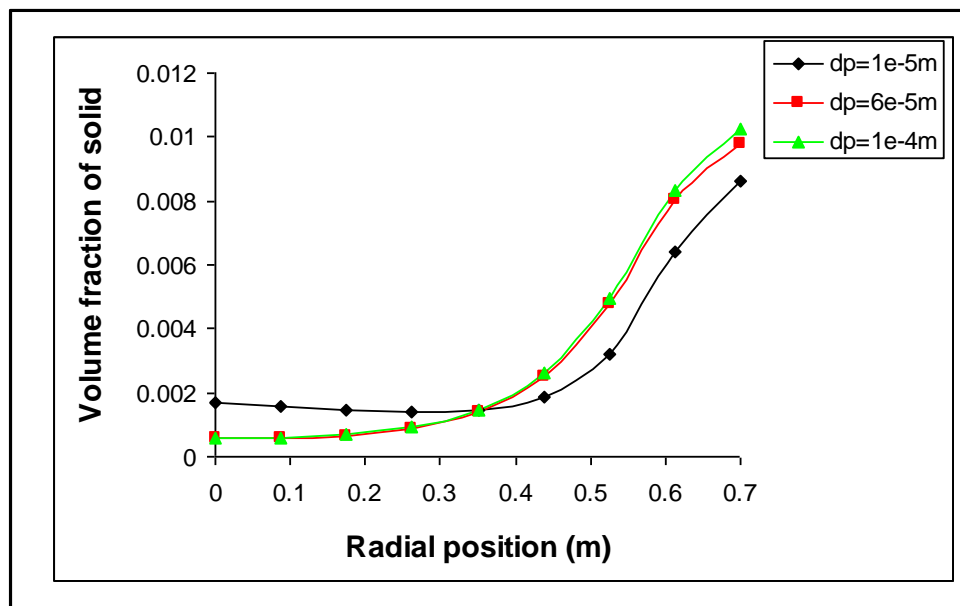t particles has been investigated using an Eulerian-Eulerian approach. The CFD model provides important information about the multiphase flow pattern, and also predicts the flow field of velocity and volume fraction on a computational grid of the solution domain.

The model was not successful in demonstrating the significant downflow of catalyst near the riser wall due to high velocity and turbulence in the gas phase. In addition, the downflow of catalyst cause overcracking of gasoline to produce dry gas and coke. The flow pattern in the bottom region of the riser is affected by the geometry of the gas-oil feed nozzle and leads to non-homogeneous flow. The flow is more uniform after the injection point and there is no instantaneous reversal flow of catalyst at wall. Catalyst and gas move upward in a flow pattern approaching more closely the plug flow. The top part of the riser is dilute and the bottom part is dense.

It is found that the velocity profiles of catalyst show an off-centre maximum due to bypassing of the catalyst particles by gas. For the axial direction, the maximum catalyst velocity is observed between the centre and the wall. The upward velocity of catalyst was quite high at the feed injection nozzles due to low acceleration occurring at the area between the nozzles.

At the higher value of the gas-oil inlet velocity, the average catalyst volume fraction in the wall region of the riser is much lower, while the central region remains effectively unchanged. The volume fraction of the solid phase decreases across the riser diameter as the gas-oil velocity is increased. It is also observed that the catalyst volume fraction is lower at the central region and increases uniformly to the wall. The model is able to describe quantitatively the accumulation of catalyst at the wall for all different catalyst sizes.

Chapter 6

HYDRODYNAMICS AND REACTION KINETICS ANALYSIS FOR STEADY-STATE CONDITIONS: EFFECT OF CATALIST-TO-OIL RATIO

6.1   Parameters and Approach – An Overview

Detailed knowledge of hydrodynamics and reactions kinetics is very important to provide an enhanced understanding of the phenomena occurring in FCC riser reactors. Optimization of the operation of FCC riser reactors is still needed due to complex interactions between a large number of dependent and independent parameters. Performance of FCC riser reactors depends on various key parameters such as temperature, catalyst-to-oil ratio (CTO), and feed injector geometry. Furthermore, the function of feed injection is to control the flow of catalyst and hydrocarbon; and to create plug flow conditions in order to minimize undesirable temperature gradients. These parameters affect the yield of the desirable products.

This chapter presents a more complete analysis involving the hydrodynamics and the kinetics of the catalytic cracking reactions in the FCC riser reactors for steady-state conditions. The hydrodynamics model of FCC riser reactor has been studied by different modelling approaches. However, accurate analysis of the flow field has not yet been achieved, and it still limited to a two-dimensional flow model. Furthermore, the catalytic cracking of hydrocarbons is a complex process due to the many reactions and chemical species involved. Therefore, the complexities of

the reactions have been investigated by lumping together several chemical compounds.

It is difficult to account for all aspects of reaction kinetics in the riser, the following process considerations are required :

1. Catalytic reactions need the presence of the catalyst. A more even catalyst distribution across the riser is important because it leads to a more uniform local catalyst-to-oil (CTO) ratio and more uniform reaction rates.

2. Catalytic reactions result in coke deposition on the catalyst, which reduces catalyst activity and selectivity. Therefore, backmixing of spent catalyst down the riser is highly undesirable.

3. Thermal cracking reactions are more sensitive to the reaction temperature. A more uniform temperature distribution across the riser is desirable because it leads to an overall reduction in the thermal cracking reactions, and more uniform catalytic reaction rates.

4. Gas radial mixing in the riser occurs relatively slowly. A more uniform gas velocity distribution across the riser is desirable because it leads to a more uniform reaction residence-time distribution.

According to Chen , the successful design of FCC riser reactors must consider the following hydrodynamics trends of a co-current gas-solid two-phase upflow:

1. Solid concentration is higher at the wall than the centre.

2. Solids always move upward in the centre zone, but can be either upward or downward flow near the wall.

3. Gas velocity is higher near the centre, and lower near the wall.

The most important reason for studying the hydrodynamics and kinetic modelling of FCC riser reactors is to accurately predict their performance. Predictive models

under various operating conditions have been studied. The Eulerian-Eulerian multiphase flow and the 3-lump kinetic model were assumed, in order to simulate three-dimensional hydrodynamics and cracking reactions occurring in the FCC riser reactors.

6.2   The Three-Lump Kinetic Model

The complexity of gas oil mixtures makes it extremely difficult to characterize and describe its kinetics at a molecular level. Therefore, the description of the complex reactions, which occur in the FCC process, has been studied by lumping large numbers of chemical compounds . The catalytic cracking of gas-oil produces a wide range of products. For simplification and less computational requirements, the three-lump kinetic scheme was used to describe the catalytic cracking reactions. In this scheme, the gas-oil feed is converted to gasoline and light gases plus coke, while a part of the gasoline is converted to light gases plus coke. The catalytic cracking reaction scheme for a three-lump model is given by:

Gas-oil ⟶ Gasoline

Light gas + coke
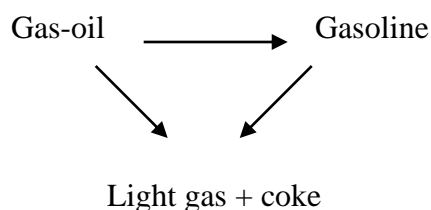
Figure 6.1. Three-lump kinetic scheme

The reaction kinetics is enclosed with the hydrodynamic model by solving the species equation of the components in the form of the reaction rates as follows:

Gas-oil cracking is a second-order reaction with rate calculated by:

$$\frac{dY_0}{dt} = K_0 Y_1^2 \phi \tag{6.1}$$

Gasoline formation is a second-order reaction with rate calculated by:

$$\frac{dY_1}{dt} = K_1 Y_1^2 \phi \tag{6.2}$$

Gasoline cracking is a first-order reaction with rate calculated by:

$$\frac{dY_2}{dt} = K_2 Y_2 \phi \tag{6.3}$$

The kinetic parameters K_0, K_1 and K_2 are related to the gas-phase temperature by the Arrhenius equation; Y_1 and Y_2 are mass fractions of gas-oil and gasoline, respectively.

Table 6.1. Reaction kinetics data (Theologos and Markatos, 1993).

Reaction	Kinetics constant (482°C)	Activation energy
Gas-oil cracking	$K_0 = 0.266 \text{ h}^{-1}$	$E_0 = 10 \text{ kcal/mol}$
Gasoline formation	$K_1 = 0.214 \text{ h}^{-1}$	
Gasoline cracking	$K_2 = 0.0188 \text{ h}^{-1}$	$E_0 = 18 \text{ kcal/mol}$

6.3   Riser Geometry and Inlet Conditions

The geometry of the riser reactors is described in Figure 6.2. The solid catalyst (zeolite) was injected from the bottom of the riser. Gas-oil feed was fed to the reactor through four nozzles. The angle between the axes of the riser and the nozzles was 30°. The riser had a diameter between 1 m at the bottom, and 1.4 m at the top. The total section of the riser height simulated was 7.8 m. A quarter of the riser height was simulated, which requires 5711 computational grids. The 3-D riser inlet was constructed using GAMBIT pre-processor. Structured (hexahedral) and unstructured (tetrahedral) grids were used throughout. Smaller grids give more accurate result; however require a large number of grids and very small time steps which need longer computational times.

The solid catalyst entered the riser at 1 m diameter. The flow rate of the catalyst inlet was 235 kg m^2 s^{-1}, with temperature of 923 K. The volume fraction of solid was 10%. The average diameter of catalyst particle was 60 μm and density of about 1400 kg m^{-3}. The gas-oil inlet velocity was 10 m s^{-1}. The temperature of the inlet gas-oil feed was varied with values of 623, 673 and 723 K. The catalyst-to-oil ratio (CTO) values were 4, 6, and 8. Turbulence intensity of the inlet gas-phase is assumed to be 5%.

At the inlet, all velocities, temperatures and volume fractions of both phases were specified. At the wall, the gas tangential and normal velocities were set to zero (non-slip condition).

The simplifying assumptions are summarized below:

- The particle size is uniform and the density of all particles is similar.
- Each phase has been described as a continuum; solid particles are defined as a particulate phase.
- Instantaneous vaporization of the feed as it enters the riser.
- A restitution coefficient for particle-particle collision has been assumed constant (0.9).
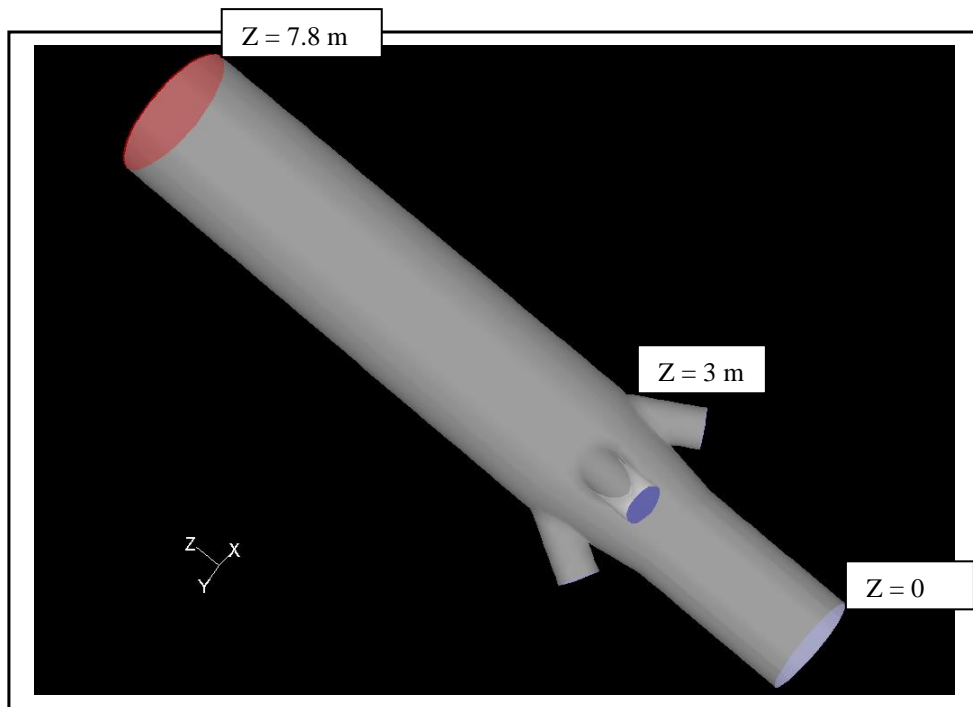

Figure 6.2. Geometry of the riser (red: outflow; blue: velocity inlet; grey: wall).

6.4   Flow Pattern of Particle Velocity

Figure 6.3 shows vector plots of the particle velocity for non-reactive and reactive flow at a fixed inlet gas-oil feed temperature of 623 K, the catalyst flow rate of 235 kg m^2 s^{-1}, the catalyst temperature of 923 K, the gas-oil inlet velocity of 10 m s^{-1} and catalyst-to-oil ratio (CTO) of 4. It can be seen that the flow patterns of particle velocity for both cases were significantly different. At the riser bottom, feed injection produced complex hydrodynamics because of the mixing of catalyst and gas-oil. However, without chemical reactions, the flow of catalyst became more defined (similar to plug flow) within about 1 m from the feed entry. For reactive flow, the linear acceleration with height is remarkable. This acceleration is probably due the expansion of the gas with the height, since the pressure decreases. In the radial direction, towards the fully developed zone of the riser, a typical turbulence velocity profile develops due to the effect of the viscous forces. It was observed for both cases that the flow pattern revealed the absence of catalyst backmixing at the riser wall. This is due to high velocity and turbulence in the gas phase. In addition, the backmixing of catalyst is undesirable due to affect on conversion and production in FCC riser reactors. Interestingly, with cracking reactions, there was an increase in catalyst velocities with riser height, particularly at the centre of the riser. This acceleration could be attributed to the increased volume of the gas phase due to the cracking reactions.

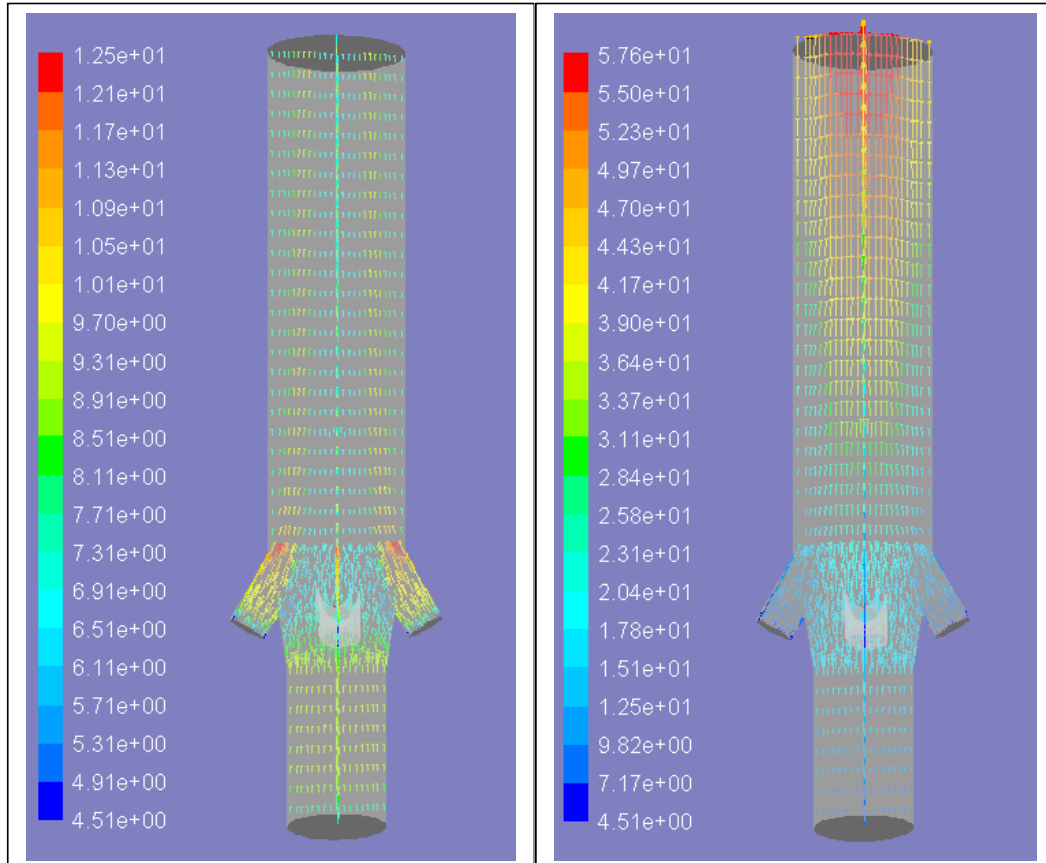**Figure 6.3.** **The computed velocity vectors of the particle for non-reactive flow (left) and reactive flow (right) (T_g = 623 K; T_s = 923 K; U_g = 10 m.s^{-1}; dp = 60 μm; $ρ_s$ = 1,400 kg.m^{-3}; G_s = 235 kg. m^2.s^{-1}; CTO = 4).**

6.5   Radial Particle Velocity Profiles in the Riser

Figure 6.4 presents the radial particle velocity profiles for five different riser heights at a fixed inlet gas-oil feed temperature of 623 K, the catalyst flow rate of 235 kg m^2 s^{-1}, the catalyst temperature of 923 K, the gas-oil inlet velocity of 10 m s^{-1} and catalyst-to-oil ratio (CTO) of 4. It can be seen that the maximum particle velocity occurred at the centre of the riser, and the particle velocity decreased from the centre to the wall. There is increased solid velocity at the riser top because many products are produced, such as gasoline and light gases. According to Das et al. (2003), the increase in the velocity is caused by the gas-phase pressure at the riser top is lower than at the bottom due to hydrostatic head of the solid. The low pressure allows the gas to expand, thus increasing the solid velocity by the drag force.
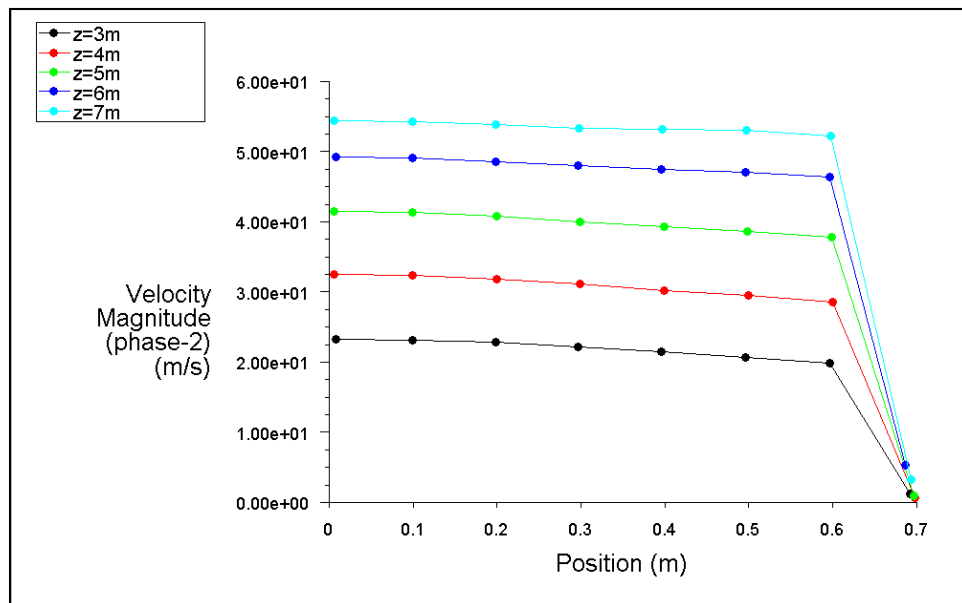

Figure 6.4. Radial velocity profiles of solid phase at different riser height (T_g = 623 K; T_s = 923 K; U_g = 10 m.s^{-1}; dp = 60 μm; $ρ_s$ = 1,400 kg.m^{-3}; G_s = 235 kg. m^2.s^{-1}; CTO = 4).

6.6   Effect of Catalyst-to-Oil Ratio (CTO)

In Figures 6.5, 6.6 and 6.7, the mass fractions of gas-oil, gasoline, and gas-coke along the riser height are predicted at a fixed inlet gas-oil feed temperature of 623 K, the catalyst flow rate of 235 kg m^2 s^{-1}, the catalyst temperature of 923 K, the gas-oil inlet velocity of 10 m s^{-1} and various catalyst-to-oil ratios of 4, 6, and 8. There were no chemical reactions with gas-oil feed injection below 3 m. These figures show that the mass fractions of gasoline and gas-coke increase with higher CTO, however, the gas-oil decreases progressively. At a CTO of 4, about 7 wt. % of gas-oil is still unconverted. The majority of the gas-oil fraction is converted within the first 3 m to 5 m from the riser bottom. Similar trends of product distribution has also been observed experimentally by Dupain et al. with CTO of 2, 4 and 6.

Figure 6.5. Gas-oil distributions along the riser height at different values of CTO   (T$_g$ = 723 K; T$_s$ = 923 K; U$_g$= 10 m.s^{-1}; dp = 60 μm; ρ$_s$ =1,400 kg.m^{-3}; G$_s$ = 235 kg. m^2.s^{-1}).
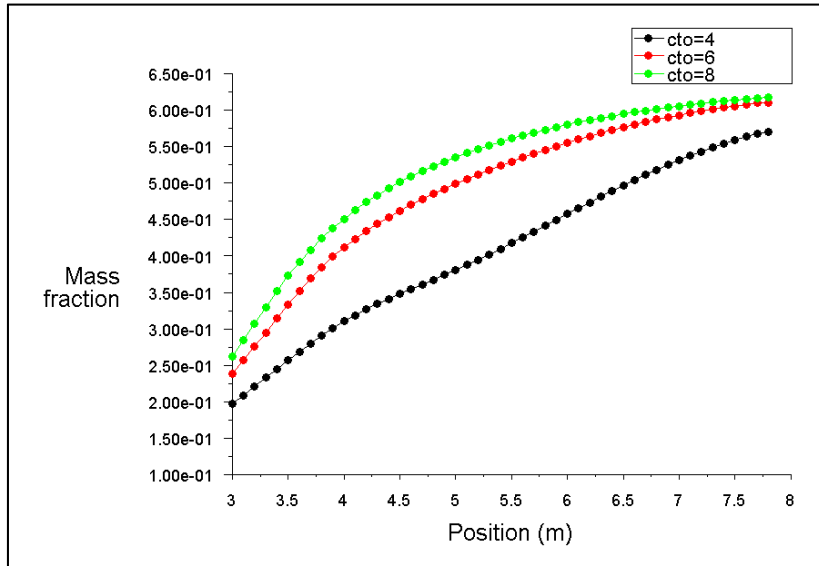
Figure 6.6. Gasoline distributions along the riser height at different values of CTO (T_g = 723 K; T_s = 923 K; U_g= 10 m.s^{-1}; dp = 60 μm; $ρ_s$ =1,400 kg.m^{-3}; G_s = 235 kg. m^2.s^{-1}).

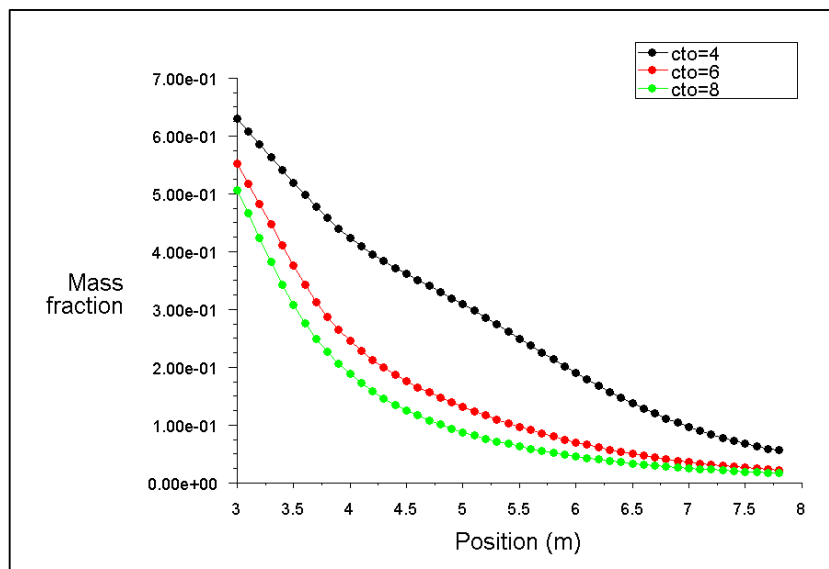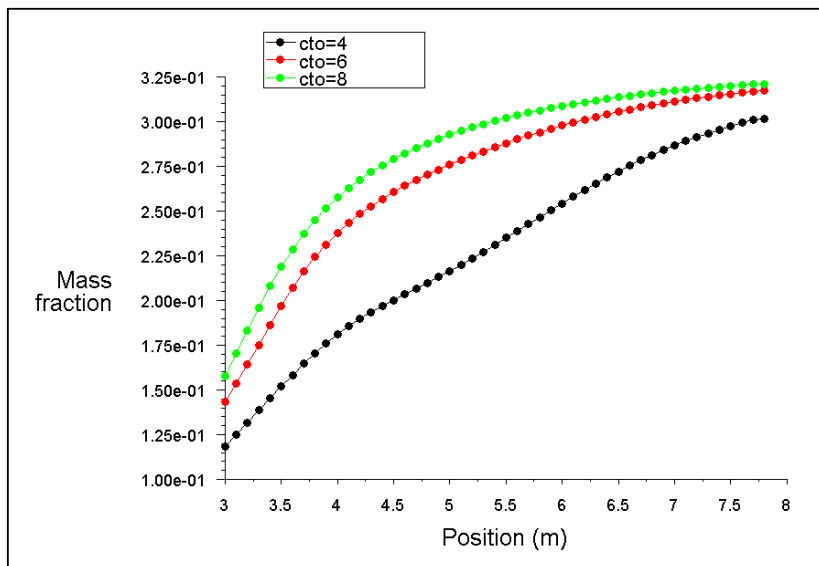**Figure 6.7. Gas-coke distributions along the riser height at different values of CTO (T_g = 723 K; T_s = 923 K; U_g= 10 m.s^{-1}; dp = 60 μm; $ρ_s$ =1,400 kg.m^{-3}; G_s = 235 kg. m^2.s^{-1}).**

6.7   Contours of Gasoline Mass Fraction

Figure 6.8 describes the contours of gasoline mass fraction over the riser cross-section at different riser heights, at a fixed inlet gas-oil feed temperature of 623 K, the catalyst flow rate of 235 kg m^2 s^{-1}, the catalyst temperature of 923 K, the gas-oil inlet velocity of 10 m s^{-1} and catalyst-to-oil ratio (CTO) of 4. It is interesting to observe how the complex flow pattern of the riser reactor has an impact on gasoline distribution especially near the feed injection zone. However, the effect of the feed injectors diminishes gradually with the riser height. As shown, a reactor flow pattern is closer to plug flow which would enhance the increasing of gasoline yield.

Figure 6.8. Contours of gasoline mass fraction at various cross sections of the riser height (T_g = 623 K; T_s = 923 K; U_g= 10 m.s^{-1}; dp = 60 µm; ρ_s =1,400 kg.m^{-3}; G_s = 235 kg. m^2.s^{-1}; CTO = 4).
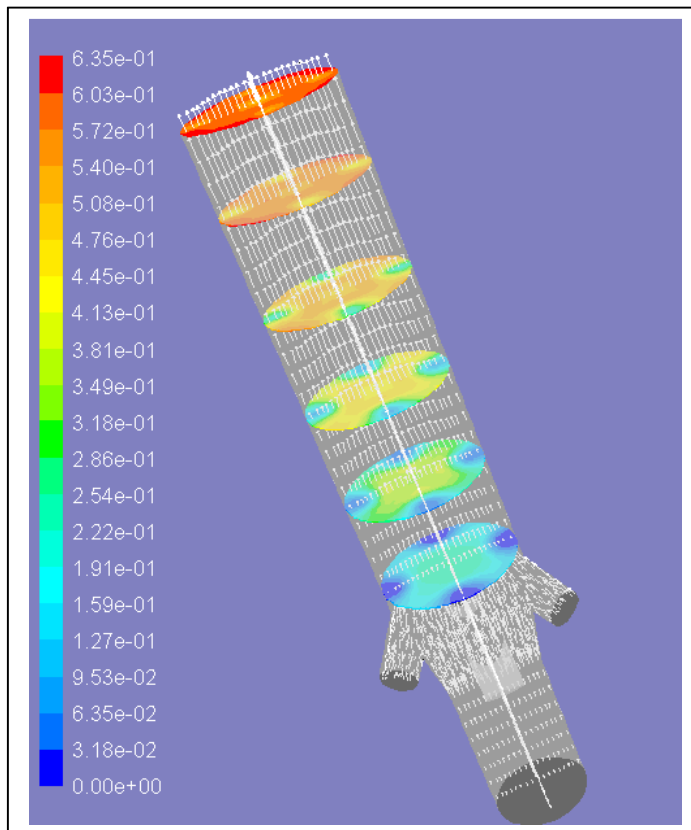
6.8   Concluding Remarks

In this chapter, we have discussed a more complete analysis involving the hydrodynamics and the kinetics of the catalytic cracking reactions in FCC riser reactors for steady-state conditions. The Eulerian-Eulerian multiphase flow and the 3-lump kinetic model were assumed in order to simulate three-dimensional hydrodynamics and the cracking reactions occurring in FCC riser reactors. It has been also described that how the FCC parameters such as catalyst-to-oil ratio (CTO) affect the final product distribution.

The simulation results show that the flow patterns for particle velocity for non-reactive and for reactive flows were significantly different. At the riser bottom, feed injection produced complex hydrodynamics because of the mixing of catalyst and gas-oil. However, without the chemical reactions, the flow of catalyst became more uniform (similar to plug flow) within about 1 m from the feed entry. For reactive flow, the linear acceleration with height is remarkable. This acceleration is probably due the expansion of the gas with the height, since the pressure decreases. In the radial direction, towards the fully developed zone of the riser, a typical turbulence velocity profile develops due to the effect of the viscous forces. It was observed for both cases that the flow pattern revealed the absence of catalyst backmixing at the riser wall. This is due to high velocity and turbulence in the gas phase. In addition, the backmixing of catalyst is undesirable due to affect on conversion and production in FCC riser reactors. Interestingly, with cracking reactions, there was an increase in catalyst velocities with riser height, particularly at the centre of the riser. This acceleration could be attributed to the increased volume of the gas-phase due to the cracking reactions. The maximum particle velocity was observed at the centre of the riser, and the particle velocity

decreased from the centre to the wall. There is increased solid velocity at the riser top because many products are produced, such as gasoline and light gases.

As shown in the predicted result, the mass fraction of gasoline and gas-coke increases with higher CTO. However, the gas-oil mass fraction decreases with the riser height. At CTO of 4, about 7 wt.% of gas-oil is still unconverted. The majority of the gas-oil fraction is converted within 3 m to 5 m from the riser bottom.

The complex flow pattern of the riser reactor has an impact on gasoline distribution, especially near the feed injection zone. However, the effect of the feed injectors diminishes gradually along the riser height. Most of the complex mixing phenomena occur in the first 3 to 5 meters of the riser reactor height.

Chapter 7

APPLICATION OF CFD FOR TRANSIENT MULTIPHASE FLOW AND REACTION MODELLING IN FCC RISER REACTORS

7.1 Problems with Modelling and its Implementation

The riser reactor is one of the most important units in the fluid catalytic cracking process. Therefore, detailed investigation of the flow pattern in the riser reactor is significant for the design and operation. The cracking reaction, when using a very active catalyst, can be completed in short-contact-time riser-reactors. Currently, the residence time of FCC riser reactors has been shortened significantly to a few seconds. In a modern FCC unit, all the reactions in the riser occur over a short period of two to four seconds before the catalyst and the products are separated in the reactor (Sadeghbeigi, 1995). For a short residence time distribution, then multiphase flow and the cracking reactions become the important processes when simulating FCC riser reactors. Since catalytic cracking reactions occur after the vaporization of the liquid hydrocarbon feedstock, both mixing and feed vaporization must take place in the riser as quickly as possible. Otherwise, thermal cracking reactions will dominate .

At present, the complexity of the flow behaviour is the main challenge for FCC riser modelling. CFD modelling for single-phase flow has been successfully applied; however, its application still remains difficult for multiphase flow, due to

the many interactions involved in the system. It is also very difficult to describe catalytic cracking reaction and combine it with multiphase hydrodynamics. This chapter presents a transient multiphase flow model for the simulation of the flow with turbulence, heat transfer and cracking reactions in FCC reactors using CFD. FLUENT version 6.2 CFD software is capable of modelling these flow systems. The model can predict many important aspects of a riser such as catalyst hold-up, temperature and enthalpy distribution of both phases, and the distribution of product yields along the riser. It was found that the reliability of the estimated parameters and predicted results were significantly improved as compared to those obtained by other studies, especially for gasoline yield.

7.2   Numerical Procedure and Boundary Conditions

The set of conservation equations along with the constitutive equations and initial and boundary conditions cannot be solved analytically. Therefore, a numerical method based on the finite volume technique was used to obtain an approximate solution. The computation was done in one quarter of the riser only due to the assumption of symmetry. The total number of grids was 5711 which consists of structured and unstructured grids.

The geometrical configuration of the riser used for the simulations is similar to Figure 6.2. The catalyst and steam are fed from the riser bottom. Gas-oil feedstock enters the riser through four feed nozzles. The riser has diameter between 1 m at the bottom to 1.4 m at the top. The height total of the riser is 7.8 m. In order to reduce the calculation time, the bottom inlet of the riser of only 7.8 m height is simulated.

For each simulation, superficial gas and solid velocities were specified. Initially, the riser was filled by 0.56 solid volume fractions at the riser height of 1.6 m from the bottom. A turbulence intensity of 5% is imposed for the gas phase. The computations are started by setting the initial guess similar to the specified velocities. A constant time step of 0.001 s with 20 iterations per time step was used. This iteration was appropriate to achieve convergence for the majority of time steps. First-order discretization schemes for the convection terms are chosen. The relative error between the iterations was specified by using a convergence criterion of 10^{-3} for each scale residual.

The catalyst is fed to the riser with velocity of 0.2 m/s and temperature of 923 K.. The volume fraction of catalyst was 40%, a mean particle diameter of 60 *µm* and density of about 1500 kg/m^3. The gas-oil inlet velocity was 10 m/s. The temperature of the inlet gas-oil feed was varied with values of 623, 673 and 723 K.

7.3 Solids Hold-up

Figure 7.1 shows the solids hold-up along the riser height for the velocity of the catalyst inlet was m/s, with temperature of 923 K; the velocity of the gas-oil inlet was 10 m/s, with temperature of 723 K. The solid hold-up was higher at the bottom of the riser. In the lower portion of the riser, the solid volume fraction decreased sharply. Then it decreased more slowly along the height of the riser, due to the increasing axial velocity and the required conservation of mass. The predicted solids hold-up along the riser is consistent with reported results in industrial riser reactors . It was suspected that the multiphase mixing due to fast acceleration of particles (gas velocity of about 10 m/s) causes these phenomena.

The predicted results indicate that most of the complex phenomena occur in the first 3 to 5 meters of the riser reactor.
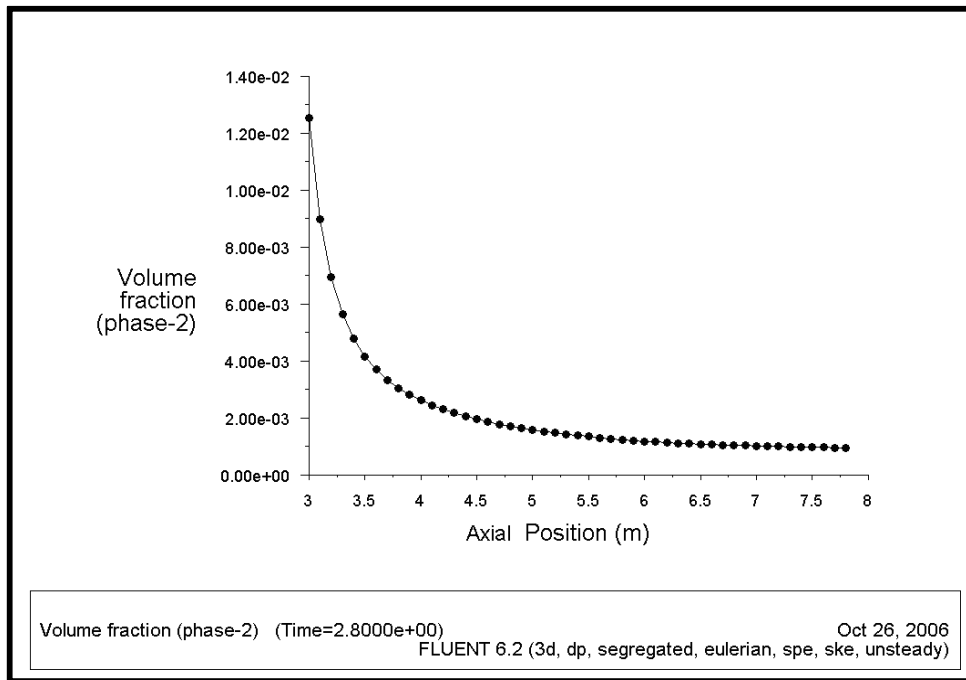
Figure 7.1. Time averaged solids hold-up distribution along the riser height (T_g = 723 K; T_s = 923 K; U_g= 10 m.s^{-1}; U_s = 0.2 m.s^{-1}; dp = 60 μm; ρ_s =1,500 kg.m^{-3}).

Figure 7.2 shows the radial distributions of volume fraction profiles of the solid phase as a function of riser height for the velocity of the catalyst inlet was m/s, with temperature of 923 K; the velocity of the gas-oil inlet was 10 m/s, with temperature of 723 K. The model predicts a profile with minima in solid volume fraction near the wall. The solid volume fraction decreased toward the wall, reaching a minimum value close to the wall. The solid volume fraction across the riser diameter decreases as the riser height increases. Miller and Gidaspow (1992) used an X-ray densitometer to determine the radial solids volume fraction profiles

in a circulating fluidized bed. Their data show that the solids volume fraction decreases with the riser height. At the riser height of 3 m, the volume fraction of solid at the wall is higher than at the centre. The profile of solid volume fraction in the riser bottom was influenced by the high inlet velocity of gas-oil feed. Therefore, the catalyst particles were pushed toward the centre by the gas-oil.

A large number of published experimental studies on a riser have observed core-annular structure. As a result, a large data base for riser operating over a wide range of solids mass fluxes and gas velocities has been established. The studies have used solids both the FCC catalyst and sand and have been carried out with risers ranging in diameter from 0.05 to 0.4 m and. However, little data is available for industrial scale risers with diameters of 1 metre or larger. The core-annular structure was not observed in this model. Ranade (1999) also predicted a similar profile for riser diameter of 0.3 m and 1.0 m (this work used diameter of 1.4 m). Moreover, a core-annular structure was found for a smaller diameter of 0.06 m. In addition, Benyahia et al. (2003) did not show a core-annular flow regime in their two-dimensional model. They concluded that the cracking reactions can significantly effect the radial solid concentration distribution due to the large increase of gas velocity along the riser. A similar trend was observed experimentally by De Wilde et al. .
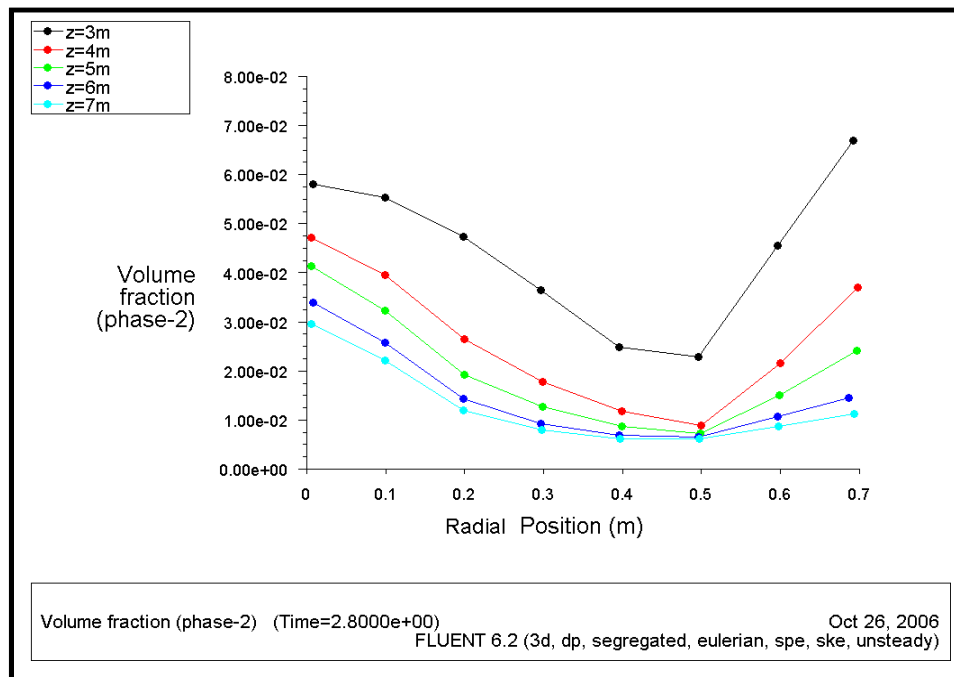
Figure 7.2. Radial solid volume fractions at different riser height (T_g = 723 K; T_s = 923 K; U_g= 10 m.s^{-1}; U_s = 0.2 m.s^{-1}; dp = 60 μm; $ρ_s$ =1,500 kg.m^{-3}).

7.4   The Profile for Axial Solid Velocity

Figure 7.3 illustrates the velocity profiles of solid along the riser height for the velocity of the catalyst inlet was m/s, with temperature of 923 K; the velocity of the gas-oil inlet was 10 m/s, with temperature of 723 K. The solid velocity increases along the riser height because of the increased amount of hydrocarbon vapours due to the cracking reaction. Catalytic cracking reactions increase the number of moles and cause a significant increase in the gas (and catalyst) velocity . Gupta in their review also concluded that the gas/solid velocity increases due to feed vaporization and molar expansion resulting from the cracking of gas-oil to form lower molecular weight products. The figure shows rapid acceleration near

the riser entrance and away from the riser entrance the acceleration is lower. Since the particles are fluidized by steam and a high-velocity of the gas-oil also injected with steam, so a number amount of drag force is applied on them. Therefore, the relative velocity between the gas and solid is very high. Moreover, the gravity force will try do decelerate these particles but the drag force is dominant in this entrance zone which is known as the acceleration zone. Because they travel away from the entrance zone, their velocity is nearer to the velocity of the gas and drag force is significantly decreased to the same magnitude order as the decelerating gravitational force. Because they flow up the riser, the drag is balanced by the solid weight and constant velocity is attained which is clearly shown in this figure.

At the riser entrance, the radial velocity of particle would be quite higher due to the entrance effect and flow instability. However, because of the presence of the wall, the particles hit the wall and are redirected back into the gas flow at the centre and are also accelerated. Furthermore, since the particles travel up the riser, the axial velocity becomes more dominant and the radial velocity becomes low.
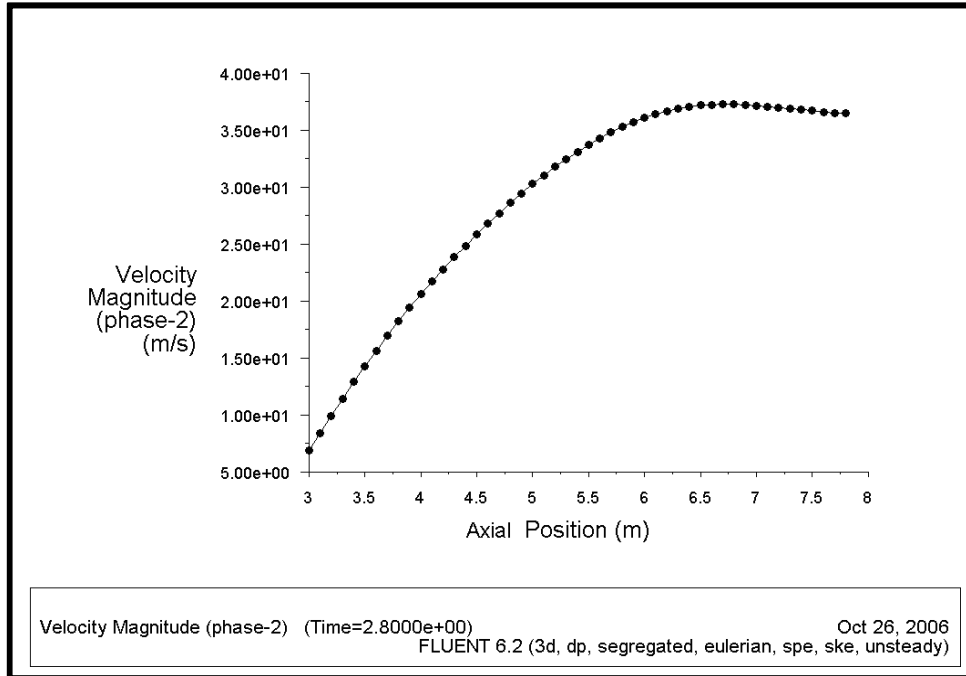
Figure 7.3 Solid velocity profiles along the riser height (T_g = 723 K; T_s = 923 K; U_g= 10 m.s^{-1}; U_s = 0.2 m.s^{-1}; dp = 60 μm; ρ_s =1,500 kg.m^{-3}).

7.5   Enthalpy Profiles

Figure 7.4 shows the enthalpy distributions of solid phase for various feed inlet temperatures. The enthalpy was higher at the bottom of the riser, and the average enthalpy was about 560 to 600 kJ/kg, which is in good agreement with the experimental value reported by Pekediz et al. (1997) and the simulation result reported by Pareek et al. .

Previous researchers have assumed a constant average heat of reaction for all cracking reactions. The assumption of constant heat reaction provides a valuable way to account for the axial temperature gradient exists in the riser. However, this work proved that the heat of cracking itself varies axially with a higher value in the riser bottom. Therefore, assuming constant heat of reactions by several researchers is oversimplification. A higher value of the enthalpy of solid phase at the bottom of the riser indicates that coking reactions are prominent at the riser bottom. The reaction leading to coke formation, in general, have a greater heat of reaction than other reactions (Arbel et al., 1995).
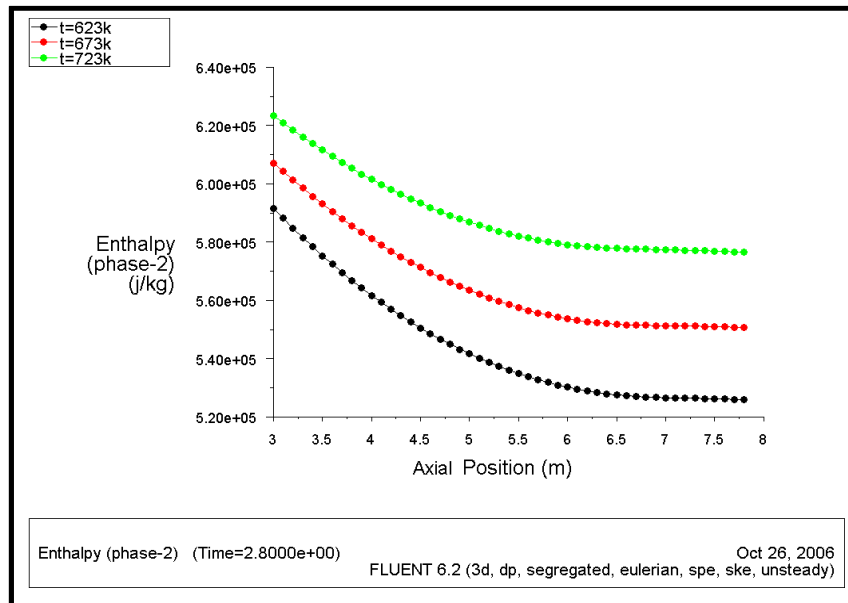
Figure 7.4. Enthalpy of the solid phase at different feed inlet temperatures ($T_s = 923$ K; $U_g = 10$ m.s^{-1}; $U_s = 0.2$ m.s^{-1}; $dp = 60$ µm; $\rho_s = 1,500$ kg.m^{-3}).

7.6 Temperature Profiles

The axial temperature profiles of the solid phase due to the endothermic cracking reactions for various inlet feed-temperatures are shown in Figure 7.5. As expected, the temperature decreased significantly from the bottom to the top of the riser. The solid temperature decreases due to the heat requirements for raising the sensible heat of the feed, and due to the endothermic heat of the cracking reactions . The temperature drop of about 35 to 55 K which is typical of industrial application was predicted. Furthermore, the maximum temperature drop of the solid phase occurs close to the riser entrance due to the higher heat of cracking reactions at the bottom. The trend of the temperature distribution along the riser height shows reasonable agreement with reported results by Pareek et al. , as shown in Figure 7.6.

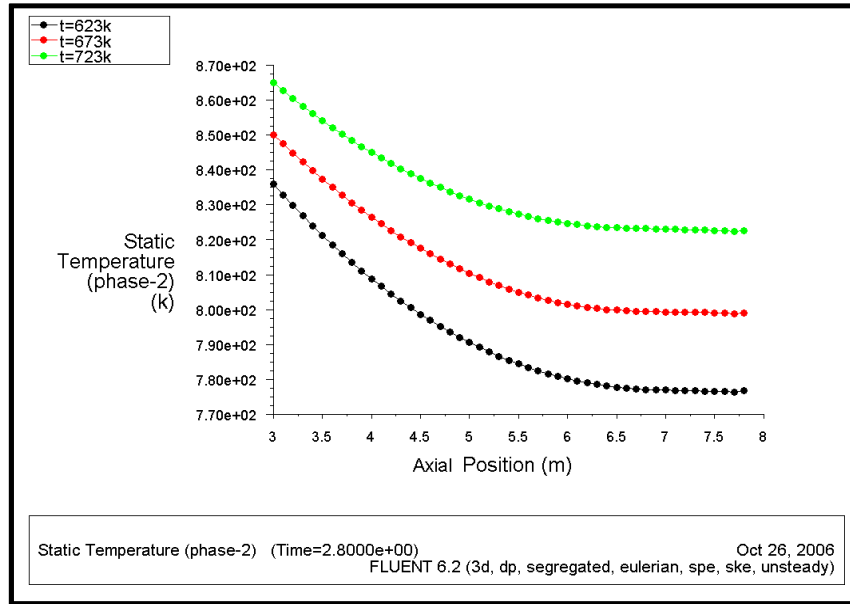**Figure 7.5. Temperature distribution of the solid phase for various feed inlet temperatures (T$_s$ = 923 K;   U$_g$= 10 m.s^{-1};   U$_s$ = 0.2   m.s^{-1}; dp = 60 μm; ρ$_s$ =1,500 kg.m^{-3}).**
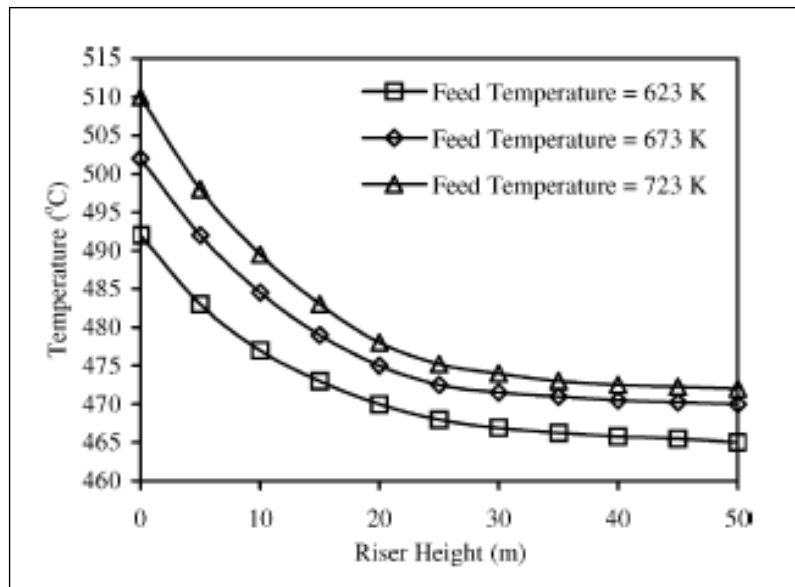
Figure 7.6. Temperature profiles along the riser height (T$_s$ = 923 K; U$_g$ = 10 m.s^{-1}; G$_s$ = 50 kg.m^2.s^{-1}; dp = 60 μm; ρ$_s$ =1,500 kg.m^{-3}).

7.7 Distribution of Reactant and Product Yields along the Riser Height

Figure 7.7 presents the concentration profiles for gas-oil, gasoline and coke along the riser height. There were no chemical reactions below the gas-oil feed injection (z = 3m). Above this region, the yield of gasoline increased along the height of the riser. However, the gas-oil concentration declined progressively. From Figure 7.7, the formation of gasoline is most significant between 3 to 5 metres from the bottom of the riser. This is due to the higher catalyst activity and the reactivity of gas-oil feedstock at the bottom. Beyond 5 m riser height, the gasoline yield only increases slightly. These profiles are in good agreement with the typically data obtained in various industrial plant and similar to reported results from other researchers .
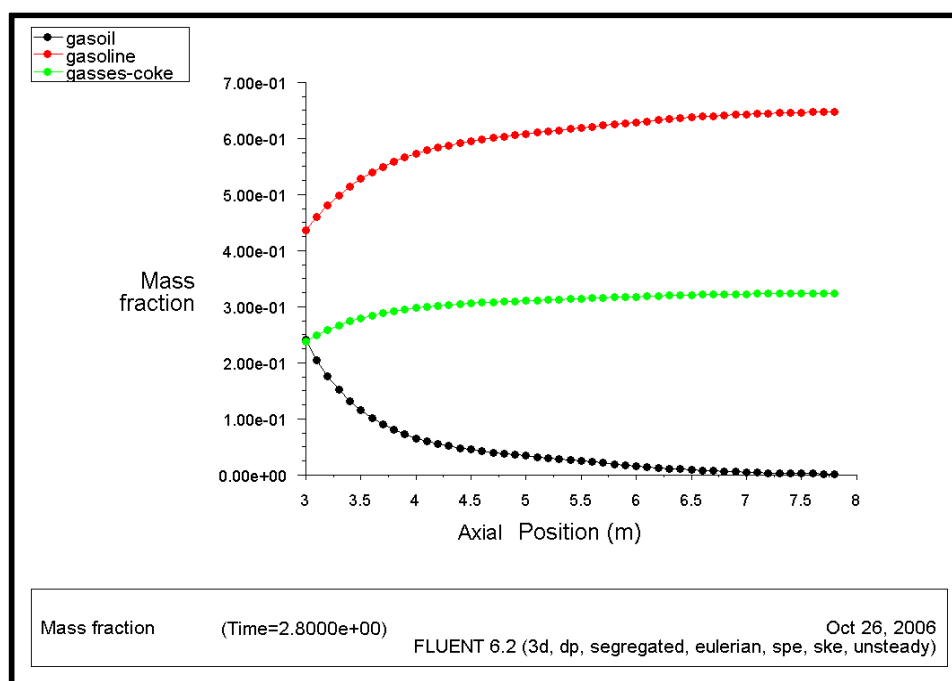
Figure 7.7. Yields distribution along the height of the riser (T_g = 723 K; T_s = 923 K; U_g= 10 m.s^{-1}; U_s = 0.2 m.s^{-1}; dp = 60 μm; $ρ_s$ =1,500 kg.m^{-3}).

7.8 Gasoline Concentration

Figure 7.8 presents the time-averaged contour plot of the gasoline concentrations over the cross section of the riser and the solid velocity vectors for the gas-oil inlet velocity and catalyst inlet velocity of 10 m/s and 0.2 m/s respectively. The blue area represents the low concentration of gasoline and the red area for higher of gasoline concentration. Interestingly, the complex flow pattern of the riser reactor has an impact on gasoline distribution, especially in the vicinity of the feed injection zone where cracking reactions commence. As shown, a low gasoline concentration occurs in this area due to effect of the injection geometry. However, the effect of feed injectors reduces continuously with the riser height. A higher concentration of gasoline can be found at the upper region of the riser. It can be seen that the flow pattern demonstrated the absence of solid recirculation at the riser wall. This is due to high velocity and turbulence in the gas phase. Pita and Sundaresan (1993) found some predicted results with similar riser geometry. They observed the recirculation of the solid at the riser wall due to lower gas velocity. They also used boundary condition of exit section with gas and solid flowing radial which is supposed to promote the solid recirculation. The recirculation of solid at the riser wall is undesirable for catalytic cracking of hydrocarbon feedstock and leads the cracking reaction to operate at a higher gas velocity than required typically in FCC riser reactor.

Figure 7.9 shows the simulated flow pattern of the gasoline concentration for the gas-oil inlet velocity and catalyst inlet velocity of 10 m/s and 0.2 m/s respectively. Contours plots refer to four different times (0.2 s; 0.6 s; 2.6 s; and 3.6 s) from the start of the simulation. The highest mass fraction of gasoline is about 0.65. The cracking reaction in the riser was completed after about 2.8 s simulation time.
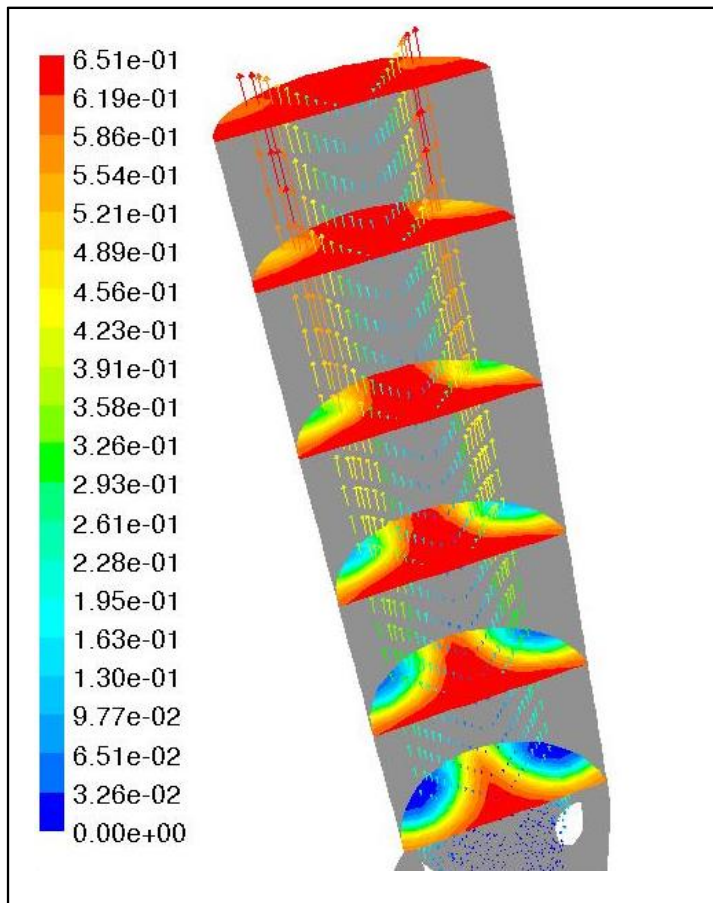
Figure 7.8. The time-averaged contours of the gasoline concentrations at the cross section of the riser, and the solid velocity vectors ($T_g = 623$ K; $T_s = 923$ K; $U_g = 10$ m.s^{-1}; $U_s = 0.2$ m.s^{-1}; dp = 60 μm; $\rho_s = 1,500$ kg.m^{-3}).
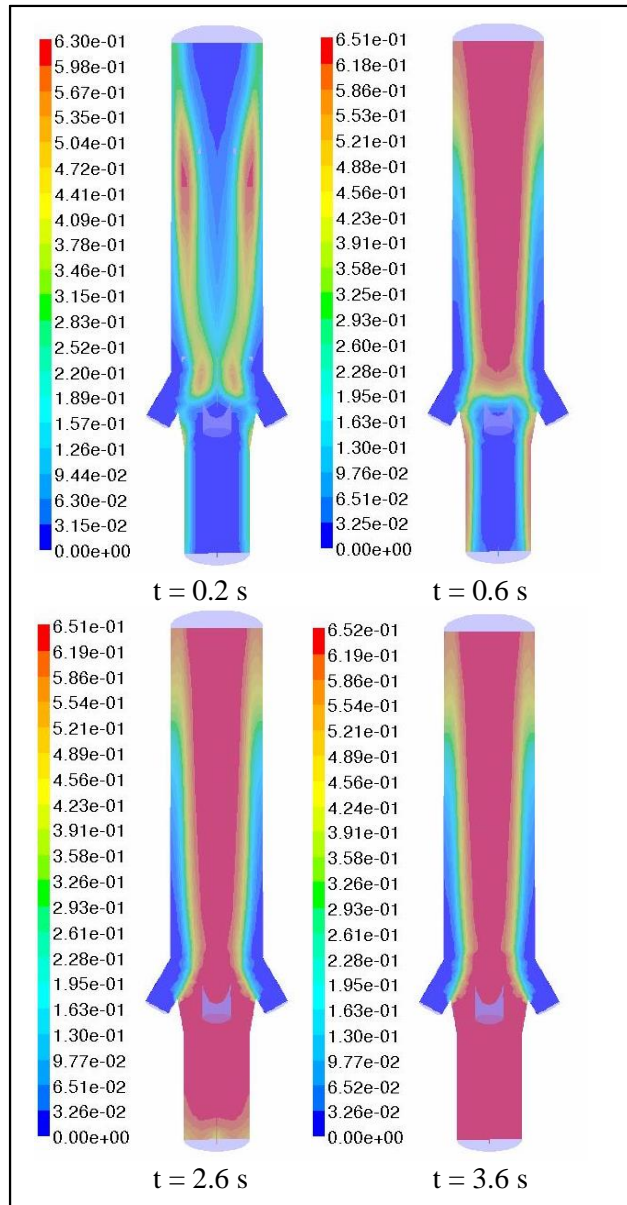
**Figure 7.9. Instantaneous contours of the gasoline mass fraction at different time simulation ($T_g = 623$ K; $T_s = 923$ K; $U_g = 10$ m.s^{-1}; $U_s = 0.2$ m.s^{-1}; dp = 60 μm; $\rho_s = 1,500$ kg.m^{-3}).**

7.9   Conclusions

We conclude that the flow pattern in an FCC riser reactor is strongly affected by the interactions of multiphase hydrodynamics, heat transfer and reaction kinetics. The predicted results indicated that most of the complex mixing phenomena occur in the first 3 to 5 meters of the riser reactor length. The increased amount of hydrocarbon vapours due to the cracking reaction increases the velocity of the gas/solid.

The predicted result shows that the solid hold-up was higher at the bottom of the riser. In the lower portion of the riser, the solid volume fraction decreased sharply. Then it decreased more slowly along the height of the riser, due to the increasing axial velocity and the required conservation of mass. The predicted solids hold-up along the riser is consistent with reported results in industrial riser reactors . It was suspected that the multiphase mixing due to fast acceleration of particles (gas velocity of about 10 m/s) causes these phenomena. The predicted results indicate that most of the complex phenomena occur in the first 3 to 5 meters of the riser reactor.

The model predicts a profile with minima in solid volume fraction near the wall. The solid volume fraction decreases towards the wall, and reaches a minimum value near the wall. The solid volume fraction across the riser diameter decreases with increasing riser height. The profile of solid volume fraction in the riser bottom was influenced by the high inlet velocity of gas-oil feed. Therefore, the catalyst particles were pushed toward the centre by the gas-oil.

As expected, the temperature decreased significantly from the bottom to the top of the riser. The solid temperature falls due to the heat requirements for raising the sensible heat of the feed, and due to the endothermic heat of the cracking reactions . Furthermore, the maximum temperature drop of the solid phase occurs close to the riser entrance due to higher heat of cracking reactions at the bottom. The enthalpy was higher at the bottom of the riser, and the average enthalpy was about 560 to 600 kJ/kg.

The complex flow pattern of the riser reactor has an impact on gasoline distribution, especially at the feed injection zone. The gasoline formation is most significant between 3 to 5 m from the bottom of the riser. This is because the gas-oil feedstock is still very reactive in this region, and the catalyst has not become deactivated. A low gasoline concentration occurs in this area due to effect of the injection geometry. A higher concentration of gasoline can be found at the upper region of the riser.

Chapter 8

Conclusions and Recommendations

8.1   Conclusions and Limitations of this Work

The literature contains many hydrodynamics CFD models that have been studied both computationally and experimentally. However, an accurate analysis of the flow field has not yet been obtained. Previous CFD models have also been limited to a two-dimensional flow model. Most researchers did not consider either turbulent flow or chemical reactions in their model. In addition, several published CFD models use cylindrical and Cartesian grid systems which are not capable of describing the complex geometries of the FCC riser reactors such as the feed injection nozzles.

In this thesis, the CFD model has been developed in order to solve three-dimensional multiphase flow and chemical reaction, together with a turbulent flow model and heat transfer under both steady-state and transient conditions. Catalytic cracking reactions were incorporated into the hydrodynamics model by solving the chemical species equations of the components in the form of reaction rates. Additional support for this model development was the availability of experimental data from the published literature, and typical operating conditions obtained from the refinery industry. This data was used for model sensitive studies. Detailed multiphase turbulent flow, heat transfer and reaction models have been obtained by a post-processing technique which provides a more complete understanding of complex phenomena in the FCC riser reactors.

In most of the cases considered, the predicted results showed good agreement with experimental data and other published CFD models. The CFD model predicted many important aspects in the FCC riser reactors such as gas-oil inlet velocity, catalyst size, temperature, catalyst-to-oil ratio (CTO), and geometry of feed injector. A number of different operating conditions were simulated in order to demonstrate the capability of the CFD model for modelling multiphase flow and chemical reactions in the FCC riser reactors. However, the application of CFD for the complete FCC system requires significant computational resources. This research has successfully provided an academic approach suitable for industrial applications, and it has also raised several issues requiring further research.

8.2   Recommendations for Further Research

The present study has demonstrated the capability of the commercial CFD code FLUENT 6.2 as a very powerful design tool which can be used to analyse the complex multiphase turbulence and reaction flows in the riser reactor. However, many fundamental aspects are still not well understood. Therefore, several advances and developments in this field are still required. Several issues that should be addressed in any future work are:

- Calculation of the vaporization of gas-oil liquid inside the riser reactors.
- In the current work, the cracking reaction rates are based on a simple three-lump kinetic scheme. Although very good results has been obtained with this simplified kinetic approach, further study is needed in order to improve the fundamental understanding of the complex chemical reactions using a more advanced kinetics scheme such as a ten-lump kinetic model.

- CFD models should be applied to a wider variety of reacting multiphase flow problems, and be used to determine refinements and improvements to the current physical models.
- Further research work should be concerned with obtaining and quantifying data for more diverse examples, and hence validating improved models which describe these industrial applications.

Chapter 9

Nomenclature

A_j	Surface area of jth face of control volume	[m^2]
C_1	Turbulence constant	[-]
C_2	Turbulence constant	[-]
C_D	Drag coefficient	[-]
C_p	Heat capacity at constant pressure	[J.kg^{-1}.K]
C_v	Heat capacity at constant volume	[J.kg^{-1}.K]
C_μ	Turbulence constant	[-]
D_i	Diffusivity of species i in the fluid	[m^2.s^{-1}]
d_s	Diameter of solid particles	[m]
e_s	Particle collisions coefficient	[-]
g	gravitational acceleration	[m.s^{-2}]
g_o	Radial distribution function	[-]
H_i	Specific enthalpy of ith phase	[J.kg^{-1}]
J_i	Rate of diffusive flux species i	[kg.m^{-2}.s^{-1}]
$k_{\Theta s}$	Diffusion coefficient	[kg.m^{-1}s^{-1}]
k_i	Turbulent kinetic energy	[J.kg^{-1}]
K_0	The kinetic parameters for Arrhenius equation	[s^{-1}]
K_1	The kinetic parameters for Arrhenius equation	[s^{-1}]
K_2	The kinetic parameters for Arrhenius equation	[s^{-1}]
P	Static Pressure	[N.m^{-1}]
P_s	Solid Pressure	[N.m^{-1}]
$\mathbf{q}_i$	The heat flux	[W.m^{-2}]
Re_s	Relative Reynolds number	[-]
T	Temperature	[K]

T_s	Solid stress tensor	[Pa]
t	Time	[s]
U_i	Velocity of ith phase	[m.s^{-1}]
Y_1	mass fractions of gas-oil	[-]
Y_2	mass fractions of gasoline	[-]
α	Turbulent kinetic energy dissipation rate	[m^2.s^{-3}]
β	Solid gas exchange coefficient	[kg.m^{-3}.s^{-1}]
ρ_i	Density of ith phase	[kg.m^{-3}]
ε_i	Volume fraction of ith phase	[-]
ϵ_i	Turbulent dissipation rate	[m^2.s^{-3}]
τ_i	Shear stress tensor of ith phase	[N.m^{-2}]
γ_s	Collisional dissipation of energy	[kg.m^{-1}.s^{-3}]
Θ_s	Granular temperature	[m^2.s^{-1}]
μ_b	Solid bulk viscosity	[kg.m^{-1}.s^{-1}]
μ_i	Viscosity of ith phase	[kg.m^{-1}.s^{-1}]
$\mu_{s,dill}$	Solid phase dilute viscosity	[kg.m^{-1}.s^{-1}]
μ_t	Turbulent viscosity	[kg.m^{-1}.s^{-1}]
σ_k	Turbulence constant	[-]
σ_C	Turbulence constant	[-]
Δt	Time step	[s]
ΔV	Cell Volume	[m^3]
Δx	cell x dimension	[m]
Δy	cell y dimension	[m]
Δz	cell z dimension	[m]

Subscripts

b	bulk material property
B	bottom direction cell volume
E	east direction cell volume
g	gas phase
N	north direction cell volume
P	current cell centre
S	south direction cell volume
s	solid phase
T	top direction cell volume
W	west direction cell volume

Chapter 10

REFERENCES

Agrawal, K., Loezos, P. N., Syamlal, M. and Sundaresan, S. (2001) *J. Fluid Mech.,* **445,** 151-185.

Arbel, A., Huang, Z., Rinard, I. H., Shinnar, R. and Sapre, A. V. (1995) *Ind. Eng. Chem. Res.,* **34,** 1228-1243.

Benyahnia, S., Arastoopour, H. and Knowlton, T. M. (2002) *Chem. Eng. Comm.,* **189,** 510-527.

Benyahnia, S., Ortiz, A. G. and Paredes, J. I. P. (2003) *International Journal of Chemical Reactor Engineering,* **1,** 1-11.

Berry, T. A., McKeen, T. R., Pugsley, T. S. and Dalai, A. K. (2004) *Ind. Eng. Chem. Res.,* **43,** 5571-5581.

Bhusarapu, S., Al-Dahlan, M. H., Dudukovic, M. P., Trujillo, S. and O'Hern, T. J. (2005) *Ind. Eng. Chem. Res.,* **44,** 9739-9749.

Bird, R. B., Stewart, W. E. and Lightfoot, E. N. (1960) *Transport Phenomena,* Wiley, New York.

Brodkey, R. S. and Hershey, H. C. (1988) *Transport Phenomena: a unified approach,* McGraw-Hill, New York.

Chang, S. L., Lottes, S. A., Zho, C. Q., Bowman, B. J. and Petrick, M. (2001) *ASME,* **123,** 544-555.

Chapman, S. and Cowling, T. G. (1970) *The Mathematical Theory of Non-uniform Gases,* Cambridge University Press, Cambridge.

Das, A. K., Baudrez, E., Marin, G. B. and Heynderick, G. J. (2003) *Ind. Eng. Chem. Res.,* **42,** 2602-2617.

Ding, J. and Gidaspow, D. (1990) *AIChE J.,* **36,** 523-538.

Ferziger, J. H. and Peric, M. (1999) *Computational Methods for Fluid Dynamics,* Springer, Berlin; New York.

Fluent (2005) *Fluent 6.2 User Guide*, Lebanon.

Froment, G. F. and Bischoff, K. B. (1990) *Chemical Reactor Analysis and Design,* Wiley, New York.

Gates, B. C., Katzer, J. R. and Schuit, G. G. (1979) *Chemistry of catalytic process,* McGraw-Hill, New York.

Hansen, K. G., Ibsen, C. H., Solberg, T. and Hjertager, B. H. (2003) *International Journal of Chemical Reactor Engineering,* **1,** 1-10.

Heynderick, G. J., Das, A. K., Wilde, J. D. and Marin, G. B. (2004) *Ind. Eng. Chem. Res.,* **43,** 4635-4646.

Ibsen, C. H., Solberg, T. and Hjertager, B. H. (2001) *Ind. Eng. Chem. Res.,* **40, 5081-5086.**

Jacob, S. M., Gross, B., Voltz, S. E. and Weekman, V. W. (1976) *AIChE J.,* **22, 701-713.**

Krishna, R. and van Baten, J. M. (2001) *Chem. Eng. J.,* **82, 247-257.**

Kunii, D. and Levenspiel, O. (1991) *Fluidization Engineering,* **Butterworth-Heinemann, Newton.**

Launder, B. E. and Spalding, D. B. (1972) *Lectures in Mathematical Models of Turbulence,* **Academic Press, London.**

Lun, C. K., Savage, S. B., Jfferey, D. J. and Chepurniy, N. (1984) *J. Fluid Mech.,* **140, 223.**

Martin, M. P., Derouin, C., Turlier, P., Forissier, M., Wild, G. and Bernard, J. R. (1992a) *Chem. Eng. Sci.,* **47, 2319-2324.**

Martin, M. P., Turlier, P. and Bernard, J. R. (1992b) *Powder Technol.,* **70, 249-258.**

Masamune, S. and Smith, J. M. (1966) *AIChE J.,* **12, 384.**

Mauleon, J. L. and Courcelle, J. C. (1985) *Oil & Gas Journal*, **64.**

Miller, A. and Gidaspow, D. (1992) *AIChE J.,* **38, 1801-1815.**

Mirgain, C., Briens, C., Pozo, M. D., Loutaty, R. and Bergougnou, M. (2000) *Ind. Eng. Chem. Res.,* **39, 4392-4399.**

Murphy, J. R. (1992) *Oil & Gas Journal,* **90, 49-58.**

Patankar, S. V. and Spalding, D. B. (1972) *Int. J. Heat Mass Transfer,* **15, 1787-1806.**

Pekediz, A., Kraemer, D. W., Blasetti, A. and de LASA, H. (1997) *Ind. Eng. Chem. Res.,* **36, 4516-4522.**

Pita, J. A. and Sundaresan, S. (1991) *AIChE J.,* **37, 1009.**

Pita, J. A. and Sundaresan, S. (1993) *AIChE J.,* **39, 541.**

Ranade, V. V. (1999) In *Second International Conference on CFD in Minerals and Process Industries***(Ed, CSIRO) Melbourne, Australia, pp. 77-82.**

Ranade, V. V. (2002) *Computational flow modeling for chemical reactor engineering,* **Academic Press, California.**

Sadeghbeigi, R. (1995) *Fluid Catalytic Cracking Handbook: design, operation, and troubleshooting of fcc facilities,* **Gulf Publishing Company, Houston,Texas.**

Samuelsberg, A. and Hjertager, B. H. (1996) *AIChE J.,* **42, 1536-1546.**

Sinclair, J. L. and Jackson, R. (1989) *AIChE J.,* **35, 1473-1486.**

Sun, B. and Gidaspow, D. (1999) *Ind. Eng. Chem. Res.,* **38, 787-792.**

Theologos, K. N. and Markatos, N. C. (1993) *AIChE J.,* **39, 1007-1017.**

Tinaburri, A. (1996) *AIChE J.,* **42, 3310-3317.**

Tsuo, Y. P. and Gidaspow, D. (1990) *AIChE J.,* **36, 885-896.**

Versteeg, H. K. and Malalasekera, W. (1995) *An Introduction Fluid Dynamics: The Finite Volume Method,* **Pearson Education Limited, U.K.**

Weekman, V. W. and Nace, D. M. (1970) *AIChE J.,* **16, 397-404.**

Weisz, P. B. and Goodwin, R. B. (1966) *J. Catal,* **6, 227.**

Xiaotao, T. B. (2004) *International Journal of Chemical Reactor Engineering,* **2(A12), 1-12.**